이학박사학위논문

Band Topology of Spacetime-Inversion-Symmetric Systems

시공간 반전 대칭이 있는 계의 띠 위상

2020 년 2 월

서울대학교 대학원

물리천문학부

안 준 영

이학박사학위논문

Band Topology of Spacetime-Inversion-Symmetric Systems

시공간 반전 대칭이 있는 계의 띠 위상

2020 년 2 월

서울대학교 대학원

물리천문학부

안 준 영

Band Topology of Spacetime-Inversion-Symmetric Systems

시공간 반전 대칭이 있는 계의 띠 위상

지도교수 양 범 정

이 논문을 이학박사 학위논문으로 제출함

2020 년 1 월

서울대학교 대학원

물리천문학부 물리학전공

안 준 영

안준영의 이학박사 학위논문을 인준함

2019 년 12 월

위 원 장	유재준	(인)
부위원장	양범정	(인)
위 원	김창영	(인)
위 원	민홍기	(인)
위 원	김영국	(인)

Abstract

We study topological phases in systems with spacetime inversion symmetry I_{ST}. I_{ST} is an anti-unitary symmetry which is local in momentum space and satisfies $I_{\mathrm{ST}}^2 = 1$ such as PT in 2D and 3D without spin-orbit coupling and C_2T in 2D with or without spin-orbit coupling where P, T, C_2 indicate inversion, time-reversal, and two-fold rotation symmetries, respectively. Under I_{ST}, the Hamiltonian and the periodic part of the Bloch wave function can be constrained to be real-valued, which makes the Berry curvature and the Chern number to vanish. In this class of systems, gapped band structures of real wave functions can be topologically distinguished by Stiefel-Whitney numbers instead. The first and second Stiefel-Whitney numbers w_1 and w_2, respectively, are the corresponding invariants in 1D and 2D, which are equivalent to the quantized Berry phase and the Z_2 monopole charge, respectively. We first describe the topological phases characterized by the first Stiefel-Whitney number, including 1D topological insulators with quantized charge polarization, 2D Dirac semimetals, and 3D nodal line semimetals. Next we show how the second Stiefel-Whitney class characterizes the 3D nodal line semimetals carrying a Z_2 monopole charge. In particular, we explain how the second Stiefel-Whitney number w_2, the Z_2 monopole charge, and the linking number between nodal lines are related. Then, we study the properties of 2D and 3D topological insulators characterized by the nontrivial second Stiefel Whitney class. After this exposure to our general theory, we explain the reformulated Nielsen-Ninomiya theorem in two dimensions as an interesting application. We derive all these results by assuming only I_{ST} symmetry. When P or C_2 symmetry is present in addition to I_{ST} symmetry

in the absence of spin-orbit coupling, we show that the second Stiefel-Whitney number can be calculated efficiently using the parity eigenvalues of P or C_2. The relation between the parity eigenvalues and the second Stiefel-Whitney number is applied to the study of odd-parity topological superconductivity in spin-polarized systems.

Keywords: band topology, spacetime inversion symmetry, topological semimetal, topological insulator, topological superconductor, topological invariant
Student Number: 2013-20372

Contents

Chapter 1

Introduction

The energy band structure of a periodic crystal consists of a mapping from a crystal momentum $\mathbf{k}$ to the Bloch Hamiltonian $H(\mathbf{k})$, which is generally complex-valued. Gapped band structures of insulators can be topologically distinguished by the equivalence class of $H(\mathbf{k})$ [1]. That is, two gapped band structures are topological distinct if one cannot be smoothly deformed to the other while keeping the energy gap. In two dimensions (2D), the gapped band structures of a complex Hamiltonian are distinguished by an integer topological invariant, called the Chern number c_1. The Chern invariant characterizes the equivalence classes of fiber bundles associated with the complex Bloch wave functions $|u(\mathbf{k})\rangle$, which is nothing but the first Chern class. The Chern number c_1 can be expressed in terms of the Berry connection $\mathbf{A}_m(\mathbf{k}) = \langle u_m(\mathbf{k})| \, i\nabla \, |u_m(\mathbf{k})\rangle$ and the Berry curvature $F_m(\mathbf{k}) = \partial_{k_x} A_{m,y}(\mathbf{k}) - \partial_{k_y} A_{m,x}(\mathbf{k})$ where $m = 1, 2, ..., N_{\text{occ}}$ with N_{occ} denoting the number of occupied bands. c_1 is given by the integral of $F_m(\mathbf{k})$ on a 2D closed manifold $\mathcal{M}$ summed over all

the occupied bands as

$$c_1 = \sum_{m=1}^{N_{\rm occ}} \int_{\mathcal{M}} \frac{d^2k}{2\pi} F_m(\mathbf{k}). \tag{1.1}$$

When the full 2D Brillouin zone torus is considered for the integration, the corresponding insulator with a nonzero c_1 is a quantum Hall insulator exhibiting a quantized anomalous Hall conductivity $\sigma_{xy} = \frac{e^2}{h} c_1$. The integration can also be performed over a 2D closed subspace of a 3D Brillouin zone enclosing Weyl points. In this case, a nonzero c_1 corresponds to the total chiral charge of the enclosed Weyl points [2–4].

On the other hand, when the system satisfies a certain symmetry condition, the corresponding Bloch wave functions can be real-valued. Here the relevant symmetry is so-called the spacetime inversion symmetry $I_{\rm ST} : (t, \mathbf{r}) \to (-t, -\mathbf{r})$, which inverts the sign of both time t and spatial coordinates $\mathbf{r}$ [5–7]. $I_{\rm ST}$ is an antiunitary symmetry operator that is local in momentum space and satisfies $I_{\rm ST}^2 = 1$. For instance, the combination of spatial inversion P and time-reversal T can be used to define $I_{\rm ST} = PT$ in systems with negligible spin-orbit coupling in any dimension. In the case of 2D systems, the combined symmetry $I_{\rm ST}$, where C_{2z} denotes two-fold rotation about the z-axis, can also play the role of $I_{\rm ST}$, irrespective of the presence or the absence of spin-orbit coupling [5]. Since $I_{\rm ST}$ can always be represented by $I_{\rm ST} = K$ with the complex conjugation operator K under a suitable basis choice [5, 8], the invariance of the Hamiltonian $H(\mathbf{k})$ under $I_{\rm ST}$ imposes the reality condition to $H(\mathbf{k})$, and then we can choose real eigenstates $|u(\mathbf{k})\rangle$, such that

$$\begin{aligned} &I_{\rm ST} H(\mathbf{k}) I_{\rm ST}^{-1} = H^*(\mathbf{k}) = H(\mathbf{k}), \\ &I_{\rm ST} \left|u(\mathbf{k})\right\rangle = \left|u(\mathbf{k})\right\rangle^* = \left|u(\mathbf{k})\right\rangle . \end{aligned} \tag{1.2}$$

Since real wave functions have zero abelian Berry curvature at every momentum

d	Physical invariant	Mathematical invariant
$d=1$	Quantized Berry phase	First Stiefel-Whitney number (w_1)
$d=2$	Z_2 monopole charge	Second Stiefel-Whitney number (w_2)

Table 1.1 The correspondence between the physics terminology and Stiefel-Whitney (Stiefel-Whitney) class in systems with spacetime inversion symmetry. d indicates the spatial dimension.

$\mathbf{k}$, all gapped real band structures have zero Chern number so that they are all topologically trivial in view of the first Chern class.

In fact, the gapped band structures of real Hamiltonians are topologically distinguished by different topological invariants, so-called the Stiefel-Whitney numbers [9–11]. The first and the second Stiefel-Whitney numbers, w_1 and w_2, respectively, are the corresponding 1D and 2D topological invariants [7, 12]. The Stiefel Whitney numbers w_1, w_2 are rooted in the mathematical structure of real vector bundles associated with real Bloch wave functions, which is nothing but the Stiefel Whitney class, characterizing the twist of real Bloch states in momentum space. Although the concept of Stiefel-Whitney numbers is not popular in condensed matter physics, their physical implication is quite transparent. Namely, w_1 is equivalent to the quantized Berry phase, while w_2 is equivalent to the Z_2 monopole charge of a nodal line, both are well-defined in systems with spacetime inversion symmetry. The correspondence between Stiefel-Whitney number and the relevant physical invariant is summarized in Table 1.

The band crossing condition changes significantly in the presence of the reality condition given in Eq. (1.2). For instance, in PT-symmetric systems with negligible spin-orbit coupling, since each band is non-degenerate at a generic

momentum $\mathbf{k}$, an accidental band crossing can be described by an effective two-band Hamiltonian given by

$$H(\mathbf{k}, m) = f_0(\mathbf{k}, m) + f_1(\mathbf{k}, m)\sigma_x + f_3(\mathbf{k}, m)\sigma_z, \tag{1.3}$$

where $\sigma_{x,y,z}$ are the Pauli matrices for the two crossing bands and $f_{0,1,3}(\mathbf{k}, m)$ are real functions of momentum $\mathbf{k}$ and a parameter m tuning the band gap. It is worth noting that the σ_y term vanishes due to the reality condition. Then because closing the band gap requires only two conditions $f_{1,3}(\mathbf{k}, m) = 0$ to be satisfied whereas the number of independent variables ($\mathbf{k}$, m) is $d+1$ where d is the spatial dimension, an accidental band crossing is possible unless $d + 1 < 2$. This means that, in 1D, a gapped band structure is generally stable but an accidental band crossing can happen at the critical point between two gapped insulators. On the other hand, in 2D, a gapless phase with point nodes can be stabilized, and an accidental band crossing induces a transition between an insulator and a stable 2D Dirac semimetal phase. Similarly, in 3D, a semimetal phase with nodal lines can be stabilized, and an accidental band crossing mediates a transition between an insulator and a 3D nodal line semimetal. It is worth noting that the 1D insulators, the 2D Dirac points, and the 3D nodal lines mentioned above are all characterized by the first Stiefel Whitney number w_1, which follows from the equivalence between w_1 and the quantized Berry phase.

In fact, a line node of a 3D nodal line semimetal can also be characterized by another topological invariant, that is, the second Stiefel-Whitney number w_2. Namely, a line node of a 3D nodal line semimetal carries two Z_2 topological indices w_1 and w_2, and thus it is doubly charged [13]. As shown in Ref. [7], w_2 is equivalent to the Z_2 monopole charge proposed in Ref. [5]. In fact, a two-band description based on Eq. (1.3) cannot capture w_2 because there should be at

least two bands below the Fermi level to characterize the band topology of a nodal line carrying nonzero Z_2 monopole charge (monopole nodal line) at the Fermi level. It is shown that the multi-band description is required due to the intrinsic linking structure of monopole nodal line with other nodal lines below the Fermi level, which can be predicted by using the mathematical property of Stiefel Whitney classes.

The significance of w_2 is not limited to the characterization of monopole nodal line in 3D nodal line semimetals. When w_2 is computed on the 2D Brillouin zone torus, it becomes a well-defined 2D Z_2 topological invariant characterizing 2D insulators in the absence of the Berry phase [7]. Thus one can classify $I_{\rm ST}$-symmetric 2D insulators into topologically trivial insulators with $w_2 = 0$ and topologically nontrival insulators with $w_2 = 1$, dubbed the 2D Stiefel Whitney insulator (Stiefel-Whitney insulator) [7, 14]. Contrary to the 2D quantum Hall insulator that has stable band topology and 1D chiral edge states, the 2D Stiefel-Whitney insulator is an obstructed atomic insulator, which can support zero-dimensional corner charges in the presence of additional chiral symmetry [7, 14–22]. The 2D Stiefel-Whitney insulator can also be used as a basic building block for novel 3D topological insulators such as 3D weak and strong Stiefel-Whitney insulators as shown in Ref. [7, 23]. Table II summarizes the correspondence between the first Chern class and the second Stiefel Whitney class.

The rest of the paper is organized as follows. The mathematical definition of the first and second Stiefel Whitney classes are given in Chapter 2. Chapter 3 describes the topological phases characterizied by the first Stiefel-Whitney number. Basically, w_1 characterizes 1D insulators with quantized charge polarization, and 2D or 3D semimetals with point or line nodes. Chapter 4 describes the relation between the second Stiefel Whitney class and the Z_2 monopole

First Chern class (c_1)	Second Stiefel-Whitney class (w_2)
2D complex wave function	2D real wave function
Chiral charge of Weyl points	Z_2 monopole charge of nodal lines
Quantum Hall insulator	Stiefel-Whitney insulator

Table 1.2 Correspondence between the first Chern class and the second Stiefel Whitney class.

charges of nodal line semimetals. Using the mathematical properties of the Stiefel Whitney classes, we show the intrinsic linking structure of semimetals with Z_2 monopole charge. Also, we explain how w_2 can be calculated from Wilson loop spectra. Topological insulators characterized by w_2 are described in Chapter 5. There we introduce the definition of 2D Stiefel-Whitney insulator, 3D weak Stiefel-Whitney insulator, and 3D strong Stiefel-Whitney insulator, and elaborate their topological properties. In Chapter 6, we explain the reformulated Nielsen-Ninomiya theorem in two dimensions as an interesting application of our theory. After that, in Chapter 7, we consider the case where spatial inversion (or twofold rotation) symmetry and time reversal symmetry are present simultaneously, while we assume only the combined spacetime inversion symmetry in the previous chapters. It allows us to calculate the second Stiefel-Whitney number using inversion parity eigenvalues very efficiently. This sets the basis for the study on odd-parity superconductivity in spin-polarized systems with spacetime inversion symmetry in Chapter 8. We conclude our review in Chapter 9 with the discussion of candidate materials and possible issues for future studies.

The text in this thesis significantly overlaps with my papers [6, 7, 14, 23–25]. The abstract, introduction, and Chapters 2, 3, 4, 5, and 9 overlap with

my review paper [24], which summarizes my research papers [6, 7, 14, 23], and Chapters 6, 7, 8, and Appendix B overlap with [14], the Supplemental Material of [7], [25], and [23], respectively.

Chapter 2

Stiefel-Whitney classes

Here we provide the mathematical definition of Stiefel-Whitney classes, which basically indicate the topological obstruction to defining real wave functions smoothly over a closed manifold.

2.1 The first Stiefel-Whitney class

The first Stiefel-Whitney class measures the orientability of real occupied wave functions over a closed 1D manifold. Namely, the real occupied wave functions are orientable (non-orientable) when $w_1 = 0$ ($w_1 = 1$).

In general, the orientation of a real vector space refers to the choice of an ordered basis. Any two ordered bases are related to each other by a unique nonsingular linear transformation. When the determinant of the transformation matrix is positive (negative), we say that the bases have the same (different) orientation. After choosing an ordered reference basis $\{v_1, v_2, ...\}$, the orientation of another basis $\{u_1, u_2, ...\}$ is specified to be positive (negative) when the

basis has the same (different) orientation with respect to the reference basis.

Real wave functions defined on the Brillouin zone can be considered as real unit basis vectors defined at each momentum, that is, they form a structure of a real vector bundle over the Brillouin zone. The basis can be smoothly defined locally on the manifold, but may not be smooth over a closed submanifold $\mathcal{M}$ of our interest. We say that the real wave functions are orientable over $\mathcal{M}$ when local bases can be glued with transition functions having only positive determinant, i.e., all transition functions are orientation-preserving. The orientable wave functions are classified into two classes with the positive and negative orientation as in the case of the real vector spaces.

Interestingly, the orientablity of real wave functions can be determined by the Berry phase computed in a smooth complex gauge, such that $w_1 = 1$ ($w_1 = 0$) indicates that the relevant wave functions carry π (0) Berry phase. Namely, the first Stiefel-Whitney number defined in a real basis is equivalent to the well-known quantized Berry phase defined in a smooth complex basis. This correspondence can be seen by investigating how the π Berry phase computed with the smooth complex state $|u_{n\mathbf{k}}\rangle$ affects the real state $|\tilde{u}_{n\mathbf{k}}\rangle$ connected by a gauge transformation as

$$|\tilde{u}_{n\mathbf{k}}\rangle = g_{mn}(\mathbf{k})\,|u_{m\mathbf{k}}\rangle\,, \tag{2.1}$$

where g is the gauge transformation matrix. In order to make the state $|u_{n\mathbf{k}}\rangle$ real, the π Berry phase should be eliminated by a local phase rotation because the diagonal components of the Berry connection are zero when the state is real. Then we have

$$0 = \int_0^{2\pi} dk\ \mathrm{Tr}\tilde{A} = \int_0^{2\pi} dk(\mathrm{Tr}A + i\nabla_k \log\det g), \tag{2.2}$$

where $\tilde{\mathbf{A}}_{mn} = \langle\tilde{u}_{m\mathbf{k}}|i\nabla_{\mathbf{k}}|\tilde{u}_{n\mathbf{k}}\rangle$ and $\mathbf{A}_{mn} = \langle u_{m\mathbf{k}}|i\nabla_{\mathbf{k}}|u_{n\mathbf{k}}\rangle$. Integrating the

$\log\det g$ term gives

$$\frac{\det g(2\pi)}{\det g(0)} = \exp\left[i\int_0^{2\pi} dk\ \mathrm{Tr}A\right]. \tag{2.3}$$

Moreover, at the Brillouin zone boundary, since the smooth complex state fulfills $|u_{n(2\pi)}\rangle = |u_{n(0)}\rangle$, the real state satisfies

$$|\tilde{u}_{n(2\pi)}\rangle = [g^{-1}(0)g(2\pi)]_{mn}\,|\tilde{u}_{m(0)}\rangle\,, \tag{2.4}$$

which, together with Eq. (2.3), shows that the total Berry phase basically determines the determinant of the transition function for $|\tilde{u}_{nk}\rangle$ at the Brillouin zone boundary. Namely, when the total Berry phase is π, the real state $|\tilde{u}_{nk}\rangle$ requires an orientation-reversal between $k = 2\pi$ and $k = 0$. Therefore we conclude that the first Stiefel-Whitney number w_1 for a closed curve C in the Brillouin zone is given by

$$w_1|_C = \frac{1}{\pi}\oint_C d\mathbf{k}\cdot\mathrm{Tr}\mathbf{A}(\mathbf{k}) \pmod 2, \tag{2.5}$$

where $\mathbf{A}(\mathbf{k})$ is the Berry connection calculated in a smooth complex gauge.

In fact, the first Stiefel-Whitney number w_1 determines the orientability of real states even in higher dimensions [10]. From the analysis in 1D, we find

$$\frac{\det g(\mathbf{q})}{\det g(\mathbf{p})} = \exp\left[i\int_{\mathbf{p}}^{\mathbf{q}} d\mathbf{k}\cdot\mathrm{Tr}\mathbf{A}(\mathbf{k})\right]. \tag{2.6}$$

Let us note that $\det g$ is globally smooth when the Berry phase is zero over every closed cycle. Otherwise, $\det g$ becomes discontinuous at some points so that the real states are non-orientable as in the 1D case. Thus, real states are orientable over an arbitrary dimensional closed manifold $\mathcal{M}$ if and only if the total Berry phase, which is calculated in a smooth complex gauge, is trivial for any 1D closed loop in $\mathcal{M}$.

2.2 The second Stiefel-Whitney class

The second Stiefel-Whitney class describes whether a spin (or pin) structure is allowed or not for given real wave functions defined on a 2D closed manifold $\mathcal{M}$. If $w_2 = 0$ ($w_2 = 1$), a spin or pin structure is allowed (forbidden). Below we give a more formal definition of the second Stiefel-Whitney number w_2.

Let us consider real occupied states $|u_{m\mathbf{k}}\rangle$ on $\mathcal{M}$. Then we introduce a covering of $\mathcal{M}$ whose geometric structure is topologically equivalent to $\mathcal{M}$. For given two open covers (or patches) A and B, one can find smooth real wave functions $|u^A_{m\mathbf{k}}\rangle$ and $|u^B_{m\mathbf{k}}\rangle$ defined in each open cover, respectively. In the overlapping region $A \cap B$, a transition function $t^{AB}_{mn}(\mathbf{k})$ is defined as

$$|u^B_{n\mathbf{k}}\rangle = t^{AB}_{mn}(\mathbf{k})\, |u^A_{m\mathbf{k}}\rangle\,. \tag{2.7}$$

For convenience, here we assume that the occupied wave functions are orientable over $\mathcal{M}$ so that $t^{AB}_{mn}(\mathbf{k}) \in \mathrm{SO}(N_{\mathrm{occ}})$. Then, since the double covering of $\mathrm{SO}(N_{\mathrm{occ}})$ is $\mathrm{Spin}(N_{\mathrm{occ}})$, the problem reduces to whether the lifting of the transition function from $t \in \mathrm{SO}(N_{\mathrm{occ}})$ to $\tilde{t} \in \mathrm{Spin}(N_{\mathrm{occ}})$ is allowed or not. If such a lifting is allowed consistently over $\mathcal{M}$, one can say that the spin structure exists, and thus $w_2 = 0$. In contrast, if such a lifting is not allowed, the spin structure does not exist, and $w_2 = 1$. The extension to the case of non-orientable manifolds is also straightforward as shown in Ref. [7].

In general, the transition functions should satisfy the following consistency conditions [9],

$$t^{AB}_{\mathbf{k}} t^{BA}_{\mathbf{k}} = 1, \tag{2.8}$$

for $\mathbf{k} \in A \cap B$ and

$$t^{AB}_{\mathbf{k}} t^{BC}_{\mathbf{k}} t^{CA}_{\mathbf{k}} = 1, \tag{2.9}$$

for $\mathbf{k} \in A \cap B \cap C$, where A, B, and C are arbitrary patches. The transition functions defined in Eq. (2.7) satisfy these consistency conditions automatically.

However, when we consider the lifting of transition functions to the double covering group at all overlapping regions in $\mathcal{M}$, the consistency conditions are not automatically satisfied everywhere. Let us write I and $-I$ to denote the 0 and 2π rotation in the double covering group. In general, after the lift $t^{AB} \to \tilde{t}^{AB}$, the lifted transition functions satisfy

$$\tilde{t}^{AB}_{\mathbf{k}} \tilde{t}^{BA}_{\mathbf{k}} = \pm I \tag{2.10}$$

for $\mathbf{k} \in A \cap B$ and

$$f^{ABC}_{\mathbf{k}} \equiv \tilde{t}^{AB}_{\mathbf{k}} \tilde{t}^{BC}_{\mathbf{k}} \tilde{t}^{CA}_{\mathbf{k}} = \pm I, \tag{2.11}$$

for $\mathbf{k} \in A \cap B \cap C$. The sign can be either $+$ or $-$ because both I and $-I$ are projected to 1 via a two-to-one mapping from $\mathrm{Spin}(N_{\mathrm{occ}})$ to $\mathrm{SO}(N_{\mathrm{occ}})$. $f^{ABC}_{\mathbf{k}}$ is gauge-invariant as one can see from the transformation of the lifted transition functions $\tilde{t}^{AB}_{\mathbf{k}} \to (\tilde{g}^{A}_{\mathbf{k}})^{-1} \tilde{t}^{AB}_{\mathbf{k}} \tilde{g}^{B}_{\mathbf{k}}$ under $|u^{A}_{n\mathbf{k}}\rangle \to g^{A}_{mn\mathbf{k}} |u^{A}_{m\mathbf{k}}\rangle$, where $\tilde{g}$ is a lift of g. Also, $f^{ABC}_{\mathbf{k}}$ has a unique value at each triple overlap, because it is fully symmetric with respect to the permutation of A, B, C, and is independent of $\mathbf{k}$ within a triple overlap.

Let us now examine the case where a lift that satisfies the consistency conditions can be found. In general, there is no obstruction for the first consistency condition in Eq. (2.8) whereas the second consistency condition in Eq. (2.9) depends on w_2. In fact, w_2 is defined as

$$(-I)^{w_2} = \prod_{A \cap B \cap C} f^{ABC}, \tag{2.12}$$

where the product is over all triple overlaps in $\mathcal{M}$. One can see that transition functions cannot be lifted to their double covering group when $w_2 = 1$ modulo two, because, in this case, there is at least one triple overlap $A \cap B \cap C$

where $f^{ABC} = -I$ violating the consistency condition. This indicates that the obstruction to the existence of a spin structure is dictated by the Z_2 invariant w_2.

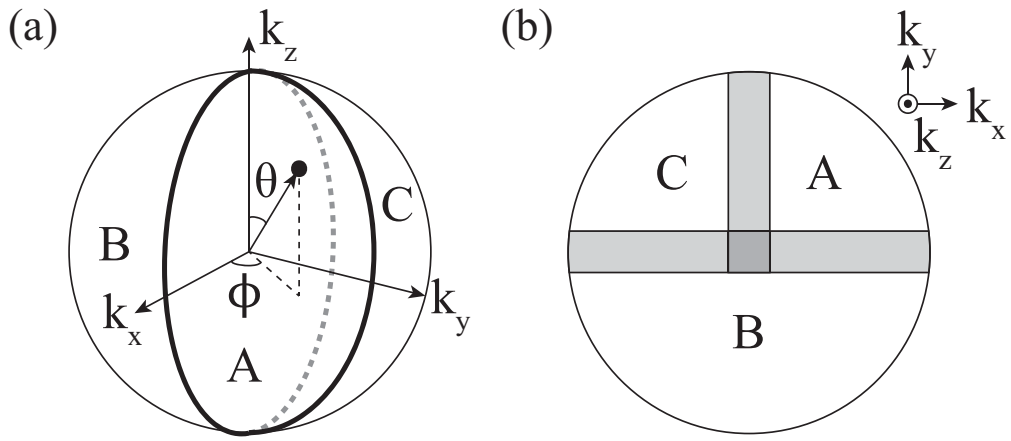

Figure 2.1 Three patches covering a sphere. (a) Orthographic view. ϕ and θ are the azimuthal and polar angles. B and A (C) overlap at $\phi = 0$ ($\phi = \pi$), and A and C overlap at $\phi = \pi/2$. The north pole at $\theta = 0$ and the south pole at $\theta = \pi$ are triple overlaps. (b) Top view. Overlapping regions are exaggerated for clarity. From the supplemental materials in Ref. [7].

For instance, let us illustrate how w_2 is defined on a spherical manifold, which is directly relevant to the Z_2 monopole charge of a nodal line. First we consider three patches A, B, and C covering a sphere shown in Fig. 2.1. In the spherical coordinates (ϕ, θ), there are three overlaps $A \cap B$, $A \cap C$, and $B \cap C$ at $\phi = 0$, $\phi = \pi/2$, and $\phi = \pi$, respectively. We restrict all transition functions on the overlaps to $\mathrm{SO}(N_{\mathrm{occ}})$, which is possible because every loop on a sphere is contractible to a point such that the first Stiefel-Whitney number is trivial. Then

$$(-I)^{w_2} = f^{ABC}(0) f^{ABC}(\pi), \tag{2.13}$$

where 0 and π denotes the polar angle θ.

Now let us define

$$\tilde{W}(\theta) = \tilde{t}^{AB}(\theta)\tilde{t}^{BC}(\theta)\tilde{t}^{CA}(\theta), \tag{2.14}$$

where we omit ϕ in the argument of transition functions because they are uniquely specified by the overlapping region. $\tilde{W}(\theta)$ is smooth for $0 < \theta < \pi$ because $\tilde{t}$ is smooth within an overlap. $\tilde{W}(0) = f^{ABC}(0) = \pm I$, and $\tilde{W}(\pi) = f^{ABC}(\pi) = \pm I$. Then we see that $w_2 = 1$ modulo two when the image of the map $\tilde{W} : [0, \pi] \to \mathrm{Spin}(N_{\mathrm{occ}})$ is an arc connecting I and $-I$, whereas $w_2 = 0$ when the image is a closed loop containing I or $-I$. Next, we project $\tilde{W}$ to W by using the two-to-one map $\mathrm{Spin}(N_{\mathrm{occ}}) \to \mathrm{SO}(N_{\mathrm{occ}})$. We have

$$W(\theta) = t^{AB}(\theta)t^{BC}(\theta)t^{CA}(\theta), \tag{2.15}$$

which is smooth for $0 < \theta < \pi$, and $W(0) = W(\pi) = 1$. Under this projection, an arc connecting I and $-I$ projects to a loop winding the non-contractible cycle an odd number of times, whereas a closed loop projects to a contractible loop or a non-contractible loop winding the non-contractible cycles an even number of times [26]. As a result, the second Stiefel-Whitney number is given by the winding number of $W(\theta)$ modulo two. This relation between w_2 and the parity of the winding number of $W(\theta)$ provides the correspondence between the second Stiefel-Whitney number and the Z_2 monopole charge of a nodal line enclosed by the sphere, which is further discussed in Sec.IV.

Chapter 3

First Stiefel-Whitney class and topological phases

Here we describe the topological phases in I_{ST}-symmetric systems characterized by the first Stiefel-Whitney number w_1. In 1D, w_1 computed over the full Brillouin zone is the bulk topological invariant of insulators with quantized charge polarization. In 2D (3D), w_1 is defined on a closed loop enclosing a point (line) nodes, and plays the role of a topological charge carried by the node. In all these cases, the low-energy properties of the system can be generally described by the 2×2 effective Hamiltonian in Eq. (1.3) and the corresponding band crossing occurs when

$$f_1(\mathbf{k}, m) = f_3(\mathbf{k}, m) = 0. \tag{3.1}$$

3.1 1D topological insulator: SSH model in a real basis

In 1D, since there is only one momentum variable k for a given tuning parameter m, the gap-closing condition in Eq. (3.1) cannot be satisfied in general, and

Topological phase	w_1	w_2
Insulator	1D TI with $P_1 = 1/2$	2D SWI
Semimetal	2D DSM or 3D NLSM	3D monopole NLSM

Table 3.1 Comparison of the topological phases characterized by the first Stiefel-Whitney number w_1 and the second Stiefel-Whitney number w_2. Here TI (SWI) indicates a topological insulator (Stiefel Whitney insulator). DSM (NLSM) denotes Dirac semimetal (nodal line semimetal). A monopole nodal line indicates a nodal line with Z_2 monopole charge.

thus an insulating phase becomes stable. However, when k and m are varied simultaneously, one can find a unique solution of Eq. (3.1) that corresponds to the critical point between two gapped insulators.

To describe the relation between the topological property of an insulator and w_1, let us consider 1D insulators described by the Su-Schuriffer-Heeger (SSH) model [27]. Although the properties of the corresponding topological insulator are already well-known, here we describe the SSH model by using a real basis and illustrate the relevant topological property in the context of the first Stiefel-Whitney number. The SSH Hamiltonian is given by

$$H_{\rm SSH} = \sin k\sigma_x + (t + \cos k)\sigma_z, \tag{3.2}$$

where the Pauli matrices $\sigma_{x,y,z}$ indicate the two sublattice sites within a unit cell. This Hamiltonian is symmetric under $PT = K$ so that the bulk charge polarization P_1 is quantized into either $P_1 = 0$ or $P_1 = 1/2$ modulo 1. It is well-known that this system describes a topologically trivial insulator with $P_1 = 0$ when $|t| > 1$ and a topologically nontrivial insulator (TI) with $P_1 = 1/2$ when $|t| < 1$. Let us see how the topology manifests in the wave function for the

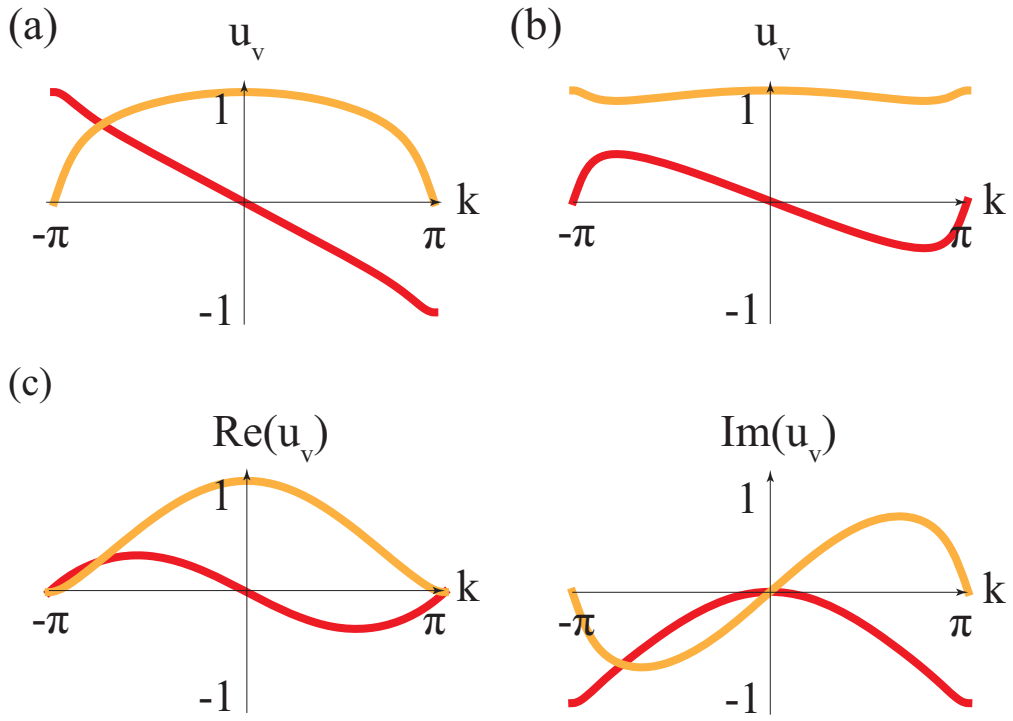

Figure 3.1 The amplitudes of the occupied state of the SSH model. Red and orange lines show the first and second components of the occupied state in Eq. (3.3). (a,b) Under reality condition. The occupied state is anti-periodic for (a) $t = 0.7$ whereas it is periodic for (b) $t = 1.3$. (c) In a smooth complex gauge with $\phi_v(k) = k/2$. The occupied state is smooth both for $|t| < 1$. From the supplemental materials in Ref. [7].

occupied state, which is given by

$$|u_v\rangle = e^{i\phi_v(k)} \frac{\mathrm{sign}(k)}{N(k)} \begin{pmatrix} t + \cos k - \sqrt{(t+\cos k)^2 + \sin^2 k} \\ \sin k \end{pmatrix}, \tag{3.3}$$

where $\phi_v(k)$ is an arbitrary overall phase factor and $N(k)$ is a positive normalization factor.

First, let us impose the reality condition on $|u_v\rangle$ over the whole 1D Brillouin

zone by choosing the gauge $e^{i\phi_v(k)} = 1$. Fig. 3.1(a) and (b) show the amplitudes of the two components of $|u_v\rangle$ along the Brillouin zone when $|t| < 1$ an $|t| > 1$, respectively. When $|t| > 1$, the real wave function is smooth and continuous over the entire 1D Brillouin zone, and thus $w_1 = 0$. In contrast, the real wave function is discontinuous at the Brillouin zone boundary at $k = \pm\pi$ when $|t| < 1$, although it is smooth over $-\pi < k < \pi$. Then at the boundaries $k = \pm\pi$, the wave function should be glued with an orientation-reversing transition function. This demonstrates that the occupied state is non-orientable, and thus $w_1 = 1$.

On the other hand, if the reality condition is relaxed by choosing $\phi_v(k) = k/2$, the occupied state becomes globally smooth in both $|t| < 1$ and $|t| > 1$ cases. [See Fig. 3.1(c), (d).] However, the discontinuity of the real wave function for $|t| < 1$ manifests as a π Berry phase of the corresponding smooth complex wave function. In this smooth complex gauge, one can easily show that $A = \langle u_v | i\nabla_k | u_v \rangle = 1/2$ and $P_1 = \int_{-\pi}^{\pi} dk A/(2\pi) = 1/2$ when $|t| < 1$. Similarly, we find $P_1 = 0$ when $|t| > 1$. This example clearly demonstrates that $w_1 = 1$ ($w_1 = 0$) in a real gauge is equivalent to the π Berry phase (0 Berry phase) in a smooth complex gauge.

3.2 2D Dirac semimetal

In 2D, the gap-closing condition in Eq. (3.1) can be satisfied by tuning two momenta k_x and k_y for given m, which indicates that a semimetal with point nodes is stable in general. When m is also treated as a tuning parameter, the number of variables (k_x, k_y, m) becomes larger than the number of equations in Eq. (3.1), which predicts a line of gapless solutions in the 3D parameter space (k_x, k_y, m). Physically, this indicates an insulator-semimetal transition acrosss the band crossing generating a stable 2D Dirac semimetal phase.

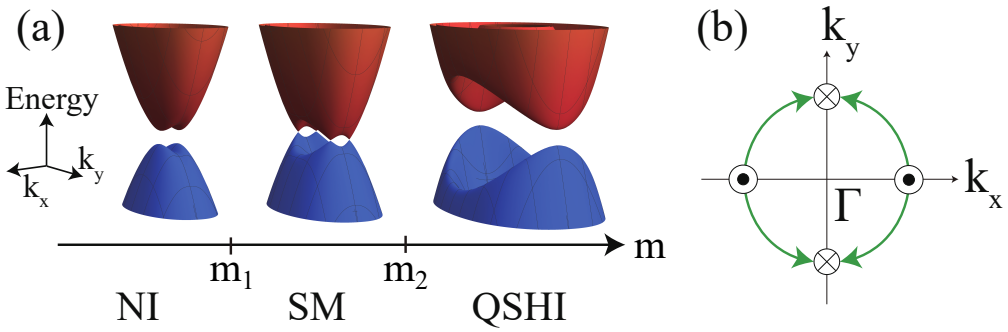

Figure 3.2 (Color online) (a) Evolution of the band structure of a 2D noncentrosymmetric system with I_{ST} symmetry as a tuning parameter m increases. (b) Trajectories of 2D Weyl points in the intermediate semimetal phase as m increases. $\odot$ and $\otimes$ are the locations where pair creation and pair annihilation happen. From the supplemental materials in Ref. [6].

The stability of the Dirac points in the resulting Dirac semimetal phase can be understood in the following way. Since the Berry curvature $F_{xy}(\mathbf{k})$ transforms to $-F_{xy}(\mathbf{k})$ under I_{ST}, $F_{xy}(\mathbf{k})$ vanishes locally unless there is a singular gapless point, which leads to the quantization of π Berry phase around a 2D Dirac point, which, at the same time, guarantees its stability [?, ?, ?, 5]. In terms of real wave functions, discontinuous real wave functions along a loop encircling an odd number of Dirac points cannot be adiabatically connected to smooth real wave functions along a loop encircling an even number of Dirac points, which again indicates the stability of Dirac points.

After the discovery of graphene, it has been well-known that a stable 2D Dirac point can exist in PT-symmetric 2D spinless fermion systems. However, in this system, it is also known that the Dirac point becomes unstable once spin-orbit coupling is turned on. Therefore finding a Dirac point stable in the presence of spin-orbit coupling was an interesting open question. One interesting

idea proposed in Ref. [28, 29] is to use the nonsymmophic crystalline symmetry which protects four-fold degenerate Dirac points at the corners of the Brillouin zone in 2D centrosymmetric systems.

On the other hand, in the case of 2D noncentrosymmetric systems, $C_{2z}T$ symmetry can protect Dirac points with two-fold degeneracy whose location can be anywhere in the Brillouin zone [5]. One can call a gap-closing point with two-fold degeneracy as a 2D Weyl point, which is distinguished from four-fold degenerate Dirac points in centrosymmetric systems. As long as the inversion is broken, and thus the spin splitting occurs at a generic momentum, the above description in Eq. (1.3) based on 2×2 matrix is still valid in $C_{2z}T$ symmetric noncentrosymmetric systems with spin-orbit coupling. In fact, near the critical point $m = m_{c1}$ for the insulator-semimetal transition, the Hamiltonian can generally be written as

$$H(\mathbf{q}) = (Aq_x^2 + m_{c1} - m)\sigma_x + vq_y\sigma_z, \tag{3.4}$$

which describes a gapped insulator (a 2D semimetal) when $m < m_{c1}$ ($m > m_{c1}$) assuming $A > 0$. Due to T symmetry, accidental band crossing happens at two momenta $\pm\mathbf{k}$. Since two Weyl points are created at each band crossing point, the semimetal phase has four Weyl points in total. Moreover, when m becomes larger than m_{c1}, four Weyl points migrate in momentum space, and eventually, they are annihilated pairwise at another critical point $m = m_{c2}$. Interestingly, when pair creation/pair annihilation is accompanied by a partner-switching between the Weyl point pairs, the two gapped phases mediated by the Weyl semimetal should have distinct topological property [6]. Namely, if one gapped phase is a normal insulator, the other one should be a 2D quantum spin Hall insulator as shown in Fig. 3.2. This theory predicts that the topological phase transition in HgTe/CdTe heterostructrue [30, 31] should be mediated by

a 2D Weyl semimetal phase inbetween. Indeed, the pair creation of 2D Weyl points across an insulator-semimetal transition was experimentally observed in few-layer black phosphorus under vertical electric field [32]. The condition for accidental band crossing in 2D noncentrosymmetric systems was systematically classified by considering 2D layer group in Ref. [33].

3.3 3D nodal line semimetals

In 3D, the gap-closing condition in Eq. (3.1) can be satisfied by tuning three momenta k_x, k_y, k_z for given m, which indicates that a semimetal with line nodes is stable in general. When m is also treated as a tuning parameter, since the number of variables (k_x, k_y, k_z, m) is four while the number of equations in Eq. (3.1) is two, a 2D sheet of gapless solutions exists in the 4D parameter space of (k_x, k_y, k_z, m). This indicates an insulator-semimetal transition acrosss the band crossing generating a stable 3D nodal line (NL) semimetal. As in the case of 2D Dirac semimetals discussed above, the stability of nodal lines in this class of nodal line semimetals (NLSMs) is guaranteed by w_1 or π Berry phase defined on a closed loop encircling a line node. NLSMs in $I_{\rm ST}$-symmetric systems were proposed in various materials [34–39]. Recent developments in the study of NLSMs are extensively reviewed in Ref. [40] where NLSM whose band degeneracy is protected by other symmetries such as mirror or nonsymmorphic symmetries are also systematically reviewed.

Chapter 4

Second Stiefel-Whitney class and 3D nodal line semimetals with monopole charge

Here we describe the properties of topological NLSM in 3D whose nontrivial topology is characterized by the second Stiefel-Whitney class. We first show that the Z_2 monopole charge of a NL defined on the wrapping sphere is equivalent to the second Stiefel-Whitney number w_2. Based on this equivalence, we apply the mathematical property of the second Stiefel-Whitney class to the problem of 3D nodal line semimetals, and predict the fundamental topological properties of the nodal line semimetals with Z_2 monopole charges.

4.1 Second Stiefel-Whitney number and Z_2 monopole charge of nodal lines

In 3D PT-symmetric spinless fermion systems, an accidental band crossing described by the 2×2 effective Hamiltonian in Eq. (1.3) generates a nodal line

that is locally stable due to π Berry phase as discussed before. However, even in the presence of π Berry phase, it is still allowed to deform a single nodal loop into a point node, which eventually disappears leading to a gapped insulator as shown in Fig. 4.1(a). Since an annihilation of a single nodal line is allowed, such a nodal line obviously carries a zero monopole charge.

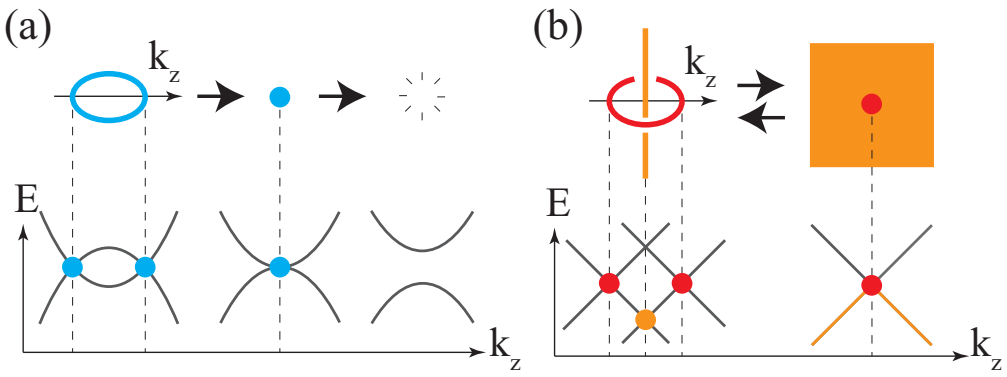

Figure 4.1 Stabilty of nodal lines in 3D PT-symmetric spinless fermion systems. (a) A Z_2 trivial nodal line can be gapped via band re-inversion. (b) A nodal line carrying Z_2 monopole charge cannot be gapped alone. From Ref. [24].

However, recently it has been proposed that there is another type of nodal lines carrying Z_2 monopole charge (monopole nodal line) [40]. A single monopole nodal line cannot be gapped and thus stable. To annihilate a monopole nodal line, one needs to introduce another monopole nodal line, and then the nodal line pair can be pair annihilated. To describe a monopole nodal line, one needs to go beyond the two-band description given in Eq. (1.3) and consider at least a four-band Hamiltonian. For instance, let us consider the following real four-band Hamiltonian

$$H(\mathbf{k}) = k_x\Gamma_1 + k_y\Gamma_2 + k_z\Gamma_3 + m\Gamma_{15}, \tag{4.1}$$

where $\Gamma_{(1,2,3)} = (\sigma_x, \tau_y\sigma_y, \sigma_z)$, $\Gamma_{15} = \tau_z\sigma_z$, and $\tau_{x,y,z}$ and $\sigma_{x,y,z}$ are the Pauli ma-

trices. The energy eigenvalues are $E = \pm\sqrt{k_x^2 + (\rho \pm |m|)^2}$ where $\rho = \sqrt{k_y^2 + k_z^2}$. One can see that the conduction and the valence bands touch along the closed loop satisfying $k_x = 0$ and $\rho = |m|$. This nodal line carries a nonzero monopole charge, which can be confirmed by directly computing the monopole charge. Let us note that once the reality condition is imposed, only three Gamma matrices, $\Gamma_{1,2,3}$ shown above, six matrices Γ_{ab} $(a = 1, 2, 3; b = 4, 5)$, and I can appear in $H(\mathbf{k})$. The presence of three real Gamma matrices, which mutually anticommutes, indicates that a 3D massless Dirac fermion can exist in this system [**?**, 41]. The Dirac point is stable against the gap opening because the mass terms associated with $\Gamma_{4,5}$ are forbidden. However, the six real matrices Γ_{ab} can deform the Dirac point into a nodal line while keeping the system gapless.

Moreover, there is another intriguing nodal structure in the bands that the Hamiltonian in Eq. (4.1) describes. That is, the occupied bands also cross and form another nodal line at $\rho = 0$ (NL*), which is linked with the monopole nodal line [7]. Because of this linking, the monopole nodal line is stable and distinct from trivial NLs. As $m \to 0$, the linking requires that the monopole nodal line becomes a four-fold degenerate Dirac point as shown in Fig. 4.1 (b). If m becomes finite after its sign-reversal, the size of the monopole nodal line increases again. A single monopole nodal line cannot be gapped and only a pair of monopole nodal lines can be created or annihilated across the band inversion.

Now let us illustrate the mechanism for the pair creation of monopole nodal lines, which is a sequence of band inversions described in Fig. 4.2(a), dubbed *a double band inversion* (DBI) [7, 42]. For concreteness, we describe a DBI by using the Hamiltonian in Eq. (4.1) after the replacement $k_z \to |\mathbf{k}|^2 - M$. The evolution of the band structure during the DBI is illustrated in Fig. 4.2 (a) as a function of the parameter M. As M is increased from $M < -|m|$, the first band inversion occurs at $M = -|m|$ between the top valence and

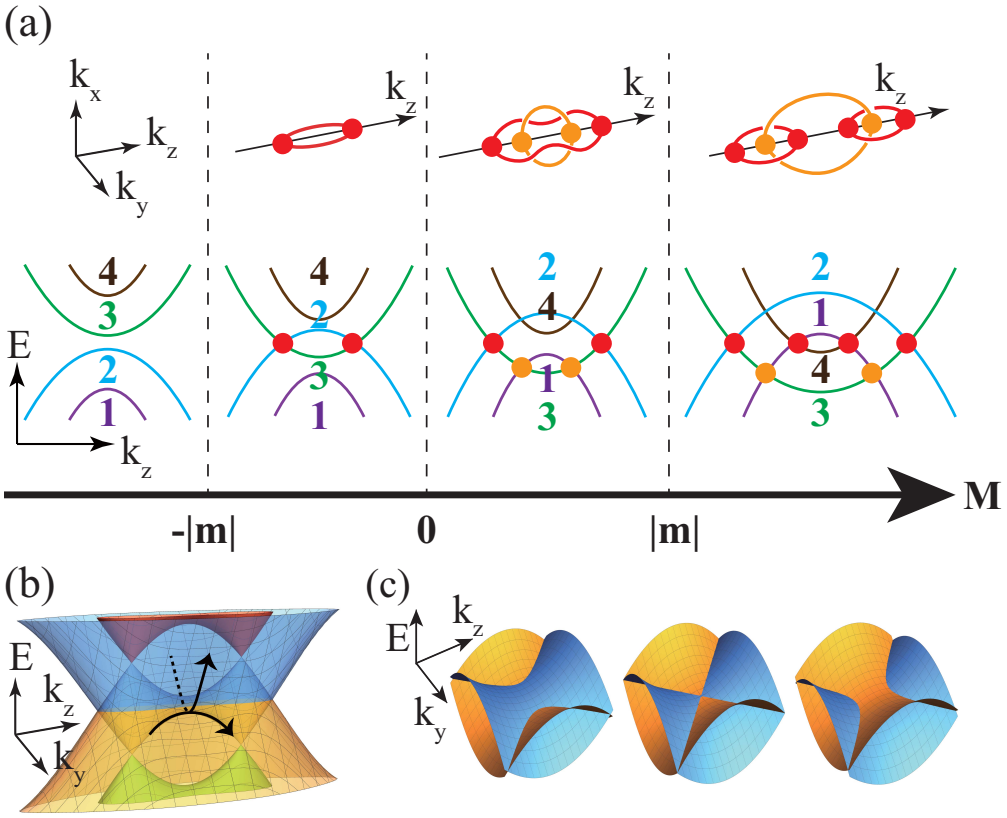

Figure 4.2 Pair creation of nodal lines carrying Z_2 monopole charge (monopole nodal lines) via a double band inversion (DBI). (a) Evolution of band structure during DBI. Red (Orange) points and lines indicate the crossing between the conduction and valence bands (two occupied bands). (b) Saddle-shaped band structure when $0 < M < |m|$. (c) Change in nodal line structure when two saddle-shaped bands cross. From the supplemental materials in Ref. [7].

bottom conduction bands, and it creates a trivial NL protected by π Berry phase. Then, the inversion at $M = 0$ between the two occupied (unoccupied) bands generates another NL below (above) the Fermi level, which we call NL*. After this band inversion, the band structure near $\mathbf{k} = 0$ develops saddle-shape

around the Fermi energy as shown in Fig. 4.2(b). Another consecutive band inversion at $M = |m|$ between the two saddle-shaped bands induces a Lifshitz transition as shown in Fig. 4.2(c), during which the trivial NL splits into two monopole nodal lines, which are linked by the NL* that are formed from the occupied bands. During DBI, each occupied (unoccupied) band crosses both of two unoccupied (occupied) bands, which is the reason why the minimal number of bands required to create a monopole nodal line is four.

Now let us discuss the equivalence between the second Stiefel-Whitney number w_2 and the Z_2 monopole charge of a nodal line. The equivalence follows from the fact that the nontrivial Z_2 monopole charge forbids the existence of the spin structure on a sphere enclosing the nodal line. Let us first briefly review the idea of the Z_2 monopole charge that is defined over a sphere enclosing a nodal line [40]. For this, we divide the wrapping sphere into two patches, each covering the northern (N) or the southern (S) hemispheres which overlap along the equator. $|u_n^N(\mathbf{k})\rangle$ and $|u_n^S(\mathbf{k})\rangle$ are real wave functions defined smoothly on the northern and the southern hemispheres, respectively. On the overlapping region, $|u_n^N(\mathbf{k})\rangle$ and $|u_n^S(\mathbf{k})\rangle$ are related by a transition function t^{NS} in a way that $|u_n^S(\mathbf{k})\rangle = t_{mn}^{NS}(\mathbf{k})\,|u_m^N(\mathbf{k})\rangle$ for $\mathbf{k} \in N \cap S$. The Z_2 monopole charge is defined by the winding number of the transition function [40]. We restrict the transition function to $\mathrm{SO}(N_{\mathrm{occ}})$, which is possible because every loop on a sphere is contractible to a point, that is, the corresponding first Stiefel-Whitney number is trivial. Then we see that the winding number of t^{NS} along a loop in $N \cap S$ gives a Z_2 number because $\pi_1(\mathrm{SO}(N_{\mathrm{occ}})) = Z_2$ for $N_{\mathrm{occ}} > 2$. This Z_2 number is nothing but the Z_2 monopole charge. When the number of occupied bands is two, the winding number is integer-valued because $\pi_1(\mathrm{SO}(2)) = Z$. In this case, the Z_2 monopole charge is given by the parity of the winding number.

Interestingly, this Z_2 monopole charge also characterizes the obstruction to

having a spin structure over the wrapping sphere. For simplicity, let us take a gauge where the transition function $t^{NS}(\mathbf{k})$ is an identity at some $\mathbf{k} = \mathbf{k}_0 \in N \cap S$. Then, the transition function undergoes a $4\pi\mathcal{N}$ rotation ($2\pi(2\mathcal{N}+1)$ rotation) for an integer $\mathcal{N}$ along a loop containing $\mathbf{k}_0$ in $N \cap S$ when the Z_2 monopole charge is trivial (nontrivial). This is because the homotopy group $\pi_1(\mathrm{SO}(N_{\mathrm{occ}}))$ is generated by the paths representing $2\pi\mathcal{N}$ rotation [26, 43] and the Z_2 monopole charge indicates the parity of the relevant winding number. While the 2π rotation and the identity are identical in $\mathrm{SO}(N_{\mathrm{occ}})$, they are not identical in $\mathrm{Spin}(N_{\mathrm{occ}})$. Therefore, the transition function is well-defined over the overlap $N \cap S$ only as a $\mathrm{SO}(N_{\mathrm{occ}})$ element when the Z_2 monopole charge is nontrivial. On the other hand, no obstruction arises when the Z_2 monopole charge is trivial because a 4π rotation is identical to the identity element even as a $\mathrm{Spin}(N_{\mathrm{occ}})$ element. Thus, the Z_2 monopole charge is identical to the second Stiefel-Whitney number over the enclosing sphere. This equivalence can be proved more rigorously by using the mathematical definition given in Eq. (2.12), (2.13) after suitable deformation of the patches and related transition functions as shown in Ref. [7]

4.2 Whitney sum formula and linking of nodal lines

Since the equivalence between the Z_2 monopole charge and the second Stiefel-Whitney number w_2 has been established, one can use the mathematical properties of Stiefel-Whitney numbers to understand the physical properties of monopole nodal lines. One important mathematical property of Stiefel-Whitney numbers is the so-called Whitney sum formula, which provides the rule for determining the total second Stiefel-Whitney number of blocks of bands from w_1 and w_2 of each block. Using the Whitney sum formula, one can show that w_2

of nondegenerate occupied bands can be expressed by the Berry connection as

$$w_2 = \sum_{n<m} \frac{1}{\pi^2} \oint_{T^2} d\mathbf{S} \cdot \mathbf{A}_n \times \mathbf{A}_m. \tag{4.2}$$

This is the central equation to be used to relate w_2 and the linking structure, which is a unique characteristic of monopole nodal lines.

To explain the Whitney sum formula, let us suppose that the set of the occupied bands $\mathcal{B}$ can be decomposed into a direct sum of n subsets.

$$\mathcal{B} = \bigoplus_i \mathcal{B}_i = B_1 \oplus \mathcal{B}_2 ... \oplus \mathcal{B}_n. \tag{4.3}$$

Here the direct sum indicates that one can find a basis in which the transition function can be block-diagonal over all the overlapping regions $A \cap B$ between two patches A and B. This is equivalent to the condition that each block is isolated from the other blocks by band gaps, because energetically isolated bands cannot be connected by transition functions. Explicitly, the Whitney sum formula is given by [10, 44]

$$w_2 \left(\oplus_i \mathcal{B}_i\right) = \sum_i w_2(\mathcal{B}_i) + \sum_{i<j} \frac{1}{\pi^2} \oint_{\mathcal{M}} d\mathbf{S} \cdot \mathbf{A}_i \times \mathbf{A}_j, \tag{4.4}$$

where $\mathcal{M}$ indicates a closed 2D manifold and $\mathbf{A}_i = \sum_{n \in \mathcal{B}_i} \langle u_{n\mathbf{k}} | i \nabla_{\mathbf{k}} | u_{n\mathbf{k}} \rangle$ is the Berry connection for the i-th block which is calculated in a smooth complex gauge. On a torus, the second term in Eq. (4.4) can be expressed as

$$\oint_{T^2} d\mathbf{S} \cdot \mathbf{A}_i \times \mathbf{A}_j = \Phi_{i,\phi} \Phi_{j,\theta} - \Phi_{i,\theta} \Phi_{j,\phi} \tag{4.5}$$

where $\Phi_{i,\psi} = \oint A_{i,\psi} d\psi$ is the Berry phase of the i-th block computed on the non-contractible cycle along the $\psi = \theta$ or ϕ direction. Because the Berry phase Φ in a smooth complex gauge is the first Stiefel-Whitney number w_1 in a real

gauge, the Berry phase $\Phi_{i,\psi}$ in Eq. (4.5) can be replaced by $\pi w_1(\mathcal{B}_i)$ leading to

$$w_2\left(\oplus_i \mathcal{B}_i\right) = \sum_i w_2(\mathcal{B}_i) + \sum_{i<j}\left[w_1^{\phi}(\mathcal{B}_i)w_1^{\theta}(\mathcal{B}_j) - w_1^{\theta}(\mathcal{B}_i)w_1^{\phi}(\mathcal{B}_j)\right], \tag{4.6}$$

which is valid on a torus $\mathcal{M} = T^2$.

One important physical implication of the Whitney sum formula given in Eq. (4.6) is that it reveals the linking structure of a monopole nodal line at the Fermi level with other nodal lines below the Fermi level. Since w_2 is equivalent to the Z_2 monopole charge of a nodal line, the relation between w_2 and the linking number of a nodal line also provides the equivalence of the Z_2 monopole charge of a nodal line to its linking number modulo two.

To show the relation between the w_2 and the linking number, let us consider a sphere enclosing a nodal line γ_1 at the Fermi level. w_2 defined on the sphere is identical to the Z_2 monopole charge of the nodal line γ_1. Now we smoothly deform the sphere into a torus while keeping the energy gap finite during the deformation. Then, w_2 computed on the sphere and the torus should be the same. If the torus T^2 wrapping γ_1 is thin enough, all the occupied bands can become non-degenerate everywhere on the torus. Then, because the w_2 of a non-degenerate band is zero, the Whitney sum formula becomes $w_2 = \sum_{n<m} \frac{1}{\pi^2} \oint_{T^2} d\mathbf{S} \cdot \mathbf{A}_n \times \mathbf{A}_m$, where $\mathbf{A}_n = \langle u_{n\mathbf{k}} | i\nabla_{\mathbf{k}} | u_{n\mathbf{k}} \rangle$ is the Berry connection for the nth topmost occupied band, and n and m run over the occupied bands.

By noting that the quantization condition of the Berry phase, $\oint_C A_n = \pi$ or 0, resembles the Ampere's law in electromagnetics, one can solve the equation and get a solution analogous to the Bio-Savart law. Explicitly, let us start from the differential form representing the quantization of the Berry phase, which is

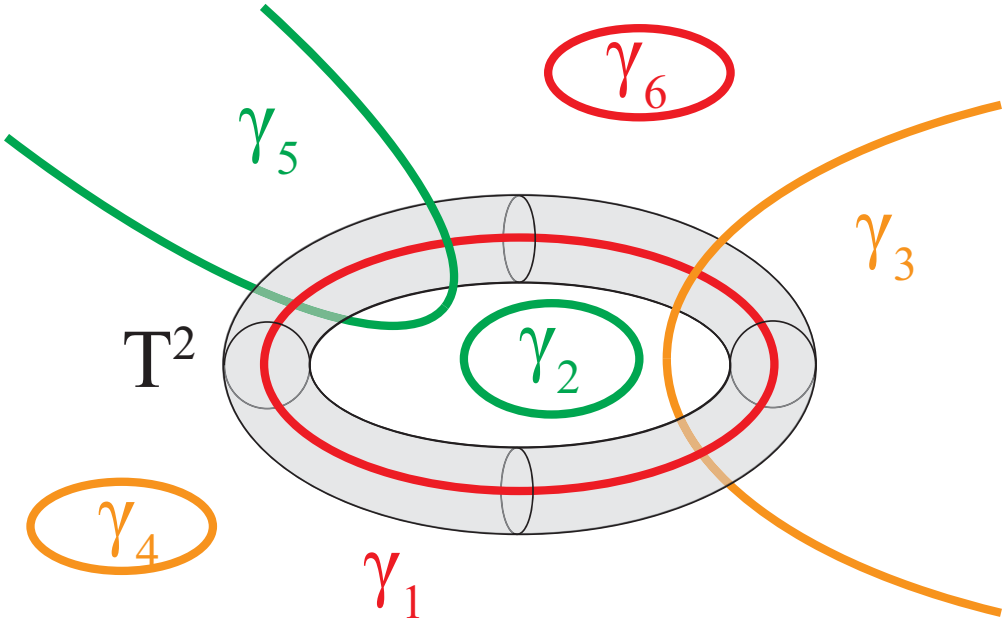

Figure 4.3 A torus T^2 wrapping the nodal line γ_1 in the Brillouin zone. T^2 is thin enough so that it does not intersect any other band degeneracies. Red lines (γ_1 and γ_6) are lines of touching between the conduction and valence band. Orange (γ_3 and γ_4) and green (γ_2 and γ_5) lines are lines of touching between the first and the second topmost occupied band and between the second and the third topmost occupied band, respectively. Only the linking between γ_1 and γ_3 is protected as it generates the nontrivial second Stiefel-Whitney number on T^2, whereas the linking between γ_1 and γ_5 is not protected [See Eq. (4.11)]. From the supplemental materials in Ref. [7].

similar to the differential form of the Ampere's law,

$$\nabla_{\mathbf{k}} \times \mathbf{A}_n(\mathbf{k}) = \sum_i I_n^i \oint_{\gamma_i} d\mathbf{k}_i \delta^3(\mathbf{k} - \mathbf{k}_i), \tag{4.7}$$

which gives

$$\mathbf{A}_n(\mathbf{k}) = \frac{1}{4\pi}\sum_i \oint_{\gamma_i} \frac{I_n^i d\mathbf{k}_i \times (\mathbf{k}-\mathbf{k}_i)}{|\mathbf{k}-\mathbf{k}_i|^3}, \tag{4.8}$$

where γ_i's are lines of band touching points, and $I_n^i = \pi$ if the line γ_i generates the Berry phase on nth band whereas $I_n^i = 0$ otherwise.

By using this formula of the Berry connection, we have

$$\frac{1}{\pi^2}\oint_{T^2} d\mathbf{S}\cdot\mathbf{A}_n\times\mathbf{A}_m = \sum_{\gamma_j}\left(\delta_{1n}\frac{I_m^j}{\pi} - \delta_{1m}\frac{I_n^j}{\pi}\right)\mathrm{Lk}(\gamma_1,\gamma_j), \tag{4.9}$$

where n and m are band indices, so that $n=1$ or $m=1$ indicate the topmost occupied band. j labels nodal lines, and

$$\mathrm{Lk}(\gamma_i,\gamma_j) = \frac{1}{4\pi}\oint_{\gamma_i}\oint_{\gamma_j}\frac{d\mathbf{k}_i\times d\mathbf{k}_j\cdot(\mathbf{k}_i-\mathbf{k}_j)}{|\mathbf{k}_i-\mathbf{k}_j|^3}, \tag{4.10}$$

is the Gauss' linking integral of the closed lines γ_i and γ_j. This eventually leads to

$$w_2(T^2) = \sum_{\tilde{\gamma}_j}\mathrm{Lk}(\gamma_1,\tilde{\gamma}_j), \tag{4.11}$$

where $\tilde{\gamma}_j$'s are nodal lines formed between the first and second topmost occupied bands. The implication of Eq. (4.11) is clear. For convenience, let us suppose that there is one nodal line γ_1 at the Fermi level and another nodal line $\tilde{\gamma}$ below the Fermi level. If the monopole charge of γ_1 is one, γ_1 and $\tilde{\gamma}$ should be linked. On the other hand, if the monopole charge of γ_1 is zero, γ_1 and $\tilde{\gamma}$ are unlinked. This relation between the Z_2 monopole charge and linking number also explain why the minimal model Hamiltonian describing monopole nodal line should be at least a 4×4 matrix. Since a monopole nodal line should be linked with other nodal lines below the Fermi level, there should be at least two occupied bands below the Fermi level.

4.3 Computation of w_2 by using Wilson loop method

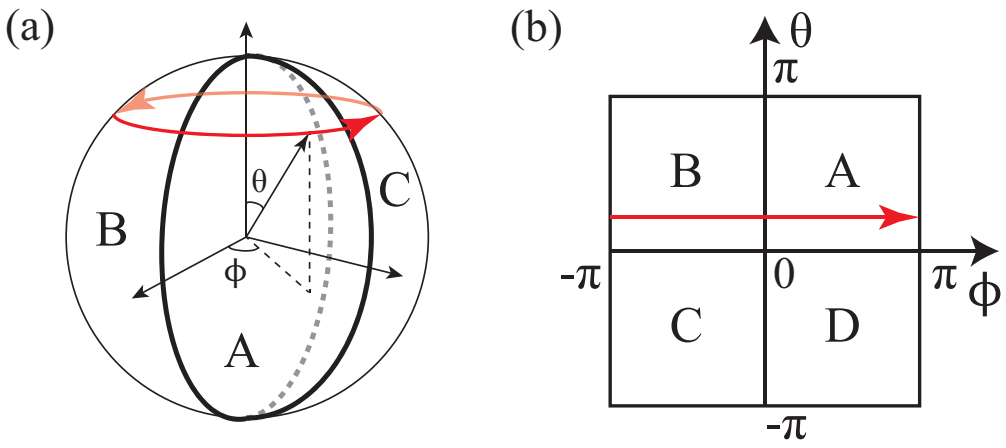

Figure 4.4 Patches covering a sphere and a torus. Wilson loop operators are calculated along the red arrows. (a) Sphere covered with three patches which overlap on $\phi = 0$, $\phi = \pi/2$, and $\phi = \pi$. (b) Torus covered with four patches. ϕ and θ are 2π-periodic. Transition functions are taken to be nontrivial only over $\theta = 0$ and $\phi = 0$ lines. From the supplemental materials in Ref. [7].

Let us explain how the second Stiefel-Whitney number w_2 can be computed by using the Wilson loop method. The Wilson loop operator is defined by [**?**, 45, 46]

$$W_{(\phi_0+2\pi,\theta)\leftarrow(\phi_0,\theta)} = \lim_{N\to\infty} F_{N-1}F_{N-2}...F_1F_0, \tag{4.12}$$

where (ϕ, θ) parametrizes a 2D subspace of the 3D Brillouin zone or the 2D Brillouin zone itself, and F_j is the overlap matrix at $\phi_j = \phi_0 + 2\pi j/N$ whose matrix elements are given by $[F_j]_{mn} = \langle u_{m\phi_{j+1}} | u_{n\phi_j} \rangle$, and $\phi_N = \phi_0$. As shown below, the homotopy class of the Wilson loop operator gives the second Stiefel-Whitney number in a special gauge known as the parallel-transport gauge [47].

In practice, the homotopy class can be simply obtained by looking at the spectrum of the Wilson loop operator. It is given by the parity of the number of spectral crossing at $\Theta = \pi$, where Θ indicates the phase eigenvalue of the Wilson loop operator.

First, let us consider a sphere in the Brillouin zone, which is covered by three patches A, B, and C whose overlaps $A \cap C$, $C \cap B$, and $B \cap A$ are at $\phi = \pi/2$, $\phi = \pi$, and $\phi = 2\pi$, respectively, for all $0 \leq \theta \leq \pi$ [See Fig. 4.4(a)]. Here ϕ and θ are the azimuthal and the polar angles of the sphere. Real occupied states $|u_{n\mathbf{k}}\rangle$ are smooth within each patch. The Wilson loop operator $W_0(\theta) \equiv W_{(2\pi,\theta)\leftarrow(0,\theta)}$ is then

$$\begin{aligned} W_0(\theta) =& \langle u^A(0,\theta)|u^B(2\pi,\theta)\rangle\, W_{(2\pi,\theta)\leftarrow(\pi,\theta)} \\ & \langle u^B(\pi,\theta)|u^C(\pi,\theta)\rangle\, W_{(\pi,\theta)\leftarrow(\pi/2,\theta)} \\ & \langle u^C(\pi/2,\theta)|u^A(\pi/2,\theta)\rangle\, W_{(\pi/2,\theta)\leftarrow(0,\theta)} \\ =& t^{AB}(\theta)\mathcal{P}e^{-i\int_{\pi}^{2\pi} d\phi' A^B_\phi(\theta,\phi')} \\ & t^{BC}(\theta)\mathcal{P}e^{-i\int_{\pi/2}^{\pi} d\phi' A^C_\phi(\theta,\phi')} \\ & t^{CA}(\theta)\mathcal{P}e^{-i\int_{0}^{\pi/2} d\phi' A^A_\phi(\theta,\phi')}, \end{aligned} \tag{4.13}$$

where we used that $W_{(\theta,\phi_2)\leftarrow(\theta,\phi_1)} = \mathcal{P}e^{-i\int_{\phi_1}^{\phi_2} d\phi' A_\phi(\theta,\phi')}$ when the states $|u_{n(\phi,\theta)}\rangle$ are smooth for $\phi_1 < \phi < \phi_2$, and $A_{nm,\phi} = \langle u_{m(\theta,\phi)}|i\partial_\phi|u_{n(\theta,\phi)}\rangle$ is the ϕ component of the Berry connection. Here $\mathcal{P}$ indicates that the integral is path-ordered. If we take the parallel-transport gauge, which is defined by

$$\begin{aligned} |u^A_{p,n(\phi,\theta)}\rangle &= \left[\mathcal{P}e^{-i\int_0^\phi d\phi' A^A_\phi(\theta,\phi')}\right]_{mn} |u^A_{m(\phi,\theta)}\rangle\,, \\ |u^B_{p,n(\phi,\theta)}\rangle &= \left[\mathcal{P}e^{-i\int_\pi^\phi d\phi' A^B_\phi(\theta,\phi')}\right]_{mn} |u^B_{m(\phi,\theta)}\rangle\,, \\ |u^C_{p,n(\phi,\theta)}\rangle &= \left[\mathcal{P}e^{-i\int_{\pi/2}^\phi d\phi' A^C_\phi(\theta,\phi')}\right]_{mn} |u^C_{m(\phi,\theta)}\rangle\,, \end{aligned} \tag{4.14}$$

the Wilson loop operator is then

$$W_0(\theta) = W_{p,0}(\theta) = t_p^{AB}(\theta) t_p^{BC}(\theta) t_p^{CA}(\theta), \tag{4.15}$$

where W_p and t_p are the Wilson loop operator and the transition function in the parallel-transport gauge. It is worth noting that the Wilson loop operator in parallel-transport gauge is given by the product of all the transition functions along the ϕ cycle for given θ, which has the same form of Eq. (2.15). Since $W_0(\theta = 0, \pi) = 1$ due to the consistency condition at triple overlaps, the image of the map $W_0(\theta)$ for $\theta \in [0, \pi]$ forms a closed loop. Then the second Stiefel-Whitney number w_2 is given by the parity of the winding number of $W_0(\theta)$ as explained in Sec.II.B, which can be obtained gauge invariantly from its eigenvalues $\Theta(\theta)$.

Fig. 4.5(a-d) shows four examples of Wilson loop spectra when $N_{\text{occ}} = 2$. As Fig. 4.5(a) and (b) both have zero winding number, Fig. 4.5(a) can be smoothly deformed to Fig. 4.5(b), and vice versa. It is possible as the crossing point on $\Theta = 0$ can be annihilated at the boundary $\theta = 0$ or $\theta = \pi$. However, Fig. 4.5(b) cannot be adiabatically deformed to Fig. 4.5(c) or (d) because they have different winding numbers.

Let us note that the parity of the winding number, which is equivalent to the second Stiefel-Whitney number, is given by the parity of the number of crossing points on $\Theta = \pi$. Thus, we can get w_2 by counting the number of the crossing points on the line. This is also true when the number of occupied bands is larger than two because the crossing points on $\Theta = \pi$ are stable even when additional trivial bands are added.

While a single linear crossing point is locally stable on the line $\Theta = n\pi$ for any integer n, two linear crossing points on the same line may be pair-annihilated. In fact, one important difference between $N_{\text{occ}} = 2$ and $N_{\text{occ}} > 2$

cases is that a pair annihilation, which is forbidden in the former case, is always possible in the latter case. In the case of two occupied bands, two linear crossing points on the line $\Theta = \pi$ at $\theta = \theta_1$ and $\theta = \theta_2$ cannot be pair-annihilated if there is a linear crossing point on the $\Theta = 0$ line at $\theta = \theta_0$ satisfying $\theta_1 < \theta_0 < \theta_2$ [See Fig. 4.5(d)]. This is because both of the eigenvalues are on $\Theta = 0$, and no eigenvalue exists on $\Theta = \pi$ at $\theta = \theta_0$. Accordingly, the crossing points at θ_1 and θ_2 on $\Theta = \pi$ cannot be pair-annihilated because they can never reach the polar angle θ_0 which is between θ_1 and θ_2. On the other hand, such protection mechanism does not exist when $N_{\rm occ} > 2$ and a pair annihilation is always possible on $\Theta = \pi$ as shown in Fig. 4.5(g,h). Hence, only the parity of the winding number is topologically meaningful when $N_{\rm occ} > 2$. This parity is the second Stiefel-Whitney number w_2 which can be determined by counting the number of the crossing points on $\Theta = \pi$.

For later use, let us briefly explain how the Wilson loop operator can be computed on a torus and it is related with the second Stiefel-Whitney number. Similar to the case on a sphere, the homotopy class of the Wilson loop operator $W_0(\theta)$ determines the second Stiefel-Whitney number w_2, gauge-invariantly from the spectrum of $W_0(\theta)$. Namely, w_2 can be determined by counting the number of the crossing points on $\Theta = \pi$. The Wilson loop operator on a torus can be related to the transition function as follows. Let us consider a torus covered with four patches shown in Fig. 4.4(b). We take a gauge where transition functions are trivial over $\theta = \pi$ line. Also, we impose on $\theta = 0$ that t^{AD} and t^{BC} are the identity (constant orientation-reversing matrices) when the occupied states are orientable (non-orientable) along θ. Then, we move to the

parallel-transport gauge which is defined by

$$|u^{A/D}_{p,n(\phi,\theta)}\rangle = \left[\mathcal{P}e^{-i\int_0^\phi d\phi' A^{A/D}_\phi(\theta,\phi')}\right]_{mn} |u^{A/D}_{m(\phi,\theta)}\rangle\,,$$
$$|u^{B/C}_{p,n(\phi,\theta)}\rangle = \left[\mathcal{P}e^{-i\int_\pi^\phi d\phi' A^{B/C}_\phi(\theta,\phi')}\right]_{mn} |u^{B/C}_{m(\phi,\theta)}\rangle\,, \tag{4.16}$$

where $0 \le \phi \le \pi$ in the first line, $\pi \le \phi \le 2\pi$ in the second line. In this gauge, the Wilson loop operator is given by the product of all the transition functions existing in the ϕ direction for given θ as

$$W_0(\theta) = \begin{cases} t^{AB}_p(0,\theta)t^{BA}_p(\pi,\theta) & \text{for } 0 \le \theta \le \pi, \\ t^{DC}_p(0,\theta)t^{CD}_p(\pi,\theta) & \text{for } \pi \le \theta \le 2\pi. \end{cases} \tag{4.17}$$

Here $W_0(\theta)$ is smoothly defined in the range $0 \le \theta < 2\pi$, but its periodic boundary condition is nontrivial:

$$W_0(2\pi) = (t^{AD}_p(0,0))^{-1} W_0(0) t^{AD}_p(0,0), \tag{4.18}$$

where we used that $t^{AD}_p(\phi,0) = t^{AD}(0,0)$ and $t^{BC}_p(\phi,0) = t^{BC}(\pi,0)$ are independent of ϕ. Let us note that since the transition function is assumed to be trivial over the $\theta = \pi$ line, $t^{AD}_p(0,0)$ determines the orientability along the θ direction. Then Eq. (4.18) means that the orientability along the θ direction constrains the Wilson loop eigenvalues along the θ direction. This information is important to understand the Wilson loop spectrum defined on the 2D Brillouin zone torus as discussed in Sec.V.A. More details for the relationship between the homotopy class of the Wilson loop operator and the mathematical definition of the second Stiefel-Whitney number on a torus is given in Ref. [7].

4.4 Candidate Materials

In Ref. [7], based on first-principles calculations, ABC-stacked graphdiyne is proposed to realize monopole nodal lines with the linking structure. ABC-

stacked graphdiyne refers to an ABC stacking of 2D graphdiyne layers composed of sp^2-sp carbon network of benzene rings connected by ethynyl chains. [See Fig. 4.6(c).] Nomura *et al.* [48] theoretically proposed ABC-stacked graphdiyne as a nodal line semimetal, and later Ahn et al. [7] found that it belongs to the monopole nodal line phase, characterized by the nontrivial second Stiefel-Whitney number. Consistent with Ref. [48], nodal lines occur off the high-symmetry Z point of the Brillouin zone. While the electronic band structure displays direct band gap along the high-symmetry lines as shown in Fig. 4.6(d), close inspection throughout the entire Brillouin zone reveals that the valence and conduction bands touch each other along a pair of closed nodal lines colored in red in Fig. 4.6(e). Additionally, the two topmost occupied bands form another nodal line [the orange line in Fig. 4.6(e)], which pierces the red nodal lines, manifesting the proposed linking structure. Moreover, it is shown that strain can induce a topological phase transition from the nodal line semimetal phase with monopole nodal lines to a 3D weak Stiefel-Whitney insulator. The pair of the monopole nodal lines appearing near the Z point fuse together and pair annihilate at the $\sim$ 3 % of tensile strain, when strain is applied along the out-of-plane (z) direction to 3D ABC graphdiyne with the rest of the lattice parameters fixed at the values obtained without strain. It is found that in the resulting insulator, any 2D slice in the momentum space with fixed k_z has $w_2 = 1$, which confirms the 3D weak Stiefel-Whitney insulator phase of 3D graphdiyne under a tensile-strain.

Let us briefly mention the influence of time-reversal symmetry breaking and spin-orbit coupling. When time-reversal symmetry is broken due to effective Zeeman effect, a monopole nodal line semimetal turns into an axion insulator with quantized magnetoelectric polarizability as shown in Ref. [7]. On the other hand, when spin-orbit coupling is not negligible, a monopole nodal

line semimetal becomes a higher-order topological insulator with helical hinge states [18]. These examples clearly show that monopole nodal line semimetal materials can be considered as a parent state leading to various novel topological insulators under suitable conditions.

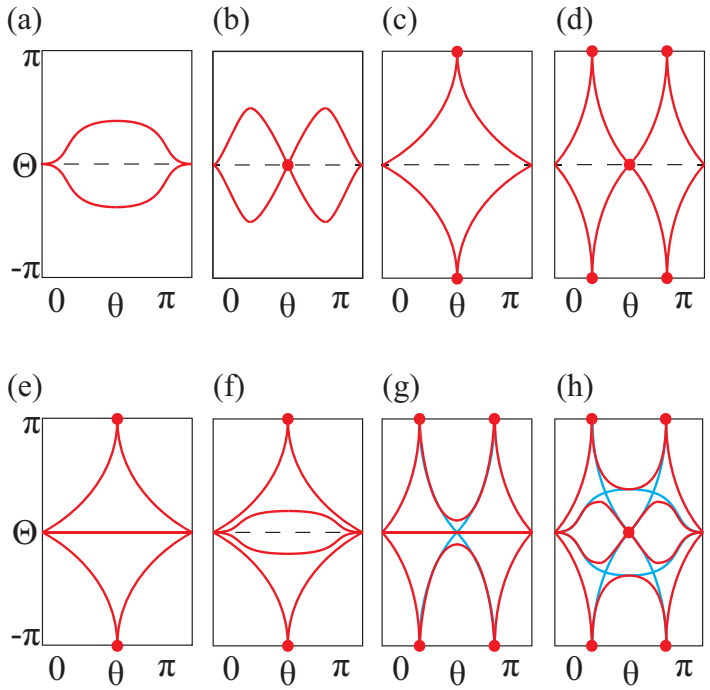

Figure 4.5 Wilson loop spectra on a sphere. The Wilson loop operator is calculated along the azimuthal direction with a fixed polar angle θ. (a-d) When the number of occupied bands $N_{\rm occ}$ is two. The winding number is (a,b) zero, (c) one, and (d) two. (b) can be adiabatically deformed to (a) as we push the crossing point on $\Theta = 0$ out of the boundary at $\theta = 0$ or $\theta = \pi$. (e-h) When $N_{\rm occ} = 3$ or $N_{\rm occ} = 4$. (e) has a flat spectrum on $\Theta = 0$ in addition to (c). Adding a small perturbation to (e) does not deform the spectrum when $N_{\rm occ} = 3$, while it deforms the spectrum to (f) when $N_{\rm occ} = 4$. (g) and (h) shows the Z_2 nature of the Wilson loop spectrum for $N_{\rm occ} = 3$ and $N_{\rm occ} = 4$, respectively. Blue lines in (g) and (h) are obtained after adding one and two flat bands to (d), respectively, whereas red lines are the spectrum after adding a PT-preserving deformation which eliminates non-protected crossing points. The crossing points on $\Theta = \pi$ can always be pair-annihilated after this deformation. From the supplemental materials in Ref. [7].

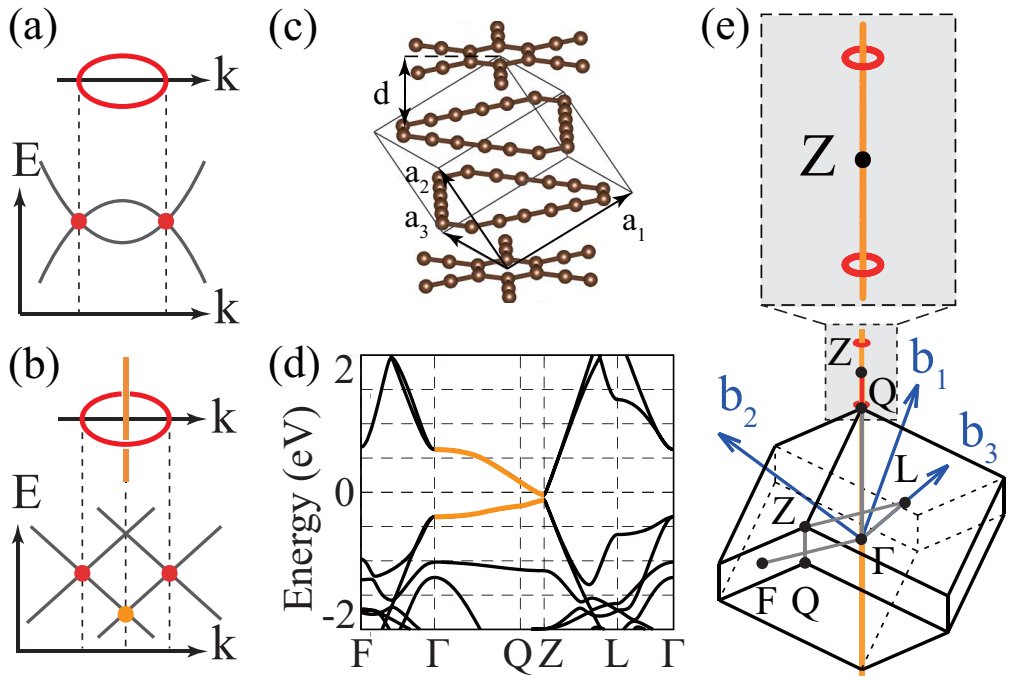

Figure 4.6 (a) Band structure near a nodal line with zero Z_2 monopole charge. (b) Band structure near a nodal line carrying a unit Z_2 monopole charge (monopole nodal line) linked with another nodal line below the Fermi level (E_F). (c) Atomic structure of ABC-stacked graphdiyne. (d) Band structure of ABC-stacked graphdiyne where thick orange lines indicate degenerate nodal lines above and below E_F. (e) The shape of two monopole nodal lines (red loops) at E_F ($E = 0$) linked with a nodal line below E_F (yellow line) in ABC-stacked graphdiyne. From Ref. [7].

Chapter 5

Stiefel-Whitney insulators in 2D and 3D

Up to now, we have considered w_2 defined on a sphere or a torus enclosing a nodal line, which is embedded in 3D momentum space. In this section, we consider w_2 as a topological invariant that classifies 2D I_{ST}-symmetric insulators, in which w_2 is defined on the entire 2D Brillouin zone torus.

5.1 Second Stiefel-Whitney number on a torus

2D I_{ST}-symmetric insulators can be characterized by the Wilson loop spectrum on the 2D Brillouin zone. The 2D Brillouin zone can be viewed as a 2D torus, parametrized by two periodic cycles $(\phi, \theta) = (k_x, k_y)$ along which occupied states may be non-orientable, contrary to the case on a sphere where occupied states are always orientable. If the Wilson loop operator is calculated along a non-orientable cycle, its spectrum cannot reveal the topological property due to the possible flat spectra existing on the $\Theta = 0$ and $\Theta = \pi$ lines. For this

reason, we only consider Wilson loop operators calculated along the orientable cycles below. More subtle issues related with the non-orientability is discussed in detail in Ref. [7]

Fig. 5.1 shows the Wilson loop spectra computed on a 2D torus. As discussed before, the second Stiefel-Whitney number on a torus indicates whether the Wilson loop operator can be continuously deformed to the identity operator or not, modulo an even number of winding on non-contractible cycles. Accordingly, the parity of the number of crossing points on $\Theta = \pi$ gives the second Stiefel-Whitney number as it does on a sphere. For example, $w_2 = 0$ in Fig. 5.1(a,b,f), and $w_2 = 1$ in Fig. 5.1(c,d,e,g,h).

What makes the Wilson loop spectrum on a torus distinct from that on a sphere is the boundary condition of the Wilson loop operator. While $W = 1$ at $\theta = 0$ and π on a sphere, the periodic boundary condition in Eq. (4.18) should be satisfied on a torus. Because the boundary condition on a torus does not require that all eigenvalues are degenerate at the end-points on $\Theta = 0$, an odd number of the crossing points on $\Theta = \pi$ does not necessarily mean that the eigenvalues wind as shown in Fig. 5.1(d,e,g,h). Moreover, when $N_{\rm occ}$ is even, crossing points on $\Theta = 0$ are protected not only locally but also globally. As crossing points are protected on both $\Theta = 0$ and π, there are three distinct topological phases characterized by an odd number of crossing points i) only on $\Theta = 0$, ii) only on $\Theta = \pi$, and iii) on both $\Theta = 0$ and $\Theta = \pi$. On the other hand, when $N_{\rm occ}$ is an odd integer, the crossing points on $\Theta = 0$ are not protected due to the flat spectrum.

When $N_{\rm occ}$ is even, there are four distinct types of Wilson loop spectra. For instance, Fig.5.1(a-d) correspond to the $N_{\rm occ} = 2$ case. Because a crossing point on $\Theta = 0$ is topologically stable, the spectrum in Fig. 5.1(a) and (b) [(c) and (d)] is distinct although $w_2 = 0$ [$w_2 = 1$] in both cases. In fact, they can be

distinguished by the first Stiefel-Whitney number along θ ($w_{1,\theta}$). To understand this, let us recall the periodic boundary condition for the Wilson loop operator shown in Eq. (4.18),

$$W(2\pi) = M^{-1}W(0)M, \tag{5.1}$$

where $\det M = -1$ when $w_{1,\theta} = 1$, in the parallel-transport gauge defined before. When $N_{\text{occ}} = 2$ and $\det M = -1$, it becomes

$$\begin{aligned} \exp(i\Theta(2\pi)\sigma_y) &= M^{-1}\exp(i\Theta(0)\sigma_y)M \\ &= \exp(-i\Theta(0)\sigma_y), \end{aligned} \tag{5.2}$$

which shows that eigenvalues are interchanged as θ goes from 0 to 2π such that an odd number of crossing points occur. As a Wilson loop operator can be diagonalized into 2×2 blocks, this applies to any case with even N_{occ}. For instance, three distinct topological phases when $N_{\text{occ}} = 4$ are shown in Fig. 5.1(f,g,h) which corresponds to $(w_{1,\theta}, w_2) = (1,0), (0,1)$, and $(1,1)$, respectively.

It is worth noting that w_2 and the corresponding Wilson loop spectrum may change depending on the unit cell choice when $w_{1,\theta} = 1$. Notice that the spectrum in Fig. 5.1(b) and (d) differ by a constant shift by π while they have different second Stiefel-Whitney numbers. The same is true for Fig. 5.1(f) and (h). To understand the origin of such unit cell dependence, let us use (k_x, k_y) to parametrize the Brillouin zone. Since the eigenstates of the Wilson loop operator calculated along k_x are Wannier states localized in the x-direction and the Wilson eigenvalues are Wannier centers, Fig. 5.1(b) and (d) (also (f) and (h)) indicate that a uniform shift of the Wannier centers changes the second Stiefel-Whitney number. In other words, the second Stiefel-Whitney number can be changed if the unit cell is shifted by a half lattice constant. Therefore, w_2 becomes a well-defined topological invariant only when $w_1 = 0$. The insulator

with $w_2 = 1$ and $w_1 = 0$ can be called a 2D Stiefel-Whitney insulator, which is an example of higher order topological insulators. In particular, the 2D Stiefel-Whitney insulator has fragile band topology when $N_{\text{occ}} = 2$ as explained in the following section.

5.2 Second Stiefel-Whitney number when $N_{\text{occ}} = 2$: Euler class, fragile topology, and corner charges

Although the general integral form of w_2 is not known, an integral form of w_2 can be found in some special cases. In particular, when $N_{\text{occ}} = 2$ and the occupied bands are orientable, w_2 is identical to the parity of the Euler invariant e_2. The Euler invariant e_2 is an integer topological invariant for two real bands which can be written as a simple flux integral form [9, 10, 41],

$$e_2 = \frac{1}{2\pi} \oint_{BZ} d\mathbf{S} \cdot \tilde{\mathbf{F}}_{12}, \tag{5.3}$$

where $\tilde{\mathbf{F}}_{mn}(\mathbf{k}) = \nabla_{\mathbf{k}} \times \tilde{\mathbf{A}}_{mn}(\mathbf{k})$ and $\tilde{\mathbf{A}}_{mn}(\mathbf{k}) = \langle \tilde{u}_m(\mathbf{k}) | \nabla_{\mathbf{k}} | \tilde{u}_n(\mathbf{k}) \rangle$ $(m, n = 1, 2)$ are 2×2 antisymmetric real Berry curvature and connection defined by real states $|\tilde{u}_n(\mathbf{k})\rangle$. It is invariant under any $SO(2)$ gauge transformation, which has the form $O(\mathbf{k}) = \exp[-i\sigma_y \phi(\mathbf{k})]$ and satisfies $\det[O(\mathbf{k})] = 1$. On the other hand, under an orientation-reversing transformation with $\det[O(\mathbf{k})] = -1$, which has the form $O(\mathbf{k}) = \sigma_z \exp[-i\sigma_y \phi(\mathbf{k})]$, e_2 changes its sign. Therefore, the Euler class is well-defined only for orientable real states, that is, the states associated only with $O(\mathbf{k})$ with a unit determinant.

The flux integral form of e_2 can be connected to transition functions in the following way. To show this relation, let us notice that the 2D Brillouin zone can be deformed to a sphere when the real states are orientable along any non-contractible one-dimensional cycles as far as the topology of the real states is concerned. Then the sphere can be divided into two hemispheres, the northern

(N) and southern (S) hemispheres, which overlap along the equator. Along the equator, the real smooth wave functions $|\tilde{u}^N\rangle$ and $|\tilde{u}^S\rangle$ defined on the northern and southern hemispheres, respectively can be connected by a transition function $t^{NS} = \langle\tilde{u}^N|\tilde{u}^S\rangle = \exp[-i\sigma_y\phi_{NS}] \in SO(2)$. It is straightforward to show that

$$\begin{aligned} e_2 &= \frac{1}{2\pi}\oint_{S^2} d\mathbf{S}\cdot\tilde{\mathbf{F}}_{12} \\ &= \frac{1}{2\pi}\int_N d\mathbf{S}\cdot\tilde{\mathbf{F}}_{12} + \frac{1}{2\pi}\int_S d\mathbf{S}\cdot\tilde{\mathbf{F}}_{12} \\ &= \frac{1}{2\pi}\oint_{S^1} d\mathbf{k}\cdot\left(\tilde{\mathbf{A}}_{N,12} - \tilde{\mathbf{A}}_{S,12}\right) \\ &= \frac{1}{2\pi}\oint_{S^1} d\mathbf{k}\cdot\nabla_{\mathbf{k}}\phi_{NS}, \end{aligned} \tag{5.4}$$

where S^1 indicates the circle along the equator. Therefore the Euler class e_2 is identical to the winding number of the transition function t^{NS}. Let us note that Eq. (5.4) is also equivalent to the definition of the monopole charge module two, and thus its parity is equivalent to w_2 according to the discussion in Sec.IV.A.

One physical consequence resulting from a nonzero Euler invariant e_2 is the existence of anomalous corner charges. The presence of corner charges can be understood in terms of the effective Hamiltonian for boundary states [18]. Here let us briefly explain the idea. Suppose that a two-dimensional system is composed of two quantum Hall insulators with Chern numbers $c_1 = 1$ and $c_1 = -1$, respectively, which are related to each other by I_{ST}. This system is an Euler insulator with $e_2 = 1$, which can be confirmed by the winding pattern of the Wilson loop spectrum. In this particular limit of the Euler insulator, two counter-propagating chiral edge states exist. The edge states are fully gapped after two I_{ST}-symmetric mass terms m_1 and m_2 are added. Each of the two mass terms has $4N_{i=1,2}+2$ zeros due to the I_{ST} symmetry condition $m_{1,2}(\theta) = -m_{1,2}(-\theta)$, where θ denotes the angular coordinate of the circular boundary

of a disk-shaped finite-size system, and $N_{i=1,2}$ are non-negative integers. The band gap of the edge spectrum $2m = 2\sqrt{m_1^2 + m_2^2}$ is nonzero because m_1 and m_2 do not vanish simultaneously in general. However, when there is additional chiral symmetry, only one mass term, which we take here as m_1, remains, so the edge band gap closes at $4N_1 + 2$ points. As the points of zero mass are domain kinks, charges are localized there. The corner charges are robust because they are energetically isolated from the bulk bands. Even when chiral symmetry is broken, the corner charges remain localized as long as they are in the bulk gap [49].

The band topology associated with the nonzero Euler class is fragile. Namely, the Wannier obstruction of an Euler insulator with $e_2 \neq 0$ disappears after additional trivial bands are introduced below the Fermi level [14]. Although the Euler class is defined only for two band systems, its parity still remains meaningful even after additional trivial bands are introduced. Namely, if the Euler class of the two-band model is even (odd), w_2 of the system should remain zero (one) after the inclusion of additional trivial bands [7]. Such a change of the topological indices from Z to Z_2 can also be observed from the variation of the winding pattern in the Wilson loop spectrum when additional trivial bands are added [7, 17].In fact, such fragility of the winding pattern in the Wilson loop spectrum reflects the fragility of the Wannier obstruction [7, 16–18]. Although the nontrivial second Stiefel-Whitney number ($w_2 = 1$) does not induce a Wannier obstruction when the number of bands is bigger than two, anomalous corner states can still exist. Here the corner charges are induced by the configuration of the Wannier centers constrained by the non-trivial second Stiefel-Whitney number [14].

5.3 Topological phase transition mediated by monopole nodal line, and 3D weak Stiefel-Whitney insulator

Since the second Stiefel-Whitney number determines not only the Z_2 monopole charge of a nodal line on its wrapping sphere but also the Z_2 topological invariant of a 2D Stiefel-Whitney insulator, an intriguing topological phase transition mediated by monopole nodal lines can occur in 3D PT-symmetric systems. To describe this, let us start with a sphere wrapping a monopole nodal line in momentum space, and deform it into two parallel 2D planes with fixed k_z. Then each 2D plane can be considered as a 2D subsystem with PT symmetry. Since the monopole charge of the nodal line is identical to the difference of w_2 of these two planes, if $w_2 = 0$ in one plane, $w_2 = 1$ in the other plane. Armed with this information, let us start from a 3D normal insulator and assume that a pair of monopole nodal line is created at the Γ point by tuning a parameter M. Then every 2D subspace with fixed k_z has $w_2 = 1$ when its k_z lies between the monopole nodal line pair whereas the other 2D subspaces with k_z on the other side of the Brillouin zone should have $w_2 = 0$. After the two monopole nodal lines are pair annihilated at the Brillouin zone boundary, one can expect that every 2D slice of the Brillouin zone with fixed k_z has $w_2 = 1$, which is the definition of a 3D weak Stiefel-Whitney insulator. This phase can be considered as a vertical stack of weakly interacting 2D Stiefel-Whitney insulators. In general, a 3D weak Stiefel-Whitney insulator is characterized by three Stiefel-Whitney numbers defined on $k_x = \pi$, $k_y = \pi$, and $k_z = \pi$ planes, respectively. The three invariants encode the three stacking directions of 2D subsystems. The invariants can be changed only when monopole nodal line pairs are created and then annihilated at the Brillouin zone boundary after traversing the full Brillouin zone, which is analogous to the topological phase transition between

a 3D Chern insulator and a normal insulator mediated by Weyl points [50].

To demonstrate the topological phase transition, let us consider a lattice regularization of Eq. (4.1),

$$H(\mathbf{k}) = \sum_{i=1}^{3} f_i(\mathbf{k})\Gamma_i + f_{15}(\mathbf{k})\Gamma_{15}, \tag{5.5}$$

where $f_1 = 2\sin k_x$, $f_2 = 2\sin k_y$, $f_3 = M + 2(\cos k_x - 1) + 2(\cos k_y - 1) + 2r(\cos k_z - 1)$, $f_{15} = m$, and r and m are positive constants. The energy spectrum has a simple analytic form $E = \pm\sqrt{f_1^2 + (f_\rho \pm |m|)^2}$, where $f_\rho = \sqrt{f_2^2 + f_3^2}$. When $r < 1 + m/2$, an insulator-semimetal-insulator transition occurs as M is varied. If we focus on $r < 1 + m/2$ and $M < 4 - m$, the system is a normal insulator when $M < -m$, a 3D weak Stiefel-Whitney insulator when $4r + m < M < 4 - m$, and it is a semimetal having two monopole nodal lines when $-m < M < 4r + m$. One can clearly see that two monopole nodal lines are linked by the line of valence band degeneracy [See Fig. 5.2(a)]. The monopole nodal lines are pair-created at $(k_x, k_y, k_z) = (0, 0, 0)$ and pair-annihilated at $(k_x, k_y, k_z) = (0, 0, \pi)$ via a double band inversion as M increases from $-m$ to $4r+m$. To verify the change of topological properties, the corresponding Wilson loop spectra are shown in Fig. 5.2(b-d).

5.4 3D strong Stiefel-Whitney insulator and quantized magnetoelectric response

Since we have a new 2D Z_2 invariant w_2 and the associated 2D Z_2 topological insulator (2D Stiefel-Whitney insulator), it is natural to ask whether one can find a 3D topological insulator associated with the second Stiefel Whitney class. In spinless fermionic systems with $I_{\mathrm{ST}} = PT$, real wave functions can be defined over the full 3D Brillouin zone. However, unfortunately, there is no

corresponding 3D topological invariant [13,51]. So we do not expect a 3D topological insulator associated with the Stiefel-Whitney number other than the 3D weak Stiefel-Whitney insulator discussed above. Instead, we focus on the 3D systems with $I_{\rm ST} = C_{2z}T$ where the z-axis is chosen as the axis for C_2 rotation. In $C_{2z}T$-symmetric 3D systems, only the wave functions on the $k_z = 0$ and $k_z = \pi$ planes can be real with the corresponding second Stiefel-Whitney numbers $w_2(0)$ and $w_2(\pi)$, respectively. Thus, a 3D strong Z_2 topological invariant Δ_{3D} may be defined as $\Delta_{3D} \equiv w_2(\pi) - w_2(0)$ in a way similar to how the 3D Fu-Kane-Mele invariant is constructed. Since Δ_{3D} originates from w_2 in $I_{\rm ST}$-invariant planes, the 3D topological insulator with $\Delta_{3D} = 1$ can be called *a 3D strong Stiefel-Whitney insulator*. Let us note that the idea of $C_{2z}T$-protected Z_2 topological insulator was already proposed in Ref. [5]. However, its bulk electromagnetic response and the related hinge excitations are studied recently in Ref. [23, 52]. In fact, a strong 3D Stiefel-Whitney insulator is an example of higher-order topological insulators whose bulk magnetoelectric response is described by the axion term with the quantized magnetoelectric polarizability $P_3 = 1/2$. As a result of the bulk boundary correspondence associated wth the quantized P_3, we show that a 3D strong Stiefel-Whitney insulator has chiral hinge states [53–62] along the edges parallel to the rotation axis and 2D massless Dirac fermions on the surfaces normal to the rotation axis as shown in Fig. 5.3.

The equivalence between Δ_{3D} and the quantized magnetoelectric polarizability can be shown by analyzing the homotopy group of the sewing matrix G for $I_{\rm ST}$ symmetry defined as

$$G_{mn}(\mathbf{k}) = \langle u_{m(-C_{2z}\mathbf{k})} | C_{2z}T | u_{n\mathbf{k}} \rangle \,, \tag{5.6}$$

which satisfies

$$G_{mn}(\mathbf{k}) = G_{nm}(-C_{2z}\mathbf{k}), \tag{5.7}$$

where $-C_{2z}\mathbf{k} = (k_x, k_y, -k_z)$ and $|u_{n\mathbf{k}}\rangle$ is the cell-periodic part of a Bloch state. If we choose smooth occupied states, the corresponding sewing matrix also becomes smooth. Then the nontrivial homotopy class of G characterizes the obstruction to taking a uniform representation $G(\mathbf{k}) = G_0$ independent of $\mathbf{k}$. At a generic momentum, $G(\mathbf{k}) \in U(N)$. On the other hand, on a $C_{2z}T$-invariant plane, either the $k_z = 0$ or $k_z = \pi$ plane, $G^T(\mathbf{k}) = G(\mathbf{k})$ according to Eq. (B.2), from which we obtain

$$G(\mathbf{k}) \in U(N)/SO(N), \tag{5.8}$$

where N denotes the number of occupied bands.

In a smooth complex gauge, the magnetoelectric polarizability P_3 takes the form of the 3D Chern-Simons invariant [63, 64]

$$P_3 = \frac{1}{8\pi^2}\int_{\mathrm{BZ}} d^3k\epsilon^{ijk}\mathrm{Tr}\left[A_i\partial_j A_k - \frac{2i}{3}A_iA_jA_k\right], \tag{5.9}$$

where $A_{mn}(\mathbf{k}) = \langle u_{m\mathbf{k}}|i\nabla_{\mathbf{k}}|u_{n\mathbf{k}}\rangle$ is the Berry connection, and BZ denotes the Brillouin zone. In terms of the sewing matrix $G(\mathbf{k})$, one can show that

$$2P_3 = \frac{1}{24\pi^2}\int_{\mathrm{BZ}} d^3k\epsilon^{ijk}\mathrm{Tr}\left[(G^{-1}\partial_i G)(G^{-1}\partial_j G)(G^{-1}\partial_k G)\right], \tag{5.10}$$

which is nothing but the 3D winding number of the sewing matrix G. Since the 3D winding number is determined by the 2D winding numbers in invariant planes, we eventually find

$$2P_3 = w_2(\pi) + w_2(0) = \Delta_{3\mathrm{D}}(\ \mathrm{mod}\ 2), \tag{5.11}$$

which is proved more explicitly in Ref. [23]. We used that w_2 is given by the 2D winding number of G, which is derived in Appendix B.

The relation between the bulk topological invariant of the axion insulator and that of the 2D Stiefel-Whitney insulator implies a similar relation between their anomalous boundary states. In fact, the chiral hinge states in an axion insulator can be considered to result from the pumping of charges at the corners of the Stiefel-Whitney insulator when k_z is regarded as a parameter for the pumping process [52]. This charge pumping picture can be extended further to the cases with strong spin-orbit coupling. Here one can consider a helical charge pumping, where the corner charges with different spins are pumped to the opposite directions, which leads to a construction of a higher-order topological insulator with helical hinge states [18, 42, 54].

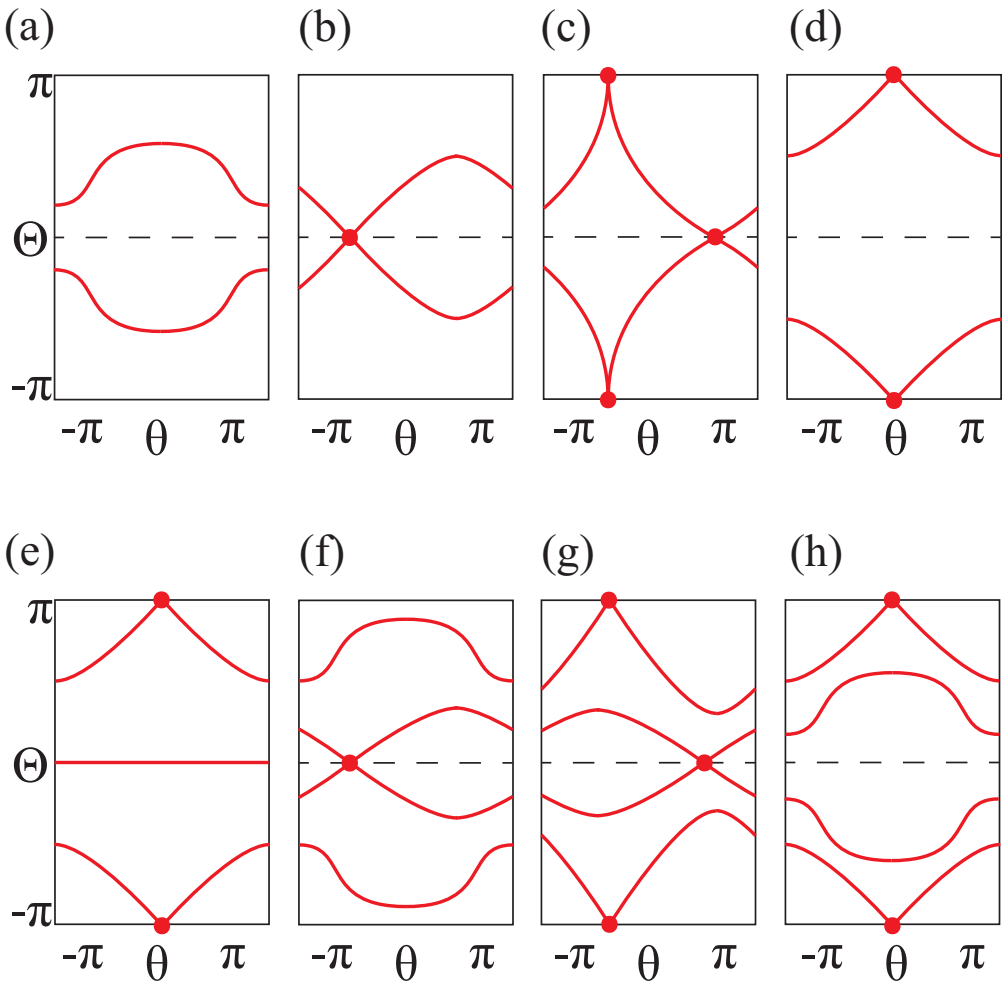

Figure 5.1 Wilson loop spectra on a torus. The Wilson loop operator is calculated along the orientable ϕ cycle at a fixed θ. (a-d) Spectrum when $N_{\text{occ}} = 2$. $(w_{1,\theta}, w_2)$= (a) $(0,0)$, (b) $(1,0)$, (c) $(0,1)$, (d) $(1,1)$. (e-h) Nontrivial spectrum when $N_{\text{occ}} = 3$ and $N_{\text{occ}} = 4$. (e) When $N_{\text{occ}} = 3$ with $w_2 = 1$. When the number of occupied bands is odd, w_2 can be determined only if we calculate the Wilson loop operator along a orientable cycle. (f-h) When $N_{\text{occ}} = 4$. $(w_{1,\theta}, w_2)$= (f) $(1,0)$, (g) $(0,1)$, (h) $(1,1)$. Here, $w_{1,\theta}$ is the first Stiefel-Whitney number computed along the θ direction. From the supplemental materials in Ref. [7].

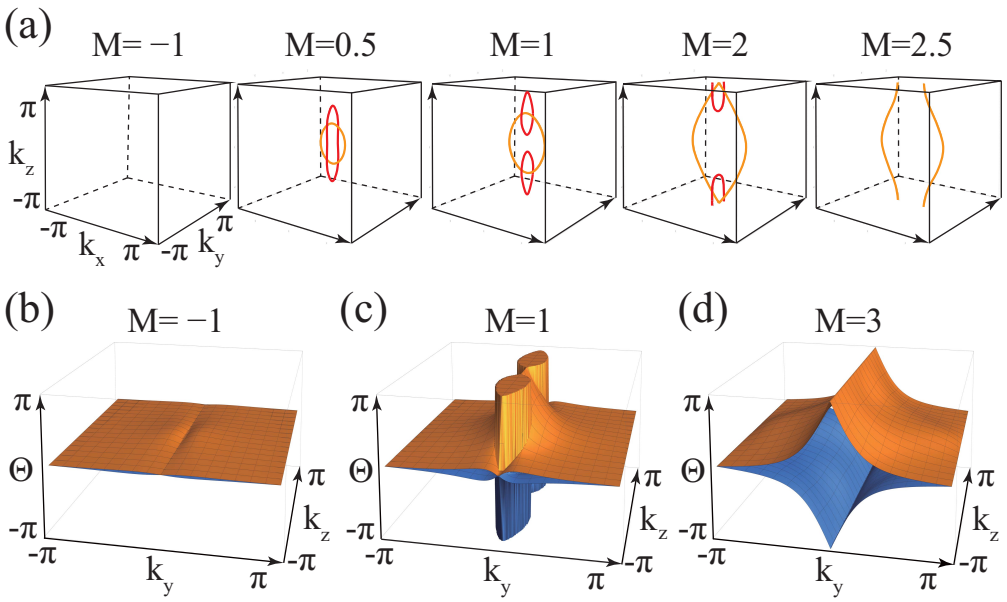

Figure 5.2 Topological phase transition from a normal insulator to a 3D weak Stiefel-Whitney insulator. The Hamiltonian in Eq. (5.5) is used with $r = 0.5$ and $m = 0.9$. (a) Shape of the nodal lines formed by touching between a conduction and a valence band (red) and between valence bands (orange). As M increases from -1 to 2.5, a pair of monopole nodal lines are created near $(0, 0, 0)$, and then they are annihilated near $(0, 0, \pi)$. (b)$\sim$(d) Wilson loop operators are calculated along the k_x direction at each value of k_y and k_z. (b) Normal insulator at $M = -1$. (c) Nodal line semimetal with monopole nodal lines at $M = 1$. (d) 3D weak Stiefel-Whitney insulator at $M = 3$.

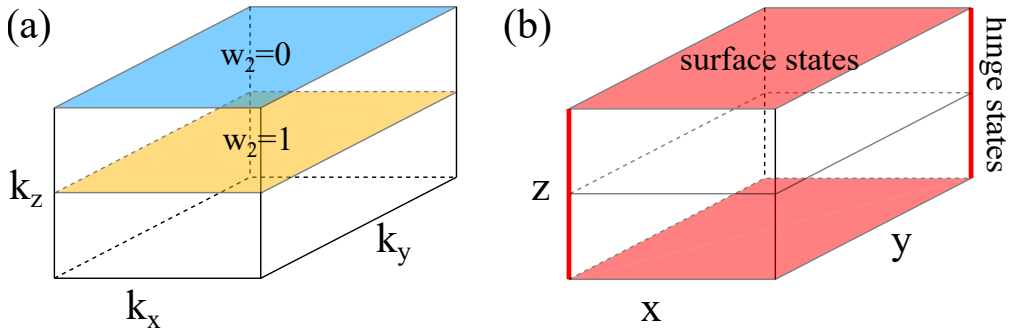

Figure 5.3 3D strong Stiefel-Whitney insulator protected by $C_{2z}T$ symmetry. (a) Schematic figure describing the second Stiefel-Whitney number on the $C_{2z}T$-invariant planes in momentum space. In a 3D strong Stiefel-Whitney insulator, $w_2(k_z = \pi) - w(k_z = 0) = 1$ modulo two. (b) Schematic figure describing the gapless states on the surface and hinges in real space. An odd number of 2D Dirac fermions appear on each of the top and bottom surfaces. 1D chiral fermions appear on the side hinges. From Ref. [23].

Chapter 6

Reformulation of the Nielsen-Ninomiya Theorem in 2D

The aim of this chapter is to show that a two-band system with the Euler class e_2 has band crossing points whose total winding number is equal to $2e_2$. This generalized the conventional Nielsen-Ninomiya theorem, which states that the total topological charge of stable band crossing in the Brillouin zone must vanish. This work was motivated by the peculiar phenomenon observed in twisted bilayer graphene.

The recent discovery of Mott insulating states and superconductivity in twisted bilayer graphene (TBG) near the first magic angle $\theta \sim 1.05^\circ$ [65, 66] has lead to a surge of research activities to understand this system [67–97]. One notable feature in the band structure of TBG is the presence of almost flat bands near charge neutrality, which are effectively decoupled from other bands by an energy gap. The reduced kinetic energy of the flat bands allows this purely carbon-based system, normally regarded as a weakly correlated system, to be an intriguing playground to examine the Mott physics and the associated

unconventional superconductivity.

For a microscopic description of correlation effect in TBG, there have been several theoretical efforts to construct a tight-binding lattice model capturing the characteristic band structure of the four almost flat bands near charge neutrality [93–97]. Here we neglect the spin degrees of freedom for counting the number of bands, which is valid because the spin-orbit coupling is negligibly small. According to the low energy continuum theory which excellently describes the qualitative feature of the almost flat bands, there are two Dirac points at each K and K' point in the Moiré Brillouin zone, whose origin can be traced back to the Dirac points at each valley of the underlying graphene layers [98, 99]. The presence of massless Dirac fermions is further supported by several theoretical studies [100–103] as well as recent quantum oscillation measurement [104]. The existence of gapless Dirac points indicates the valley charge conservation $U_v(1)$ and the spacetime inversion symmetry $C_{2z}T$, where C_{2z} denotes a two-fold rotation about the z-axis and T is time-reversal symmetry [93, 94]. In the presence of $U_v(1)$ and $C_{2z}T$, the four nearly flat bands are decoupled into two independent valley-filtered two-band systems, and each two-band system possesses Dirac points at K and K'. The fact that both the valley charge conservation and $C_{2z}T$ are not the exact symmetry of the TBG indicates that the symmetry of the low energy physics is larger than the exact lattice symmetry [93].

Interestingly, by putting together all the emergent symmetry including $U_v(1)$ and $C_{2z}T$, Po et al. have found an obstruction to constructing well-localized Wannier functions describing the four nearly flat bands in TBG [93, 94]. Moreover, it is shown that the obstruction originates from the fact that the two Dirac points in each valley-filtered two-band system have the same winding number, which is generally not allowed in 2D periodic systems due to the

Nielsen-Ninomiya theorem [105].

The main purpose of the present study is to unveil the topological nature of the nearly flat bands in TBG near a magic angle and propose a general framework to understand the band topology of 2D systems sharing the same symmetry. In particular, we show that, two bands having two Dirac points with the same winding number is endowed with an integer topological invariant, the Euler class e_2, when the 2D spinless fermion system has spacetime inversion symmetry $I_{\mathrm{ST}} \equiv C_{2z}T$. We explicitly show that two bands having a nonzero Euler class cannot have exponentially localized Wannier representation, that is, there is a Wannier obstruction. Moreover, the nonzero Euler class e_2 implies that there are band crossing points, henceforth called vortices, between the two bands, whose total winding number is equal to $2e_2$. Thus, a real two-band system carrying a nonzero e_2 evidences the violation of the Nielsen-Ninomiya theorem.

This chapter is organized as follows. We first present the topological properties of a simple four-band lattice model proposed by Zou et al. [93], which captures all the essential properties of the nearly flat bands in TBG at magic angle. After clarifying the issues related with the band topology of TBG by using the toy model, we provide a general description of the band topology of spacetime (I_{ST}) symmetric spinless fermion systems in 2D. In Sec 6.2. we prove the correspondence between the vortex winding number and the Euler class, and demonstrate the violation of Nielsen-Ninomiya theorem in real two band systems with a nonzero Euler class.

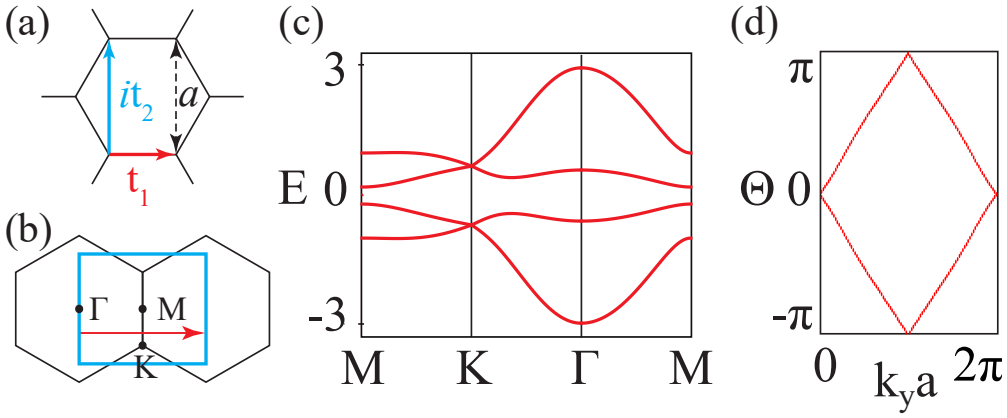

Figure 6.1 (a) The definition of the hopping amplitudes $t_{1,2}$ for a four-band lattice model proposed by Zou et. al. [93]. a is the lattice constant representing the lattice vector for a Moiré superlattice of TBG at magic angle. (b) High symmetry points in the Brillouin zone. $\Gamma = (0,0)$, $M = (2\pi/\sqrt{3}a, 0)$, and $K = (2\pi/\sqrt{3}a, 2\pi/3a)$. The blue rectangle is the Brillouin zone used to compute the Wilson loop spectrum. (c) Band structure along high-symmetry lines. Both of the occupied and unoccupied bands have gapless Dirac points at K and K'. (d) Wilson loop spectrum for the lower two bands. The Wilson loop operator is calculated along the k_y direction at fixed k_x, as shown by the red arrow in (b). The unit winding of the spectrum indicates the unit Euler class $|e_2| = 1$. From Ref. [14].

6.1 Band topology of nearly flat bands in twisted bilayer graphene

Let us first clarify the issues related with the band topology of the nearly flat bands in TBG at magic angle. For this purpose, we study a simple four-band model Hamiltonian proposed by Zou et al. [93], which captures the essential characteristics of the nearly flat bands in TBG.

6.1.1 A four-band lattice model

The model is defined on a honeycomb lattice which represents the Moiré superlattice of TBG at magic angle [93]. Putting two orbitals per site, one can construct a four-band Hamiltonian given by

$$H = \sum_{\langle ij \rangle} c_i^\dagger (\hat{t}_1)_{ij} c_j + \sum_{\langle\langle ij \rangle\rangle} c_i^\dagger s_{ij} (i\hat{t}_2)_{ij} c_j, \tag{6.1}$$

where $\hat{t}_1 = 0.4 + 0.6\tau_z$ and $\hat{t}_2 = 0.1\tau_x$ indicate the hopping amplitudes between the nearest-neighbor and next-nearest neighbor sites with the Pauli matrices $\tau_{x,y,z}$ representing the orbital degrees of freedom. Here we choose $s_{ij} = +1$ for $\mathbf{r}_i = \mathbf{r}_j + a\hat{y}$, which determines the rest of the s_{ij}'s because of the C_{3z} symmetry. Then the full Hamiltonian is invariant under a three-fold rotation about the z-axis C_{3z}, a two-fold rotation about the y-axis C_{2y}, and $I_{\mathrm{ST}} = C_{2z}T$. Namely, the lattice model has D_6 point group symmetry. This model Hamiltonian inherits the essential features of the nearly flat bands of TBG with enlarged emergent symmetries. In momentum space, the Hamiltonian becomes

$$\begin{aligned} H(\mathbf{k}) = \hat{t}_1 \Bigg[& \left(1 + 2\cos\frac{\sqrt{3}k_x a}{2} \cos\frac{k_y a}{2} \right) \sigma_x \\ & + 2\sin\frac{\sqrt{3}k_x a}{2} \cos\frac{k_y a}{2} \sigma_y \Bigg] \\ & + \hat{t}_2 \left(4\cos\frac{\sqrt{3}k_x a}{2} \sin\frac{k_y a}{2} - 2\sin k_y a \right), \end{aligned} \tag{6.2}$$

where the Pauli matrices $\sigma_{x,y,z}$ denote the sublattice degrees of freedom of the honeycomb lattice.

6.1.2 Band topology of lower two bands

The band structure of the four-band model is shown in Fig. 6.1(c). One can see that two lower bands are fully separated from the two upper bands. The

two lower bands cross at two corners of the BZ, K and K', forming two Dirac points with the same winding number. As pointed out in [93], the winding number of the two Dirac points can be determined by examining the mirror eigenvalues of the two occupied bands at the M point: if their mirror eigenvalues are opposite (equal), the winding numbers of the Dirac points at K and K' points are equal (opposite). In the case of the model Hamiltonian in Eq. (6.1), the mirror symmetry along the ΓM line can be represented by τ_z, and it can be explicitly checked that the mirror eigenvalues of the two occupied bands are indeed opposite along this line. Similarly, the two upper bands also possess two Dirac points sharing the same winding number whose winding direction is opposite to that between the lower two bands. Both the lower two bands and the upper two bands possess the same topological characteristic of the nearly flat bands of TBG in a single valley while preserving all D_6 point group symmetry [93].

Let us focus on the topological properties of the lower two bands to understand the band topology and the relevant obstruction of the nearly flat bands in TBG. One direct evidence showing the nontrivial topology of the lower two bands is the winding of the Wilson loop spectrum shown in Fig. 6.1(d), which is computed from the transition function in a real gauge by using the technique developed in [7]. Here the Wilson loop operator corresponds to the transition function. In the Wilson loop spectrum in Fig. 6.1(d), two eigenvalues change symmetrically about $\Theta = 0$ line due to the I_{ST} symmetry, and each eigenvalue winds once as k_x is varied. Below we show that the unit winding of the transition function in a real gauge indicates the unit Euler class $|e_2| = 1$, which imposes an obstruction to Wannier representation and leads to the violation of the Nielsen-Ninomiya theorem.

6.2 Failure of Nielsen-Ninomiya Theorem due to the Euler class

Let us now show that the Euler class is the topological invariant that explains the band topology for nearly flat bands in TBG, which was attributed to the non-zero total winding number in the Brillouin zone. More explicitly, we show that the Euler class is equivalent to half the total winding number. To introduce some notations and set the stage for the discussion that follows, we first give a short proof of the 2D Nielsen-Ninomiya theorem, in analogy to the three-dimensional (3D) case [106]. Our main result will follow by carefully investigating the failure of the 2D Nielsen-Ninomiya theorem.

6.2.1 Two-dimensional Nielsen-Ninomiya theorem

We give a short proof of the 2D Nielsen-Ninomiya theorem that the total winding number is zero in 2D periodic systems and point out what the assumptions are. Note that we have stated this theorem by using the winding number instead of Berry phase because Berry phase is defined only modulo 2π.

Let us take two real basis states $|\tilde{u}_{1\mathbf{k}}\rangle$ and $|\tilde{u}_{2\mathbf{k}}\rangle$ such that I_{ST} is represented by the complex conjugation K (i.e., $I_{\mathrm{ST}} = K$), so the I_{ST} symmetry condition $I_{\mathrm{ST}} H(\mathbf{k}) (I_{\mathrm{ST}})^{-1} = H(\mathbf{k})$ requires that the matrix elements of the Hamiltonian $H_{mn}(\mathbf{k}) = \langle \tilde{u}_{m\mathbf{k}} | H(\mathbf{k}) | \tilde{u}_{n\mathbf{k}} \rangle$ to be real, that is, $H_{mn}(\mathbf{k}) = H^*_{mn}(\mathbf{k})$. Therefore,

$$H(\mathbf{k}) = r(\mathbf{k}) \cos\theta(\mathbf{k}) \sigma_1 + r(\mathbf{k}) \sin\theta(\mathbf{k}) \sigma_3 \tag{6.3}$$

where $r(\mathbf{k}) \geq 0$, σ_1 and σ_3 are Pauli matrices defined in the basis $\{|\tilde{u}_{1\mathbf{k}}\rangle, |\tilde{u}_{2\mathbf{k}}\rangle\}$, and a term proportional to σ_0 is ignored. Let us define a unit vector $\mathbf{n}(\mathbf{k}) = (\cos\theta(\mathbf{k}), \sin\theta(\mathbf{k}))$ away from points at which $r(\mathbf{k}) = \mathbf{0}$. The winding number of the Hamiltonian along a loop C is defined to be the winding number of

$\mathbf{n}(\mathbf{k})$ [107]:$N_C = \frac{1}{2\pi} \oint_C d\mathbf{k} \cdot \nabla_{\mathbf{k}} \theta(\mathbf{k})$. Let D_i be a disk enclosing an ith vortex, so that the total winding number is given by

$$N_t = \frac{1}{2\pi} \oint_{\cup_i \partial D_i} d\mathbf{k} \cdot \nabla_{\mathbf{k}} \theta(\mathbf{k}), \tag{6.4}$$

where ∂D_i is the boundary of D_i. Using the Stokes' theorem, we have

$$N_t = -\int_{BZ - \cup_i D_i} d\mathbf{S} \cdot \nabla_{\mathbf{k}} \times \nabla_{\mathbf{k}} \theta(\mathbf{k}) = 0 \tag{6.5}$$

Here, we have made an obvious assumption that the matrix elements of the two-band Hamiltonian are continuously defined throughout the Brillouin zone. This has two important implications. The first one is that when the matrix elements of the two-band Hamiltonian cannot be defined continuously in the presence of I_{ST} symmetry, a non-vanishing total winding number is allowed. We will discuss this in the following subsection. The second implication is that when the two bands are no longer isolated from the other bands, the winding number may lose its meaning. This is discussed in [14].

6.2.2 Winding number and the Euler class

Let us now prove that e_2 is equal to half the total winding number of a two band Hamiltonian. We again consider the Hamiltonian in Eq. (6.3).

In the case when the total Berry phase, i.e. the sum of the Berry phases of the two bands, along any non-contractible 1D cycle in the Brillouin zone is trivial, we can take a spherical gauge in which we neglect the non-contractible 1D cycles and instead view the Brillouin zone as a sphere [Fig. B.1]. We refer readers to [14] for a discussion on the case in which the Berry phase is nontrivial.

One immediate consequence of the non-vanishing total winding number is that it is impossible to define a continuous Hamiltonian matrix element throughout the sphere. Thus, let us divide the sphere into N and S hemispheres such

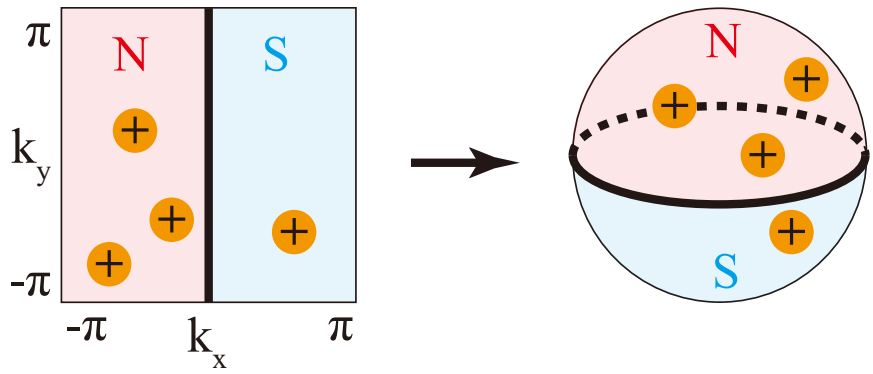

Figure 6.2 Deformation of the Brillouin zone to a sphere. When the total winding number is non-zero in the Brillouin zone, Hamiltonian matrix elements are smooth only over local patches N and S, respectively. When the nontrivial transitions are restricted to $k_x = 0$ (the black bold line), the boundary of the Brillouin zone can be contracted to a point so that the Brillouin zone becomes a sphere on the right. From Ref. [14].

that each vortex is located in the interior of either the N or S hemisphere [Fig. B.1]. On the equator, we need a transition function, $O_{NS}(\phi) \in SO(2)$, where ϕ is the azimuthal angle parametrizing the equator. The two Hamiltonian on the N and S hemispheres are connected along the equator as

$$(H_N)_{mn} = (O_{NS})_{mp}(H_S)_{pq}(O_{NS}^{\dagger})_{qn} \tag{6.6}$$

Thus, we must have $O_{NS} = \exp(-i\sigma_y(\theta_S - \theta_N)/2)$. Before moving on, note that we may assume that the two bands of our interest arise as sub-bands of a lattice Hamiltonian. Then, this transition matrix is the transition function between the two sub-bands of interest. Because the full lattice Hamiltonian is continuous, any discontinuity of the projected 2×2 Hamiltonian must originate from that of the basis states of the two subbands. Accordingly, the Euler class,

which is given by the winding number of the transition function, is equal to

$$\frac{1}{4\pi}\oint_{\text{equator}} d\mathbf{k}\cdot(\nabla_{\mathbf{k}}\theta^N-\nabla_{\mathbf{k}}\theta^S)=(N_N+N_S)/2, \tag{6.7}$$

where $N_{N/S}$ are the sum of the winding number within N/S patch. The negative sign in the definition of N_S is there because the winding number is defined by the counterclockwise line integral with respect to the normal direction of the sphere. In conclusion, we have proved that

$$e_2=-\frac{1}{2}N_t. \tag{6.8}$$

Let us note that this is a generalization of the Poincaré-Hopf theorem [108–110], which relates zeros of a tangent vector field to the Euler characteristic of the manifold, to rank two real Bloch bundles (i.e., two real Bloch states).

Chapter 7

Inversion Parity Formulae

We have developed our theory by requiring only the combination of inversion and time reversal symmetries. Many PT-symmetric (or, in 2D, C_2T-symmetric) systems, however, have both inversion (or two-fold rotation) and time reversal symmetries. Inversion symmetry helps us to identify the topological phase of matter because the phase is partially determined by the inversion eigenvalues at the inversion-invariant momenta (which is commonly called time-reversal-invariant momenta or TRIM in short) [38, 42, 111–114]. Here we derive the formula for calculating the second Stiefel-Whitney class using inversion eigenvalues, which is

$$(-1)^{w_2} = \prod_{i=1}^{4} (-1)^{[N^-_{\mathrm{occ}}(\Gamma_i)/2]}, \tag{7.1}$$

where $\Gamma_{i=1,2,3,4}$ are four TRIM on the inversion-invariant plane where w_2 is evaluated, $N^-_{\mathrm{occ}}(\Gamma_i)$ is the number of occupied bands with negative inversion eigenvalues at Γ_i, and the bracket means the greatest integer function, i.e., $[n+x] = n$ for $n \in \mathbb{Z}$ and $0 \leq x < 1$. After we derive Eq. (7.1), we discuss

about using the formula to count the Z_2 monopole charges in the Brillouin zone. Finally, we show that the quantized magnetoelectric polarization can be induced by applying a magnetic field on a nodal line semimetal with odd pairs of Z_2 monopoles.

7.1 The first Stiefel-Whitney class from parity

Before we move on, let us briefly review the relation between the Berry phase and inversion eigenvalues following Ref. [38, 112], because it is needed in the derivation of our formula. Here the Berry phase is calculated in a smooth complex gauge. As shown in Sec. 2.1, this Berry phase corresponds to the first Stiefel-Whitney class w_1 of real gauges.

Inversion symmetry imposes a constraint on the Berry connection by

$$\mathrm{Tr}A(\mathbf{k}) + \mathrm{Tr}A(-\mathbf{k}) = -i\nabla_{\mathbf{k}} \log\det B(\mathbf{k}), \tag{7.2}$$

where $B_{mn}(\mathbf{k}) = \langle u_{m-\mathbf{k}}| P |u_{n\mathbf{k}}\rangle$ is the sewing matrix for inversion symmetry. Accordingly, the Berry phase along an inversion-invariant line is given by [**?**, **?**]

$$\begin{aligned}\int_{-\pi}^{\pi} dk \mathrm{Tr}A(k) &= \int_0^{\pi} dk \left(\mathrm{Tr}A(k) + \mathrm{Tr}A(-k)\right) \\ &= \int_0^{\pi} dk - i\nabla_k \log\det B(k) \\ &= -i\log\frac{\det B(\pi)}{\det B(0)}.\end{aligned} \tag{7.3}$$

That is,

$$\begin{aligned}\exp\left[i\int_{-\pi}^{\pi}dk\mathrm{Tr}A(k)\right] &= \frac{\det B(\pi)}{\det B(0)} \\ &= \det B(\pi)\det B(0) \\ &= \prod_{i=1}^{2}\prod_{n=1}^{N_{\mathrm{occ}}}\xi_n(\Gamma_i) \\ &= \prod_{i=1}^{2}\xi(\Gamma_i), \end{aligned} \tag{7.4}$$

where we used $\det B(0) = \pm 1$, $\Gamma_1 = 0$ and $\Gamma_2 = \pi$, $\xi_n = \pm 1$ is the inversion eigenvalue of the nth occupied band, and $\xi(\Gamma_i)$ is the product of all inversion eigenvalues of occupied states over the TRIM Γ_i for simplicity of notation. The product of ξ at two TRIM gives the Berry phase along the inversion-invariant line passing through the two TRIM.

By applying the above relation, we can investigate the inversion-required band degeneracies [38]. Let us recall that, in PT-symmetric systems, the non-trivial Berry phase along a contractible loop indicates that band degeneracies are enclosed by the loop. The band degeneracies appear as nodal lines in the 3D Brillouin zone. If we consider the Berry phase Φ around the half of an inversion-invariant plane, which we parametrize by $0 \le k_x \le \pi$ for simplicity, it is given by

$$\begin{aligned}(-1)^{\Phi/\pi} &= \exp\left[i\oint_{\partial(\mathrm{hIP})}d\mathbf{k}\cdot\mathrm{Tr}\mathbf{A}(\mathbf{k})\right] \\ &= \exp\left[i\oint dk_y\mathrm{Tr}A_y(\pi,k_y) - i\oint dk_y\mathrm{Tr}A_y(0,k_y)\right] \\ &= \prod_{i=1}^{2}\xi(\Gamma_i)\left[\prod_{i=3}^{4}\xi(\Gamma_i)\right]^{-1} \\ &= \prod_{i=1}^{4}\xi(\Gamma_i), \end{aligned} \tag{7.5}$$

where ∂(hIP) is the boundary of the half invariant plane, and Γ_i's are contained in the invariant plane. Therefore, when the product of all inversion eigenvalues over four TRIM is -1 $(+1)$, an odd (even) number of nodal lines penatrating through the half of the inversion-invariant plane containing the four momenta. Here only the parity of the number of nodal lines can be counted because an even number of nodal lines can be removed from an invariant plane without changing the inversion eigenvalues.

7.2 The second Stiefel-Whitney class from parity

We are now ready to derive an analogous formula for the second Stiefel-Whitney class. While we have taken a complex smooth gauge to associate the first Stiefel-Whitney class with inversion eigenvalues, we now take a real gauge to associate the second Stiefel-Whitney class charge with inversion eigenvalues.

7.2.1 Two occupied bands

First we consider two orientable occupied bands over an invariant plane. Because the first Stiefel-Whitney class is trivial for orientable occupied bands, there are two cases according to Eq. (7.4): the product of two inversion eigenvalues at each TRIM is all negative or all positive.

In the former, the second Stiefel-Whitney class is trivial because the occupied bands can be deformed to topologically trivial bands without closing the band gap between the conduction and valence band as follows. We invert the occupied bands such that the topmost occupied band has the positive inversion eigenvalue and the other has the negative eigenvalue at each TRIM. Then, by applying Eq. (7.5) to the lowest occupied band rather than the whole occupied bands, we find that inversion eigenvalues do not require a degener-

acy between the occupied bands because the product of inversion eigenvalues is positive for the lowest occupied bands. In other words, all degeneracies between the occupied bands can be removed without changing the inversion eigenvalues. After removing all the accidental degeneracies, we have two non-degenerate orientable occupied bands. The Whitney sum formula shows that the second Stiefel-Whitney class is trivial for the resulting bands. As the band gap is not closed during the deformation we have described, the second Stiefel-Whitney class of the original phase is also trivial.

In the latter case where the inversion eigenvalues are the same at each TRIM, it may be impossible to isolate the two occupied bands from each other without closing the band gap between the conduction and valence band. For example, when the eigenvalues are -1 at one or three TRIM and $+1$ at the other TRIM, the degeneracy of the occupied bands is required by Eq. (7.5) applied to the lowest occupied band. The second Stiefel-Whitney class is nontrivial in this case. We will show this by associating the flux integral form of the second Stiefel-Whitney class with inversion eigenvalues. As we did when reviewing the result for the Berry phase, we begin by defining an 1D integral with inversion eigenvalues and then extend the result to 2D integrals.

Inversion symmetry gives the following constraints on the real Berry connection and curvature by

$$\begin{aligned} A^R(\mathbf{k}) &= -B^T(\mathbf{k})A^R(-\mathbf{k})B(\mathbf{k}) - B^T(\mathbf{k})\nabla_{\mathbf{k}}B(\mathbf{k}), \\ F^R(\mathbf{k}) &= B^T(\mathbf{k})F^R(-\mathbf{k})B(\mathbf{k}), \end{aligned} \tag{7.6}$$

where $A^R_{mn} = \langle u_{m\mathbf{k}}|\nabla_{\mathbf{k}}|u_{n\mathbf{k}}\rangle$, and $|u_{n\mathbf{k}}\rangle$ is real.

We consider an inversion-invariant line and take a smooth real gauge over the line where the sewing matrix is also smooth over the line. It is always possible because we consider orientable occupied bands. Then, because the sewing

matrix is smooth and $\det B = 1$ at TRIM over the line, the sewing matrix belongs to SO(2), i.e.,

$$B(\mathbf{k}) = \exp \begin{pmatrix} 0 & \phi(\mathbf{k}) \\ -\phi(\mathbf{k}) & 0 \end{pmatrix} \tag{7.7}$$

It follows that the constraint equation for the real Berry connection becomes

$$\begin{aligned} A^R(\mathbf{k}) + A^R(-\mathbf{k}) &= -(B^T(\mathbf{k})\nabla_{\mathbf{k}} B(\mathbf{k})) \\ &= \begin{pmatrix} 0 & -\nabla_{\mathbf{k}}\phi(\mathbf{k}) \\ \nabla_{\mathbf{k}}\phi(\mathbf{k}) & 0 \end{pmatrix}, \end{aligned} \tag{7.8}$$

from which we find

$$\begin{aligned} \int_{-\pi}^{\pi} dk A_{12}^R(k) &= \int_0^{\pi} dk \left(A_{12}^R(k) + A_{12}^R(-k) \right) \\ &= -\int_0^{\pi} dk \nabla_k \phi(k), \end{aligned} \tag{7.9}$$

and so

$$\begin{aligned} \exp\left[i \int_{-\pi}^{\pi} dk A_{12}^R(k) \right] &= \exp\left[-i \int_0^{\pi} dk \nabla_k \phi(k) \right] \\ &= \exp\left[-i \left(\phi(\pi) - \phi(0) \right) \right] \\ &= \prod_{i=1}^{2} \xi_1(\Gamma_i), \end{aligned} \tag{7.10}$$

where $\xi_1(\Gamma_i)$ is the eigenvalue of the sewing matrix, i.e., $B(\Gamma_i) = \xi_1(\Gamma_i) I_{2\times 2}$.

Next, we consider an inversion-invariant plane. As the occupied states may not be smooth over the whole plane, the sewing matrix also may not be smooth. The sewing matrix defined on C and D patches are related to the one defined on A and B patches as

$$B^{CD}(\mathbf{k}) = (t^{AC}(-\mathbf{k}))^{-1} B^{AB}(\mathbf{k}) t^{BD}(\mathbf{k}), \tag{7.11}$$

where A and C covers $-\mathbf{k}$, and B and D covers $\mathbf{k}$, and t^{AB} and t^{CD} are the transition functions defined by $|u^C_{n-\mathbf{k}}\rangle = t^{AC}_{mn}(-\mathbf{k})\,|u^A_{n-\mathbf{k}}\rangle$ and $|u^D_{n\mathbf{k}}\rangle = t^{BD}_{mn}(\mathbf{k})\,|u^B_{n\mathbf{k}}\rangle$. We require all the transition functions be orientation-preserving. Then, the above relation shows that the sewing matrix belongs to SO(2) everywhere on the plane because it belongs to SO(2) within the patches covering a TRIM. The symmetry constraint on F^R becomes

$$F^R(\mathbf{k}) = F^R(-\mathbf{k}). \tag{7.12}$$

The second Stiefel-Whitney class over the invariant plane is then given by

$$\begin{aligned}
\exp\left[i\pi w_2\right] &= \exp\left[\frac{i}{2}\int_{-\pi}^{\pi} dk_x \int_{-\pi}^{\pi} dk_y F^R_{12}(k_x,k_y)\right] \\
&= \exp\left[i\int_{0}^{\pi} dk_x \int_{-\pi}^{\pi} dk_y F^R_{12}(k_x,k_y)\right] \\
&= \exp\left[i\oint dk_y A^R_{12}(\pi,k_y) - i\oint dk_y A^R_{12}(0,k_y)\right] \\
&= \prod_{i=1}^{2}\xi_1(\Gamma_i)\left[\prod_{i=3}^{4}\xi_1(\Gamma_i)\right]^{-1} \\
&= \prod_{i=1}^{4}\xi_1(\Gamma_i),
\end{aligned} \tag{7.13}$$

where we applied the Stokes' theorem on a patch fully covering the half Brillouin zone to get the second line.

Next, we consider two non-orientable occupied bands. Because the invariant plane should be gapped in order that the second Stiefel-Whitney class is defined, $\xi(\Gamma_i)$ can be negative at an even number of TRIM. When ξ is negative at none or all the four TRIM, the occupied bands are orientable, which we have discussed. The remaining is the case where $\xi(\Gamma_i)$ is negative at two TRIM, which we take as Γ_1 and Γ_2. There are three configuration of inversion eigenvalues up to the permutation $\Gamma_1 \leftrightarrow \Gamma_2$ and $\Gamma_3 \leftrightarrow \Gamma_4$ and up to a band inversion between the

occupied bands. They are

$$\begin{array}{ccc} \Gamma_1\Gamma_2\Gamma_3\Gamma_4 & \Gamma_1\Gamma_2\Gamma_3\Gamma_4 & \Gamma_1\Gamma_2\Gamma_3\Gamma_4 \\ --++ & ++-- & +-+- \\ ++++ & ---- & -++- \end{array} \tag{7.14}$$

After removing all the accidental degeneracies, the lowest occupied band can be isolated by a band gap from the other band in all three configurations. In the first and second case, the second Stiefel-Whitney class for the occupied bands is trivial according to the Whitney sum formula. Here, the Whitney sum formula is $w_2(\mathcal{B}_1 \oplus \mathcal{B}_2) = w_{1\phi}(\mathcal{B}_1)w_{1\theta}(\mathcal{B}_2) - w_{1\theta}(\mathcal{B}_1)w_{1\phi}(\mathcal{B}_2)$ modulo two, where $\mathcal{B}_1$ and $\mathcal{B}_2$ is the bottom and top occupied bands. Because $w_1(\mathcal{B}_1) = 0$ for trivial $\mathcal{B}_1$, we find $w_2 = 0$. On the other hand, the second Stiefel-Whitney class is nontrivial in the last case according to the Whitney sum formula, because $(w_{1\phi}(\mathcal{B}_1), w_{1\theta}(\mathcal{B}_1), w_{1\phi}(\mathcal{B}_2), w_{1\theta}(\mathcal{B}_2)) = (\pi, \pi, 0, \pi)$ or $(0, \pi, \pi, 0)$ or their permutation by $\phi \leftrightarrow \theta$.

Let us notice that the second Stiefel-Whitney class is nontrivial only when there is an odd number of TRIM at which inversion eigenvalues for the two occupied bands are both -1. Thus, we can summarize the result for two occupied bands as

$$(-1)^{w_2} = \prod_{i=1}^{4} (-1)^{[N_{\mathrm{occ}}^{-}(\Gamma_i)/2]}, \tag{7.15}$$

where the bracket is the greatest integer function.

7.2.2 General occupied bands

We now extend the above derivation to the case with $N_{\mathrm{occ}} > 2$. We do this by decomposing occupied states into two-level blocks and applying the Whitney sum formula.

Let us consider $2N+1$ or $2N+2$ occupied bands with a non-negative integer N on an inversion-invariant plane. At each TRIM, we decompose the occupied bands into N pairs which have inversion eigenvalues $--$ or $++$ and the remaining band or bands through the band inversion only between the occupied bands. Also, we re-order the energy level of the occupied bands such that the remaining block is at the highest level. We have, for example, the following pattern. We have N blocks with degenerate inversion eigenvalues e.g.,

$$\begin{aligned} & \Gamma_1\Gamma_2\Gamma_3\Gamma_4 \\ 2N+0 &: -+-+ \\ 2N-1 &: -+-+ \\ & \vdots \\ 2 &: ++-- \\ 1 &: ++-- \end{aligned} \tag{7.16}$$

for the $1, 2, ..., 2N$th lowest energy level, and we have a remaining block at the highest energy level, which consists of one and two bands for $N_{\rm occ} = 2N+1$ and $2N+2$, respectively, e.g.,

$$\begin{aligned} \Gamma_1\Gamma_2\Gamma_3\Gamma_4 \qquad & \qquad \Gamma_1\Gamma_2\Gamma_3\Gamma_4 \\ 2N+1 : -++- \qquad & \qquad 2N+2 : -++- \\ & \qquad 2N+1 : +-+- \end{aligned} \tag{7.17}$$

where $\Gamma_1, ..., \Gamma_4$ are TRIM on the inversion-invariant plane. After this decomposition, the product of all inversion eigenvalues is positive within each of $N+1$ blocks. This is obvious for the lowest N blocks, and for the $N+1$ block it follows from that the band gap between the conduction and valence band is open. Hence, each block can be isolated from the other bands by removing all

the accidental degeneracies without changing the inversion eigenvalues. After lifting all the accidental degeneracies, the second Stiefel-Whitney class of the whole occupied bands is given by summing up the second Stiefel-Whitney class of $N+1$ blocks according to the Whitney sum formula [See Eq. (4.4)]. From the relation between the inversion eigenvalues and the second Stiefel-Whitney class for each block, we find that

$$(-1)^{w_2} = \prod_{i=1}^{4} (-1)^{[N_{\mathrm{occ}}^{-}(\Gamma_i)/2]}. \tag{7.18}$$

7.2.3 Z_2 monopole charge

Suppose that the band gap is open on two invariant planes which do not intersect each other [1]. In such a case, we can detect the Z_2 monopole charges in the Brillouin zone using the relation between the inversion eigenvalues and the second Stiefel-Whitney class. It is because the difference of the second Stiefel-Whitney classes measure the Z_2 monopole charges in the half-Brillouin zone. Let two planes $k_z = 0$ and $k_z = \pi$ be gapped for convenience. We have

$$\begin{aligned}
\exp\left[i\pi N_{mp}\right] &= \exp\left[i\pi\left(w_2(\pi) - w_2(0)\right)\right] \\
&= \prod_{i=1}^{4} (-1)^{[N_{\mathrm{occ}}^{-}(\Gamma_i)/2]} \left(\prod_{i=5}^{8} (-1)^{[n_{\mathrm{occ}}^{-}(\Gamma_i)/2]} \right)^{-1} \\
&= \prod_{i=1}^{8} (-1)^{[N_{\mathrm{occ}}^{-}(\Gamma_i)/2]},
\end{aligned} \tag{7.19}$$

where N_{mp} is the number of Z_2 monopoles in the half Brillouin zone. Eq. (7.19) can be intuitively understood as counting the number of double band inversions modulo two. Suppose we start with a trivial insulator whose inversion eigenvalues are all positive. In order to have $[N_{\mathrm{occ}}^{-}(\Gamma_i)/2]$ pairs of negative inversion

[1] This condition is not satisfied when $\prod_{i=1}^{8} \xi(\Gamma_i) = -1$ because the band gap is closed on at least one of the two plane according to Ref. [38] [See Eq. (7.5)].

eigenvalues at Γ_i, we need $[N^-_{\rm occ}(\Gamma_i)/2]$ times of double band inversions at Γ_i modulo two. As a double band inversion creates a pair of Z_2 monopoles in the Brillouin zone, it creates one Z_2 monopole in the half Brillouin zone in the presence of inversion symmetry. The parity of the number of Z_2 monopoles in the half Brillouin zone is then given by summing $[N^-_{\rm occ}(\Gamma_i)/2]$ over all TRIM. This is exactly what Eq. (7.19) shows.

Chapter 8

Topological Superconductivity

In this chapter, we study the superconductivity of spin-polarized electrons in centrosymmetric ferromagnetic metals. When spin-orbit coupling is negligible, which we assume, the system has spacetime inversion symmetry under the combination of effective spinless time reversal and spatial inversion. So, we can define the Stiefel-Whitney numbers in the system, and our results developed above can be applied here.

Recently, odd-parity superconductivity has received great attention due to their potential to realize topological superconductors (TSCs) [115–119]. Fu and Berg [120], and also Sato [121, 122] proposed a simple but powerful parity formula relating the parity configuration in the normal state and the topological property of the odd-parity superconducting state. The simplicity of the formula allows fast diagnosis of the topological nature of a superconducting state by just counting the number of Fermi surfaces, which greatly facilitates the search of TSCs in centrosymmetric materials.

One limitation of the Fu-Berg-Sato formula is that it can be applied only

to conventional first-order TSCs in which d-dimensional bulk topology supports gapless Majorana states on $(d-1)$-dimensional boundaries. However, recent studies on topological crystalline phases have uncovered higher-order TSCs whose d-dimensional bulk topology protects gapless Majorana fermions on the boundaries with dimensions lower than $(d-1)$ [55, 123–127]. In general, kth-order TSCs in d dimensions host $(d-k)$-dimensional boundary Majorana states. In the case of dth-order TSCs in d dimensions, Majorana zero modes (MZMs) exist at corners, which can be potentially useful for topological quantum computations [116–119].

Up to now, several interesting ideas have been proposed to realize 2D second-order TSCs in various different settings, such as using the superconducting proximity effect on quantum Hall insulators [128], quantum spin Hall insulators [126, 129,130], second-order topological insulators [131], Rashba semiconductors [132] and nanowires [133]; breaking time reversal symmetry of TSCs with helical Majorana edge states by applying external magnetic field [55,134–137] or attaching antiferromagnets [138]; and some other ideas [126, 136, 139–141]. In 3D, on the other hand, there are only few mechanisms proposed for realizing a third-order TSC such as applying magnetic field to a 3D second-order TSC with helical hinge modes [55]. For more systematic investigations of higher-order TSCs, a simple criterion for diagnosing higher-order band topology, similar to the Fu-Berg-Sato parity formula for first-order TSCs, is highly desired. Although some formulae for higher-order TSCs having gapless boundary states were proposed recently [142], the parity formula for dth-order TSCs hosting MZMs is still lacking.

In this chapter, we establish generalized parity formulae for higher-order TSCs and apply them to ferromagnetic metals where odd-parity superconductivity naturally arises. Using the generalized parity formulae, we classify all

possible spin-polarized band structures of centrosymmetric ferromagnetic metals that can realize inversion-protected higher-order TSC. From this analysis, we find doped ferromagnetic nodal semimetals as an ideal normal state that realizes higher-order TSCs. Explicitly, in 2D, odd-parity pairing of a doped Dirac semimetal (DSM) induces a 2D second-order TSC. In 3D, odd-parity pairing of a doped nodal line semimetal (NLSM) generates a nodal line superconductor with monopole charges. Furthermore, in the case of a doped monopole NLSM [5, 7], odd-parity pairing induces a 3D third-order TSC. These findings show that the combination of superconductivity and spin-polarized 2D and 3D nodal semimetals can be promising platforms for topological quantum computations using MZMs.

8.1 Symmetry and nodal structures

Let us first clarify the symmetry of the normal and superconducting states of ferromagnetic metals with inversion symmetry P_0 and classify the relevant nodal structures. We assume that an electron's spin is polarized along the z-direction. Also, we neglect spin-orbit coupling, but its influence is discussed later. In this setting, although time reversal symmetry $\mathcal{T} = i\sigma_y K$ is broken, the ferromagnetic metallic state is symmetric under the effective time reversal $T \equiv e^{i\pi\sigma_y/2}\mathcal{T} = K$ defined as the product of $\mathcal{T}$ and a 180° spin rotation around the y axis, $e^{i\pi\sigma_y/2}$. Here σ_y is a Pauli matrix for spin degrees of freedom, and K denotes the complex conjugation operator. Also, $P_0 = P_0^*$ because $[P_0, T] = 0$. Then, the system is invariant, locally at each momentum $\mathbf{k}$, under P_0T symmetry satisfying $(P_0T)^2 = 1$. Such a P_0T symmetric system belongs to the $\mathbf{k}$-local symmetry class AI+$\mathcal{I}$ proposed by Bzdusek and Sigrist [13], where the 1D and 2D topological phases are classified by Z_2 invariants [5, 13]. Here the 1D Z_2 invariant is the quantized Berry phase, which is the topological charge of 2D

Dirac points and also of 3D nodal lines. The 2D Z_2 invariant is the monopole charge of 3D nodal lines.

To describe the superconducting state, we introduce a $2N$-component Nambu spinor $\hat{\Psi}(\mathbf{k}) = [\hat{c}_{\uparrow\alpha}(\mathbf{k}), \hat{c}^\dagger_{\uparrow\beta}(\mathbf{k})]^T$, where $\hat{c}_{\uparrow\alpha}(\mathbf{k})$ $[\hat{c}^\dagger_{\uparrow\alpha}(\mathbf{k})]$ is an electron creation [annihilation] operator with spin up and orbital $\alpha = 1, \ldots, N$. The corresponding Bogoliubov-de Gennes (BdG) Hamiltonian can be written as $\hat{H} = \hat{\Psi}^\dagger H_{\rm BdG} \hat{\Psi}$, where

$$H_{\rm BdG} = \begin{pmatrix} h(\mathbf{k}) & \Delta(\mathbf{k}) \\ \Delta^\dagger(\mathbf{k}) & -h^T(-\mathbf{k}) \end{pmatrix}. \tag{8.1}$$

Here, $h(\mathbf{k})$ indicates the Hamiltonian for the normal state, and the pairing function $\Delta_{\alpha\beta}(\mathbf{k})$ with orbital indices $\alpha,\ \beta$ satisfies $\Delta_{\alpha\beta}(\mathbf{k}) = -\Delta_{\beta\alpha}(-\mathbf{k})$ because of the Fermi statistics of electrons. Since the pairing function forms an irreducible representation of the symmetry group, it can have either odd-parity $P_0\Delta(\mathbf{k})P_0^{-1} = -\Delta(-\mathbf{k})$ or even-parity $P_0\Delta(\mathbf{k})P_0^{-1} = +\Delta(-\mathbf{k})$.

In the weak-pairing limit, we can focus on the pairing at the Fermi energy E_F and define the corresponding pairing function as $\Delta_{E_F}(\mathbf{k})$. Then, $P_0\Delta_{E_F}(\mathbf{k})P_0^{-1} = \Delta_{E_F}(\mathbf{k})$ because Δ_{E_F} is a 1×1 matrix. The Fermi statistics $\Delta_{E_F}(\mathbf{k}) = -\Delta_{E_F}(-\mathbf{k})$ naturally shows that the pairing function satisfies the odd-parity condition

$$P_0\Delta_{E_F}(\mathbf{k})P_0^{-1} = -\Delta_{E_F}(-\mathbf{k}). \tag{8.2}$$

Therefore, in Eq. (8.1), we consider only odd-parity pairing functions that satisfy $P_0\Delta(\mathbf{k})P_0^{-1} = -\Delta(-\mathbf{k})$. The corresponding odd-parity BdG Hamiltonian is symmetric under inversion $P = \tau_z P_0$ which anticommutes with the particle-hole symmetry $C = \tau_x K$, where $\tau_{x,y,z}$ are Pauli matrices for the Nambu space. PT and CP symmetries satisfying $(PT)^2 = 1$ and $(CP)^2 = -1$, which show that the BdG Hamiltonian belongs to the $\mathbf{k}$-local symmetry class CI+$\mathcal{I}$ [13]. In this class, 2D Dirac points or 3D nodal lines can be protected as in the case of

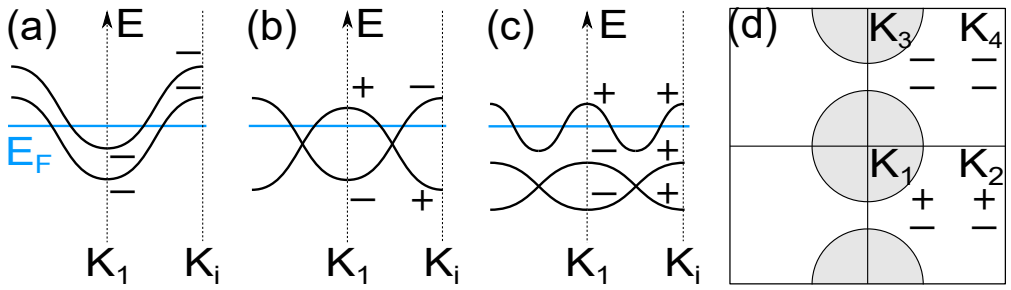

Figure 8.1 Band structure and parity configuration of spin-polarized metals leading to 2D second-order TSCs in the weak pairing limit. (a) Two electron-like (or hole-like) Fermi surfaces surrounding the same TRIM. (b) Doped DSM with $\nu_1 = 1$. (c) Normal state whose whole bands, including both occupied and unoccupied bands, have the higher-order topology with $\nu_2 = 1$. The horizontal axes in (a,b,c) schematically represent the 2D Brillouin zone: $\mathbf{K}_1 = (0, 0)$, and $\mathbf{K}_i$ indicates the other three TRIMs with the same parity configuration. $\pm$ represents the parity at TRIM. (d) The fourth way to obtain the higher-order TSCs. Here, the $\pm$ sign on the top (bottom) row at each TRIM represents the parity of the higher-energy (lower-energy) states. One (no) band is occupied in the gray (white) regions, and the boundaries show the relevant Fermi surfaces. From Ref. [25].

the class AI+$\mathcal{I}$. The only difference is that the 1D invariant is integer-valued in the class CI+$\mathcal{I}$, but this is irrelevant in our analysis below because we are only interested in the parity of the 1D invariant that can be related to the eigenvalues of P.

8.2 Nodal structure of TSC and parity formula

According to Eq. (8.2), an odd-parity pairing function $\Delta(\mathbf{k})$ changes its sign on the Fermi surfaces surrounding a time-reversal-invariant momentum (TRIM) so that an even number of nodes should appear at the points where the sign of $\Delta(\mathbf{k})$ changes. The number of nodal points can be related with the inversion parities of occupied bands using the idea proposed in Refs. [120–122] as follows. In 2D, the parity of the number of Dirac node pairs related by inversion can be

counted by the Z_2 invariant $\nu_1 \equiv \sum_{\mathbf{K}\in\mathrm{TRIM}} n_-^{\mathrm{o}}(\mathbf{K}) \mod 2$ [38], where $n_-^{\mathrm{o}}(\mathbf{K})$ is the number of occupied states with negative parity at $\mathbf{K}$. Here ν_1 can be understood as the number of band inversions at TRIM that create pairs of Dirac points, starting from the trivial phase with only positive-parity occupied states.

One can define a similar parity index ν_1^{BdG} for the BdG Hamiltonian as

$$\begin{aligned}\nu_1^{\mathrm{BdG}} &\equiv \sum_{\mathbf{K}\in\mathrm{TRIM}} n_-^{\mathrm{BdG;o}}(\mathbf{K}) \\ &= \sum_{\mathbf{K}\in\mathrm{TRIM}} n_-^{\mathrm{o}}(\mathbf{K}) + n_+^{\mathrm{u}}(\mathbf{K}) \\ &= \sum_{\mathbf{K}\in\mathrm{TRIM}} n^{\mathrm{u}}(\mathbf{K}) \mod 2, \end{aligned} \tag{8.3}$$

where $n_\pm^{\mathrm{o(u)}}$ is the number of occupied (unoccupied) states with $\pm$ parity in the normal state, $n^{\mathrm{u}} = n_+^{\mathrm{u}} + n_-^{\mathrm{u}}$, and $n_\pm^{\mathrm{BdG;o(u)}}$ is defined similarly for the BdG Hamiltonian with an odd-parity pairing function. The second line in Eq. (8.3) results from the odd-parity pairing, and the third line follows from $n_-^{\mathrm{o}}(\mathbf{K}) = n_-^{\mathrm{o}}(\mathbf{K}) + n_-^{\mathrm{u}}(\mathbf{K}) - n_-^{\mathrm{u}}(\mathbf{K}) = n_-^{\mathrm{o}}(\mathbf{K}) + n_-^{\mathrm{u}}(\mathbf{K}) + n_-^{\mathrm{u}}(\mathbf{K}) \mod 2$ together with $\sum_{\mathbf{K}} n_-(\mathbf{K}) = 0 \mod 2$ following from that, when all the bands are occupied, no band crossing exists at the Fermi level. Equation (8.3) shows that $\nu_1^{\mathrm{BdG}} = 1 \mod 2$ only when there exists an odd number of Fermi surfaces. This is consistent with the odd-parity condition of the pairing function $\Delta(\mathbf{k})$ on the Fermi surface in Eq. (8.2), which guarantees an odd number of Dirac node pairs in the superconducting state per each normal state Fermi surface enclosing a TRIM.

8.3 Generalized parity formula for second-order TSC in 2D

To derive the condition for higher-order superconductivity of spin-polarized electrons, let us introduce generalized parity formulae. According to the Dirac Hamiltonian formalism for inversion-protected higher-order topological phases [49, 55], we can obtain a higher-order TI by inverting 2^n bands at a TRIM starting from a topologically trivial phase. Here, n denotes a nonnegative integer. Therefore, counting the number of the simultaneous inversion of 2^n bands at TRIM leads to the following Z_2 index,

$$\nu_{2^n} \equiv \sum_{\mathbf{K}\in\mathrm{TRIM}} \left[\frac{n_-^{\mathrm{o}}(\mathbf{K})}{2^n}\right]_{\mathrm{floor}} \mod 2, \tag{8.4}$$

where $[m+a]_{\mathrm{floor}} = m$ for an integer m and $0 \le a < 1$. We can also introduce similar indices $\nu_{2^n}^{\mathrm{BdG}}$ for the BdG Hamiltonian by replacing $n_-^{\mathrm{o}}(\mathbf{K})$ by $n_-^{\mathrm{BdG;o}}(\mathbf{K})$. These indices characterize higher-order TSCs.

Let us first discuss the physical meaning of ν_2^{BdG} in 2D. Recently, it was shown that $\nu_2 = 1$ indicates the second-order topology of a PT-symmetric topological insulator with chiral symmetry, characterized by fractional corner charges on the boundary [14, 18, 49]. A straightforward extension of this idea shows that $\nu_2^{\mathrm{BdG}} = 1$ characterizes a second-order TSC with Majorana corner modes. Explicitly, ν_2^{BdG} can be decomposed as

$$\begin{aligned}\nu_2^{\mathrm{BdG}} = &\sum_{\mathbf{K}\in\mathrm{TRIM}} \left[\frac{n^{\mathrm{u}}(\mathbf{K})}{2}\right]_{\mathrm{floor}} + \sum_{\mathbf{K}\in\mathrm{TRIM}} n_-^{\mathrm{o}}(\mathbf{K}) \\ &+ \sum_{\mathbf{K}\in\mathrm{TRIM}} \left[\frac{n_-(\mathbf{K})}{2}\right]_{\mathrm{floor}} + \sum_{\mathbf{K}\in\mathrm{TRIM}} \delta_2(\mathbf{K}) \mod 2,\end{aligned} \tag{8.5}$$

where $\delta_2(\mathbf{K}) = [n^{\mathrm{u}}(\mathbf{K}) + 1]n_-(\mathbf{K}) \mod 2$. In Eq. (8.5), the first term counts the parity of the number of "double Fermi surfaces", that is, two electron-like (or hole-like) Fermi surfaces enclosing the same TRIM, in the normal state. The

second term is ν_1 for the occupied bands in the normal state and the third term is ν_2 when all bands are occupied in the normal state. Finally, the last term counts the number of TRIM with an even number of unoccupied state and an odd number of negative-parity eigenstates. Figures 8.1(a-d) show four different normal state band structures leading to $\nu_2^{\mathrm{BdG}} = 1$ in weak-pairing limit, which arise from the nontrivial value of the first, second, third, and fourth terms in Eq. (8.5), respectively.

The analysis of Eq. (8.5) becomes much simpler in systems with an inversion-symmetric unit cell, where all atoms in a unit cell can be adiabatically shifted to its center without breaking inversion symmetry. In this case, the third term in Eq. (8.5) vanishes because an inversion-symmetric unit cell gives a topologically trivial state with $\nu_2 = 1$ when all bands are occupied. Similary, the zero Berry phase of the whole bands makes the fourth term vanish.

Then, there remain two different channels leading to $\nu_2^{\mathrm{BdG}} = 1$: one is odd-parity pairing in a metal with double Fermi surfaces, and the other is odd-parity pairing in a doped DSM, whose nontrivial band topology arises from the first and second terms in Eq. (8.5), respectively. In general, the former induces nodal superconductivity rather than a fully gapped TSC. This is because each of the two Fermi surfaces encloses a TRIM so that an odd-parity pairing function accompanies the sign reversal at two points on the Fermi surface, generating Dirac nodes. A strong pairing is required to get a fully gapped superconducting state via pair annihilations of Dirac nodes, unless the system is fine-tuned so that the two Fermi surfaces are very close to each other. On the other hand, even weak pairing generates a fully gapped superconducting state in doped DSMs because two disconnected Fermi surfaces, each centered at a generic momentum, are paired in this case.

8.4 Higher-order TSCs in 3D and further generalization

In 3D, $\nu_1 = 1$ indicates an odd number of nodal lines [38], and $\nu_2 = 1$ indicates an odd number of pairs of monopole nodal lines in the Brillouin zone [7,42]. Similarly, $\nu_1^{\rm BdG} = 1$ ($\nu_2^{\rm BdG} = 1$) indicates a superconductor with an odd number of nodal lines (monopole nodal line pairs). In particular, the superconductor with a monopole nodal line pair exhibits the second-order topological property and carries anomalous hinge Majorana states, as in the case of chiral-symmetric monopole NLSMs [18]. Similar to 2D cases, the most promising way to get $\nu_2^{\rm BdG} = 1$ is the process with a nontrival second term in Eq. (8.5), which corresponds to doping spin-polarized NLSMs. The third term in Eq. (8.5) always vanishes when the whole bands are fully considered. Also the fourth term vanishes if we take an inversion-symmetric unit cell as in 2D. In the case of the first term, it may be relevant in a strong pairing limit. A double Fermi surface normally generates a superconducting state with nodal lines carrying trivial monopole charges from each Fermi surface. When the pairing amplitude is sufficiently strong, however, the two trivial nodal lines may recombine and turn into two monopole nodal lines. We note that the same mechanism corresponding to the second term in Eq. (8.5) was also proposed in Ref. [13] for systems with SU(2) spin rotation symmetry.

The above formulation can be generalized further to $\nu_{2^n}^{\rm BdG}$ with an arbitrary n:

$$\begin{aligned}\nu_{2^n}^{\rm BdG} = &\sum_{\mathbf{K}\in{\rm TRIM}} \left[\frac{n^{\rm u}(\mathbf{K})}{2^n}\right]_{\rm floor} + \sum_{\mathbf{K}\in{\rm TRIM}} \left[\frac{n_-^{\rm o}(\mathbf{K})}{2^{n-1}}\right]_{\rm floor} \\ &+ \sum_{\mathbf{K}\in{\rm TRIM}} \left[\frac{n_-(\mathbf{K})}{2^n}\right]_{\rm floor} + \sum_{\mathbf{K}\in{\rm TRIM}} \delta_{2^n}(\mathbf{K}) \mod 2, \end{aligned} \tag{8.6}$$

where the definition of $\delta_{2^n}(\mathbf{K})$ is given in the Appendix C. In particular,

$\nu_4^{\mathrm{BdG}} = 1$ characterizes the third-order TSC in 3D [49]. By the same reason discussed above, one can show that the best way to get a fully gapped superconductivity with $\nu_4^{\mathrm{BdG}} = 1$ is to use the process related with the second term in Eq. (8.6), which can be achieved by doping a monopole NLSM (see the Supplemental Material for details [143]). To sum up, in ferromagnetic systems with an inversion-symmetric unit cell, doped nodal semimetals are the best normal state to get a higher-order TSC in the weak-pairing limit.

8.5 Lattice model

We demonstrate our theory by using simple tight-binding models defined on rectangular or orthorombic lattices. We construct three models in which the spin-polarized normal states are a 2D DSM, a 3D NLSM, and a 3D monopole NLSM, respectively. When an odd-parity superconducting pairing is introduced, we show that the three nodal semimetals turn into a 2D second-order TSC, a 3D monopole nodal line superconductor, and a 3D third-order TSC, respectively.

First, a 2D DSM can be described by the nearest-neighbor tight-binding Hamiltonian for s and p_x orbitals as

$$h = -\mu + 2t \sin k_x \sigma_y + (M - 2t \cos k_x - 2t \cos k_y)\sigma_z, \tag{8.7}$$

where the Pauli matrices $\sigma_{y,z}$ describe the orbital degrees of freedom with $\uparrow$ ($\downarrow$) indicating a s (p_x) orbital. The corresponding band structure exhibits two Dirac points on the $k_x = 0$ line when $0 < M/t < 4$ at the energy $E = -\mu$. To induce superconductivity, we consider the following interaction term $H_{\mathrm{int}} = -U \sum_{i,\sigma\neq\sigma'} n_{i,\sigma} n_{i,\sigma'} - V \sum_{\langle i,j\rangle,\sigma} n_{i,\sigma} n_{j,\sigma}$ where U (V) indicates the on-site interorbital (nearest-neighbor intraorbital) interaction, which is to be treated by mean-field approximation. The resulting odd-parity pairing leads to a fully gapped TSC whose second order band topology is clearly demon-

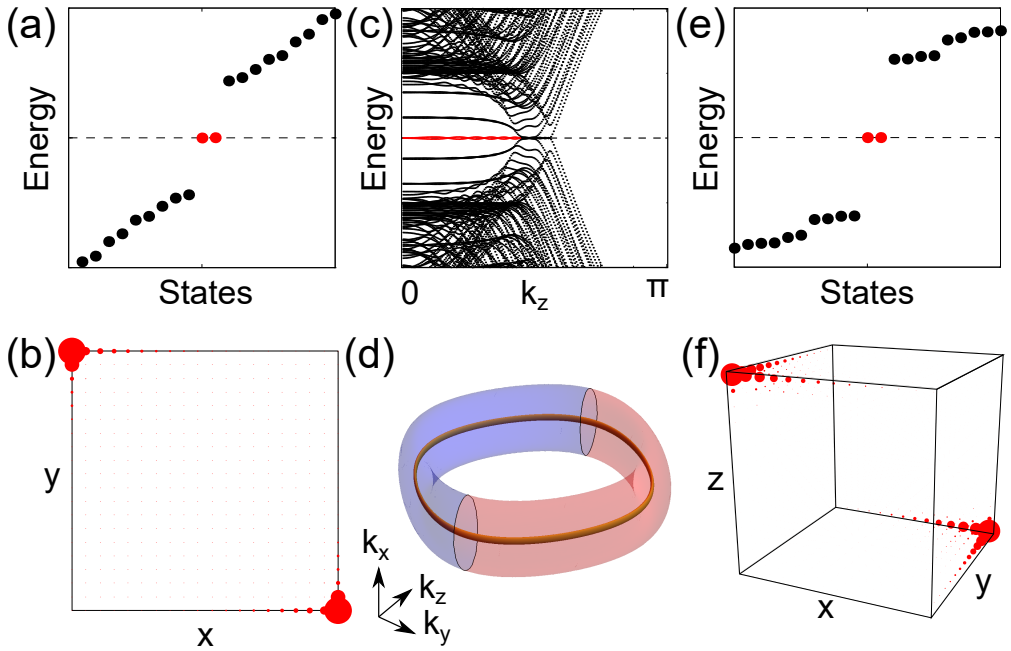

Figure 8.2 Higher-order topological superconductivity from lattice models. (a,b) 2D second-order TSC obtained by adding an odd-parity pairing function to the doped 2D DSM described in Eq. (8.7). (a) Energy spectrum on a finite-size lattice. (b) Probability density of a Majorana zero mode (c,d) Monopole nodal line superconductor derived from a doped 3D NLSM. (c) Energy spectrum of the system, finite-sized along x and y directions. (d) Nodal structure in the Brillouin zone. The torus indicates the Fermi surface enclosing a nodal line (thick gold line) in the normal state. The blue (red) color indicates the region where the pairing function has positive (negative) sign. Two monopole nodal loops appear at the interection, where the pairing function changes its sign. (e,f) 3D third-order TSC derived from a doped 3D monopole NLSM (e) Energy spectrum on a finite-size lattice. (f) Probability density of a Majorana zero mode. From Ref. [25].

strated in Fig. 8.2(a,b). Vetically stacking the 2D DSM and introducing interlayer hopping, described by $-2t\cos k_z\sigma_z$, we obtain the Hamiltonian for a 3D NLSM. Also, by further adding p_y and d_{xy} orbitals at each lattice site and introducing nearest-neighbor hopping, we obtain a 3D monopole NLSM. Adding an odd-parity pairing function in these NLSMs leads to a 3D monopole nodal

line superconductor and a 3D third-order TSC whose topological properties are demonstarted in Fig. 8.2(c-f). Detailed information about the tight-binding models is given in the Supplemental Material [143].

8.6 Discussions

We first discuss the effect of the inversion asymmetry of the unit cell. For instance, in the Kagome lattice, the unit cell always breaks inversion symmetry if all atoms are required to be strictly within the unit cell. One may choose a unit cell, invariant under inversion up to lattice translations, only when the atoms in a unit cell are located on its boundary. In this case, $\nu_2 = 1$ when each atom is occupied by one electron, so the third term in Eq. (8.5) is nontrivial [143] for a three-band tight-binding model. Then, we have $\nu_2^{\mathrm{BdG}} = 0$ even when the normal state is a doped DSM. However, this does not mean that MZM is absent on the boundary. In fact, one can show that MZMs exist (do not exist) when $\nu_2^{\mathrm{BdG}} = 0$ ($\nu_2^{\mathrm{BdG}} = 1$) in constrast to systems having inversion-symmetric unit cell. To obtain more conventional bulk-boundary correspondence where $\nu_2^{\mathrm{BdG}} = 1$ always indicates the existence of MZMs independent of symmetry of the unit cell, one may define a reference trivial phase of the TSC as the limit $\mu \to -\infty$ where all electrons are unoccupied in the normal state as proposed in [144]. This gives a well-defined trivial phase for TSCs because Majorana fermions are confined to form electrons in such a limit: $|\mu|$ serves as the binding energy for Majorana fermions because $\mu c_{\mathbf{x}}^\dagger c_{\mathbf{x}} = 2i\mu\gamma_{1\mathbf{x}}\gamma_{2\mathbf{x}}$ at each site $\mathbf{x}$ [145], where Majorana operators $\gamma_{1,2}$ are defined from the electron annihilation operator $c_{\mathbf{x}} = \gamma_{1\mathbf{x}} + i\gamma_{2\mathbf{x}}$.

Next, let us discuss the effect of spin-orbit coupling. When spin-orbit coupling is included, T symmetry is broken because the electron's spin cannot rotate freely independent of the orbital degrees of freedom. Since the protec-

tion of the nodal structures in both normal and superconducting states requires the combination of time reversal and inversion symmetries, the nodal structures become unstable when spin-orbit coupling exists. However, our formula in Eq. (8.6) is still applicable as long as inversion symmetry is preserved. Accordingly, a gapped higher-order TSC can still survive if the parity configuration does not change due to spin orbit coupling, since their topology can be protected by inversion symmetry only. In the case of the monopole nodal line superconductor, the nodes are fully gapped when T symmetry is broken due to spin-orbit coupling. The resulting gapped superconductor is a second-order TSC hosting chiral hinge states [7, 55, 146]. In fact, in the normal state, NLSM transforms to a Weyl semimetal by spin-orbit coupling as long as the parity configuration does not change. This means that, when spin-orbit coupling exists, what we observe is the transition from a Weyl semimetal to a fully gapped second-order TSC.

One way to realize spin-triplet pairing in 2D ferromagnetic nodal semimetals is to use a superconductor-ferromagnet-superconductor heterostructure with inversion symmetry. Here, we can use conventional spin-singlet s-wave superconductors and a ferromagnet with in-plane magnetization. After spin-singlet Cooper pairs penetrate into the ferromagnet, they can turn into spin-triplet Cooper pairs because of the spin polarization in the ferromagnet [147]. In 3D, on the other hand, an intrinsic superconducting pairing is required because the proximity effect is not effective. In fact, there are several materials where the coexistence of ferromagnetism and superconductivity is reported including, uranium-based materials UGe_2, URhGe, UCoGe, UTe_2 [148–154], and more recently proposed twisted double bilayer graphene [155–157]. We hope that our work stimulates the research on higher-order TSC in ferromagnets. This will open a new route to Majorana quantum computations, where ferromag-

netic nodal semimetals with spin-polarized band crossing serve as platforms for higher-order TSCs.

Finally, let us briefly comment on the extension of our result to other symmetry classes. We note that our parity formula Eq. (8.4) is generally applicable to any odd-parity superconductors, while we focus on ferromagnetic systems with effective time reversal symmetry since odd-parity pairing is natural in these systems. Furthermore, we expect that nodal semimetals required by eigenvalues of symmetry operator G can lead to a G-protected dth-order TSCs, which can be shown by extending Eq. (8.4) to eigenvalues of G, as is outlined in [142] for kth-order TSCs with $k < d$. We leave more detailed theoretical analysis for futur

Chapter 9

Discussion

The Stiefel-Whitney classes are examples of characteristic classes, which are the cohomology classes associated to vector bundles, describing how the corresponding vector bundle is twisted [10, 11]. There are mainly four different types of characteristic classes known up to now: Chern classes, Stiefel Whitney classes, Euler Classes, and Pontryagin classes [10, 11]. While the idea of Chern classes and associated topological invariants, such as Chern numbers, mirror or spin Chern numbers, Fu-Kane invariants, have been widely applied to condensed matter physics, the implication of the other characteristic classes in the context of condensed matter physics is not well established yet. In this paper, we have reviewed the recent progress in the study of topological physics associated with Stiefel-Whitney numbers. More explicitly, we showed that the first Stiefel-Whitney number is equivalent to the quantized Berry phase so that the nontrivial first Stiefel-Whitney number w_1 indicates either a 1D insulator with quantized charge polarization or a stable Dirac point (nodal line) in 2D Dirac semimetals (3D nodal line semimetals) in systems with spacetime inversion

symmetry I_{ST}. Moreover, we proved that the second Stiefel-Whitney number not only characterizes the monopole charge of nodal lines in I_{ST}-symmetric systems but also serves as a well-defined 2D topological invariant characterizing a 2D Stiefel-Whitney insulator. This idea is further extended to 3D systems with $I_{\mathrm{ST}} = PT$ and $I_{\mathrm{ST}} = C_{2z}T$ leading to the 3D weak and strong Stiefel-Whitney insulators, respectively. However, materials that realize 2D Stiefel-Whitney insulator and 3D strong Stiefel-Whitney insulator composed of spinless fermions are still lacking, which provides new research opportunities to find novel topological materials and phenomena.

One important research direction to pursue is to investigate the physical responses in topological phases characterized by the second Stiefel-Whitney number. While we have throughly studied the topological nature of the second Stiefel-Whitney number through band theory, the studies have been restricted to the study of band structures. It is now definitely an important issue to reveal the characteristic physical responses to electric, magnetic, optical, and thermal perturbations of Stiefel-Whitney insulators and monopole nodal line semimetals. Since the Stiefel-Whitney insulator belongs to the category of fragile topological insulators or obstructed atomic insulators, this study would be able to be generalized to the constructin of a response theory for general fragile topological and obstructed atomic insulators. Only after we understand the responses, we will be able to say that we really understand those topological materials.

Also, as briefly explained, I_{ST}-symmetric two-band systems in 2D can be characterized by another characteristic class, so-called the Euler class. The Euler class is an integer topological invariant classifying real orientable two-band systems. As discussed before, a two-band system with a nonzero Euler invariant e_2 has fragile band topology and supports corner charges. In fact, an Euler

insulator with $e_2 \neq 0$ has an intriguing topological properties which are not discussed in this review article. If an additional trivial band is coupled to the original two-band system and band crossing happens between them, the newly generated Dirac points play the role of the source of π Berry phase with a Dirac string in between, which strongly affects the braiding properties of the original Dirac points. Such a nontrivial braiding is a manifestation of the non-abelian topological charge of real wave functions, which is discussed thoroughly in Ref. [14, 158]. To unveil novel topological physics associated with other characteristic classes is definitely one important issue for future research.

Appendix A

Reality condition from spacetime inversion symmetry

Here, we show that $I_{\rm ST}$ symmetry imposes the reality condition on the Hamiltonian with a suitable choice of basis. Since $I_{\rm ST}$ does not change momentum, we make the momentum dependence of the Hamiltonian implicit in the following to simpilfy the notation.

Let $\{|\alpha\rangle, |\beta\rangle, \ldots\}$ be the basis for the Hilbert space we consider. Then, $I_{\rm ST}$ symmetry condition $I_{\rm ST} H I_{\rm ST}^{-1} = H$ in this basis becomes

$$\langle\alpha|H|\beta\rangle = \langle\alpha|PT|\gamma\rangle\langle\gamma|H|\delta\rangle\langle\delta|PT|\beta\rangle = [\langle\alpha|I_{\rm ST}|\gamma\rangle][\langle\gamma|H|\delta\rangle]^*[\langle\delta|I_{\rm ST}|\beta\rangle]^*. \tag{A.1}$$

We have the reality condition $\langle\alpha|H|\beta\rangle = \langle\alpha|H|\beta\rangle^*$ when $\langle\alpha|I_{\rm ST}|\gamma\rangle = \delta_{\alpha\gamma}$.

Note that it is always take a basis where $\langle\alpha|I_{\rm ST}|\gamma\rangle = \delta_{\alpha\gamma}$. When $I_{\rm ST}|\alpha\rangle = e^{i\phi_\alpha}|\alpha\rangle$, we can define a $I_{\rm ST}$-invariant state $e^{i\phi_\alpha/2}|\alpha\rangle$. When $I_{\rm ST}|\alpha\rangle$ and $|\alpha\rangle$ are linearly independent, we can define two linearly independent $I_{\rm ST}$-invariant states as $|u_\alpha^+\rangle = \frac{1}{2}(|\alpha\rangle + I_{\rm ST}|\alpha\rangle)$ and $|u_\alpha^+\rangle = \frac{1}{2i}(|\alpha\rangle - I_{\rm ST}|\alpha\rangle)$.

Therefore, if we take an I_{ST}-invariant basis $\{|\alpha\rangle, |\beta\rangle, \ldots\}$ through this procedure, we find that I_{ST} symmetry imposes that the Hamiltonian matrix elements in this basis are real, i.e., $\langle\alpha|H|\beta\rangle = \langle\alpha|H|\beta\rangle^*$.

Appendix B

Alternative formulation of Stiefel-Whitney numbers using homotopy theory

In this Appendix, we study the homotopy classification of symmetry representations to describe the bulk topological invariants protected by spacetime inversion I_{ST} symmetry. We define topological invariants as obstructions to having smooth Bloch wave functions compatible with a momentum-independent symmetry representation. When the Bloch wave functions are required to be smooth, the information on the band topology is contained in the symmetry representation. This implies that the d-dimensional homotopy class of the unitary matrix representation of the symmetry operator corresponds to the d-dimensional topological invariants. Here, we prove that the second Stiefel-Whitney number, a two-dimensional topological invariant protected by I_{ST}, is the homotopy invariant that characterizes the second homotopy class of the matrix representation of I_{ST}.

B.1 Homotopy groups of the sewing matrix

Let us begin by studying general aspects of the homotopy groups of the sewing matrix G for I_{ST}. G is defined as

$$G_{mn}(\mathbf{k}) = \langle u_{mI_{\mathrm{ST}}\mathbf{k}} | I_{\mathrm{ST}} | u_{n\mathbf{k}} \rangle \,, \tag{B.1}$$

where $I_{\mathrm{ST}}\mathbf{k} = (k_x, k_y) = \mathbf{k}$ and $|u_{n\mathbf{k}}\rangle$ is the cell-periodic part of a Bloch state. We are interested in the ground state of the system and study the topology of the occupied states, so hereafter we assume that m and n run over the indices of occupied bands. Since $(I_{\mathrm{ST}})^2 = (I_{\mathrm{ST}})^2 T^2 = 1$ in both spinless and spinful systems, G satisfies

$$G_{mn}(\mathbf{k}) = G_{nm}(\mathbf{k}). \tag{B.2}$$

Under a gauge transformation $|u_{n\mathbf{k}}\rangle \to |u'_{n\mathbf{k}}\rangle = U_{mn}(\mathbf{k}) \, |u_{m\mathbf{k}}\rangle$, the sewing matrix transforms as

$$G_{mn}(\mathbf{k}) \to G'_{mn}(\mathbf{k}) = [U^\dagger(\mathbf{k}) G(\mathbf{k}) U^*(\mathbf{k})]_{mn}, \tag{B.3}$$

where $G'_{mn}(\mathbf{k}) = \langle u'_{m\mathbf{k}} | I_{\mathrm{ST}} | u'_{n\mathbf{k}} \rangle$. If we choose smooth wave functions for occupied states, the corresponding sewing matrix also becomes smooth. The nontrivial homotopy class of G characterizes the obstruction to taking a uniform representation $G(\mathbf{k}) = G_0$ independent of $\mathbf{k}$.

Note that $G^T(\mathbf{k}) = G(\mathbf{k})$ according to Eq. (B.2). Such a symmetric unitary matrix can be written as

$$G(\mathbf{k}) = U_G(\mathbf{k}) U_G^T(\mathbf{k}), \tag{B.4}$$

where U_G is a unitary matrix describing a unitary transformation from a smooth gauge to a real gauge. As a redefinition $U_G(\mathbf{k}) \to O(\mathbf{k}) U_G(\mathbf{k})$ for any $O(\mathbf{k}) \in$

$O(N)$ does not change $G(\mathbf{k})$, we obtain

$$G(\mathbf{k}) \in U(N)/O(N), \tag{B.5}$$

on I_{ST}-invariant planes, where N denotes the number of occupied bands.

Since a nontrivial homotopy class of $G(\mathbf{k})$ is an obstruction to taking a constant symmetry representation, it classifies possible topological phases for N occupied bands. Since a smooth gauge transformation can change the homotopy class of G, one should carefully identify the homotopy classes that are related to each other by gauge transformations, to get a well-defined classification of topological phases. This should be consistent with the classification of the Hamiltonian space. In fact, we show below that

$$\frac{\pi_d\left[U(N)/O(N)\right]}{\mathrm{GaugeDOF}} \simeq \pi_d\left[\frac{O(N+M)}{O(N)\times O(M)}\right]_{M\to\infty}, \tag{B.6}$$

where $d = 1, 2$ [1], GaugeDOF is the image of the map $j^* : \pi_d[U(N)] \to \pi_d[U(N)/SO(N)]$ that is induced by the projection $j : U(N) \to U(N)/O(N)$, and $O(N+M)/[O(N)\times O(M)]$ is the classifying space of the real (i.e., I_{ST}-symmetric) Hamiltonians for N occupied and M unoccupied bands [13].

The above equivalence can be explicitly shown in two steps. First, we use that

$$\pi_d\left[\frac{O(N+M)}{O(N)\times O(M)}\right]_{M\to\infty} \simeq \pi_{d-1}[O(N)], \tag{B.7}$$

which states that the d-dimensional topological phase described by a real Hamiltonian is characterized by the $(d-1)$-th homotopy class of the transition function for real wave functions [10, 11, 40]. Then, we use the equivalence between

[1] We focus on $d = 1, 2$ here because we consider I_{ST} symmetry. However, this equation can be extended to higher-dimensional systems with PT symmetry with $(PT)^2 = 1$. In general, it is valid for any $d \neq 4n$ for a positive integer n as shown in Appendix B.4. When $d = 4n$ for some positive integer n, the band topology is characterized by the $2n$-th Chern class, so the nontrivial band topology does not require PT symmetry and persists without the symmetry. Therefore, the classification of the sewing matrix does not give the full classification of band topology in the case.

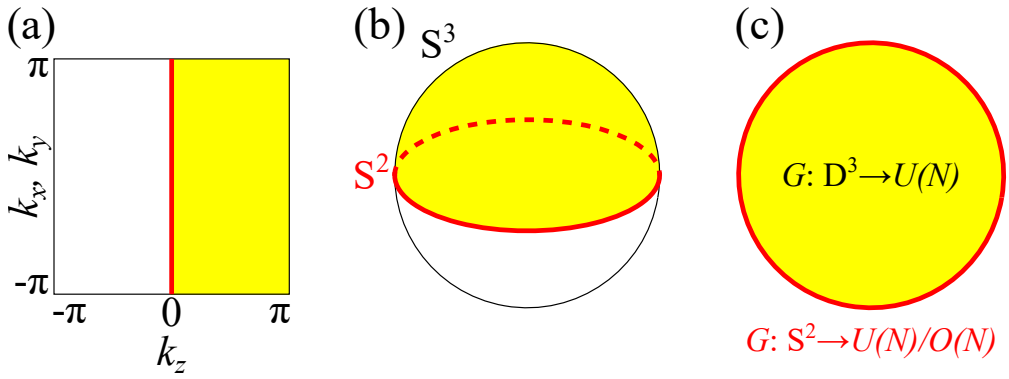

Figure B.1 Effective domain for the sewing matrix. (a) A plane representing the 3D Brillouin zone. The yellow region shows the effective Brillouin zone, and the red region with $k_z = 0$ is a $I_{\rm ST}$-invariant plane. The $k_z = \pi$ plane is assumed to be topologically trivial. (b) A 3-sphere equivalent to the 3D Brillouin zone. (c) The sewing matrix G in the yellow region and on its boundary (red). From Ref. [23].

the formalism in the smooth gauge and that in the real gauge:

$$\frac{\pi_d\left[U(N)/O(N)\right]}{\text{GaugeDOF}} \simeq \pi_{d-1}[O(N)], \tag{B.8}$$

where $d = 1, 2$, which can be derived from the exact sequence of homotopy groups [See Appendix B.4]. We demonstrate the relation between the smooth gauge and the real gauge in more detail for $d = 1, 2$ in the following sections B.2 and B.3, respectively.

B.2 The first homotopy class

Here, we review the correspondence between the 1D winding number of G in a smooth gauge and the first Stiefel-Whitney number w_1 in a real gauge [7], since the same idea is used to derive the correspondence between the second homotopy class of G and the second Stiefel-Whitney number in the next section.

Let us suppose that $|u_{n\mathbf{k}}\rangle$ is smooth and the sewing matrix G is defined in this basis. Then, we perform a gauge transformation to get new basis states

$|\tilde{u}_{nk}\rangle = U_{mn}(k)\,|u_{mk}\rangle$ such that $\tilde{G}(k) = U^\dagger(k)G(k)U^*(k)$ and $U(k)$ is smooth for $0 < k < 2\pi$, where $0 \le k < 2\pi$ parametrizes a closed loop in the $I_{\rm ST}$-invariant plane. If we require the reality condition $\tilde{G}(k) = 1$ for the new basis, we have $\det[U^\dagger(k)G(k)U^*(k)] = \det\tilde{G}(k) = 1$, so $\partial_k \log\det U(k) = \frac{1}{2}\partial_k \log\det G(k)$. We have the transition function $t_{mn} \equiv \langle\tilde{u}_{m0}|\tilde{u}_{n2\pi}\rangle = U^*_{pm}(0)U_{pn}(0+2\pi)$ since $\langle u_{p0}|u_{q2\pi}\rangle = \delta_{pq}$ due to the smoothness of the original basis. Its determinant is given by the winding number of G, which we write as w, namely, $\det t = \det[U^*(0)U(2\pi)] = \exp[\int_0^{2\pi}\partial_k \log\det U(k)] = \exp[\frac{1}{2}\int_0^{2\pi}\partial_k \log\det G(k)] = (-1)^w$. As the first Stiefel-Whitney number w_1 is defined by $(-1)^{w_1} = \det t$, we have $w_1 = w$ modulo 2.

The above construction shows the relation Eq. (B.8). Here, $\det t = \pm 1$ characterizes $\pi_0[O(N)]$ because $t \in O(N)$, and $\exp[\int_0^{2\pi}\partial_k \log\det U(k)] = \pm 1$ characterizes the gauge-invariant part of $\pi_1[U(N)/O(N)]$. Let us explain more about this. Although U is not periodic when $\det t = -1$ because then $\det U$ is antiperiodic, U is periodic as an element of $U(N)/O(N)$ (recall $U(2\pi) = U(0)t$). Smooth gauge transformations can change the winding number of U, but it does not change the periodic condition of U. Therefore, among nontrivial elements in $\pi_1[U(N)/O(N)]$, only the loops along which $\det U$ changes sign is robust against gauge transformations.

B.3 The second homotopy class

In this section, we show that the second homotopy class of G in a smooth gauge corresponds to the second Stiefel-Whitney number in a real gauge. Below we begin with the definition of the second Stiefel-Whitney number in a real gauge, and then go to a smooth gauge. The gauge transformation matrix is associated with the sewing matrix by Eq. (B.4).

We take a real gauge and cover the Brillouin zone torus with two patches A

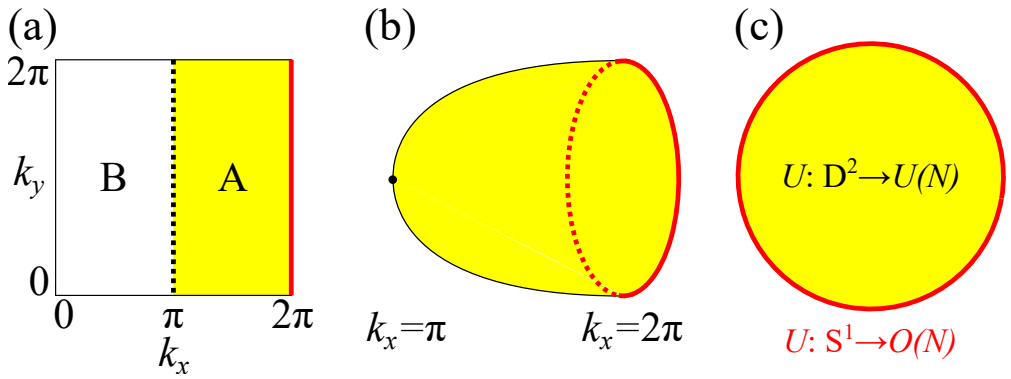

Figure B.2 Gauge transformation from a real to a smooth complex gauge in a $I_{\rm ST}$-invariant plane. (a) $I_{\rm ST}$-invariant 2D Brillouin zone covered by two patches A and B in a real gauge. (b) The patch A whose $k_x = \pi$ line is contracted to a point. (c) The gauge transformation matrix U on the patch A. From Ref. [23].

and B, overlapping on the lines $k_x = 0$ and $k_x = \pi$ [See Fig. B.2(a)]. When the first Stiefel-Whitney numbers are nontrivial along both k_x and k_y directions, we should introduce more patches so that there exist discontinuous transitions along the k_y direction [7]. However, we can always Dehn twist the Brillouin zone in those cases as shown in Fig. B.3 such that only one cycle has nontrivial w_1 at most, and we take the nontrivial cycle to be along the k_x direction [7]. We assume that such a Dehn twist is done. Also, we take the transition function at $k_x = \pi$ to be trivial. That is, we require that real occupied states $|\tilde{u}_{n\mathbf{k}}\rangle$ are smooth within the patches, but there can exist a nontrivial transition function on the equator defined by

$$t^{AB}_{mn}(k_y) \equiv \langle \tilde{u}^{A}_{m(2\pi,k_y)} | \tilde{u}^{B}_{n(0,k_y)} \rangle \,, \tag{B.9}$$

which is an element of the orthogonal group $O(N)$ for N occupied bands. The second Stiefel-Whitney number w_2 is defined by the 1D winding number of the transition function t^{AB} modulo 2.

Then, we consider a gauge transformation to smooth states $|u_{n(k_x,k_y)}\rangle$ via

$$\begin{aligned} |u_{n(k_x,k_y)}\rangle &= U_{mn}(k_x,k_y)\,|\tilde{u}^A_{m(k_x,k_y)}\rangle\,,\ \pi \le k_x \le 2\pi, \\ |u_{n(k_x,k_y)}\rangle &= U_{mn}(k_x,k_y)\,|\tilde{u}^B_{m(k_x,k_y)}\rangle\,,\ 0 \le k_x \le \pi, \end{aligned} \tag{B.10}$$

where $U(k_x,k_y)$ is smooth for $0 \le k_x, k_y \le 2\pi$. The gauge transformation matrix U satisfies

$$\begin{aligned} t^{AB}_{mn}(k_y) &= \langle \tilde{u}^A_{m(2\pi,k_y)} | \tilde{u}^B_{n(0,k_y)} \rangle \\ &= U_{mp}(2\pi,k_y)\,\langle u_{p(2\pi,k_y)} | u_{q(0,k_y)} \rangle\, U^*_{nq}(0,k_y) \\ &= U_{mp}(2\pi,k_y)\delta_{pq}U^*_{nq}(0,k_y), \end{aligned} \tag{B.11}$$

where we used that $|u_{n\mathbf{k}}\rangle$ is smooth in the last line. By choosing a gauge $U(0,k_y) = 1$, we have

$$U(2\pi,k_y) = t^{AB}(k_y) \in O(N). \tag{B.12}$$

We further require that $U(\pi,k_y)$ is independent of k_y, i.e.,

$$U(\pi,k_y) = U_0 \in U(N), \tag{B.13}$$

as shown in Fig. B.2. It is possible to take this gauge because the 1D topological invariant, the first Stiefel-Whitney number, is trivial along the k_y direction.

Now, the information on the wave function topology, encoded in the transition function t^{AB} in a real gauge, is reflected in the unitary matrix U under the constraint of Eq. (B.12). Since U is constant on $k_x = 0$ and $k_x = \pi$ lines, the lines can be shrunk to a point as long as topology is concerned. After the shrinking, the B region becomes a sphere, and the A region becomes a cap as shown in Fig. B.2(b). All possible Us are homotopically equivalent in the region B because they are classified by the homotopy group $\pi_2[U(N)] = 0$. Therefore, we only need to study the homotopy class of U on the region A. The homotopy

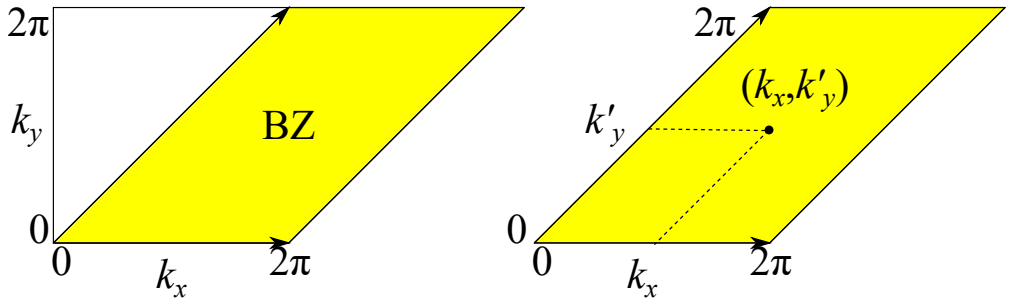

Figure B.3 Dehn twist of the Brillouin zone. A Brillouin zone defined by $0 \leq k_x, k_y \leq 2\pi$ is Denn-twisted to a tilted Brillouin zone shown as a yellow (shaded) region. When both 1D cycles along k_x and k_y have nontrivial 1D topological invariants, i.e., $w_{1x} = w_{1y} = 1$, we have a trivial 1D cycle k'_y by a Denn twist because $w_{1y'} = w_{1x} + w_{1y} = 0 \mod 2$. From Ref. [23].

group of U on the region N with the boundary condition Eq. (B.13) is the relative homotopy group $\pi_2[U(N), O(N)]$ [See Fig. B.2(c)]. Here, $[U(N), O(N)]$ means that $U \in U(N)$ inside the region A and $U \in O(N)$ on its boundary, which is the equator. Because $\pi_2[U(N)] = 0$, the relative homotopy class of U is in one-to-one correspondence with the homotopy class of U on its boundary, which is nothing but the homotopy class of the transition function $t^{AB} \in \pi_1[O(N)]$. That is, $\pi_2[U(N), O(N)] \simeq \pi_1[O(N)]$. Moreover, the relative homotopy group of U is isomorphic to the homotopy group of $G = UU^T$. In other words, $\pi_2[U(N), O(N)] \simeq \pi_2[U(N)/O(N)]$ [11], where the isomorphism is provided by the projection from $[U(N), O(N)]$ to $U(N)/O(N)$. Therefore,

$$\pi_2[U(N)/O(N)] \simeq \pi_1[O(N)]. \tag{B.14}$$

As the homotopy groups for smooth and periodic gauge transfomations are trivial, the process described here provides an explicit mapping for the isomorphism in Eq. (B.8) in the $d = 2$ case.

Using this formulation of the second Stiefel-Whitney number as a homotopy class of the sewing matrix, we can simply derive the the unique characteristic

of the Stiefel-Whitney numbers, the Whitney sum formula [7, 10], if we require some natural algebraic rules for the second homotopy classes on the Brillouin zone torus. Let us first consider a real gauge and suppose that the occupied bands are grouped into blocks $\mathcal{B}_i$ of bands isolated from each other, so that different blocks are not connected by transition functions. For example, transition functions are block-diagonalized when there are finite energy gaps between blocks, though a gapped energy spectrum is not necessary in general to have a block-diagonal form of transition functions. On the Brillouin zone torus having noncontractible 1D cycles along k_x and k_y directions, the second Stiefel-Whitney number of the whole occupied bands $\oplus\mathcal{B}_i$ is related to the Stiefel-Whitney numbers of blocks by the *Whitney sum formula* [7, 10]

$$w_2(\oplus_i \mathcal{B}_i) = \sum_i w_2(\mathcal{B}_i) + \sum_{i\neq j} w_1^x(\mathcal{B}_i) w_1^y(\mathcal{B}_j), \tag{B.15}$$

where $w_1^{a=x,y}$ is the first Stiefel-Whitney number along $k_{a=x,y}$. The appearance of the second term in the summation is a unique characteristics of the second Stiefel-Whitney number.

From the relation between the transition function in a real gauge and the sewing matrix in a smooth gauge derived above, we can infer that the Whitney sum formula should be applicable to the blocks that decouple the sewing matrix in a smooth gauge. For instance, let us consider two blocks $\mathcal{B}_1$ and $\mathcal{B}_2$ of occupied bands that block-diagonalize the sewing matrix as

$$G(\mathbf{k}) = \begin{pmatrix} e^{i\theta_1(\mathbf{k})} G_1^{(0)}(\mathbf{k}) & 0 \\ 0 & e^{i\theta_2(\mathbf{k})} G_2^{(0)}(\mathbf{k}) \end{pmatrix}, \tag{B.16}$$

where the $U(1)$ factor $e^{i\theta_{i=1,2}}$ of each block is singled out. Let N_1 and N_2 be the number of the bands in the blocks $\mathcal{B}_1$ and $\mathcal{B}_2$, respectively. Then, the second homotopy class of $G : T^2 \to U(N_1)/O(N_1) \times U(N_2)/O(N_2)$ is determined by the

second homotopy classes of $G_1^{(0)} \in SU(N_1)/SO(N_1)$, $G_2^{(0)} \in SU(N_2)/SO(N_2)$, and $(e^{i\theta_1}, e^{i\theta_2}) \in U(1) \times U(1) \simeq T^2$. The parities of the second homotopy class for $G_1^{(0)}$ and $G_2^{(0)}$ correspond to $w_2(\mathcal{B}_1)$ and $w_2(\mathcal{B}_2)$, respectively. Because the generators of $\pi_2[SU(N_i)/SO(N_i)]$ for $i = 1, 2$ are mapped to the generators of $\pi_2[U(N_1 + N_2)/O(N_1 + N_2)]$ by the inclusion maps, we have $w_2(\mathcal{B}_1 \oplus \mathcal{B}_2) = w_2(\mathcal{B}_1) + w_2(\mathcal{B}_2)$ when the $U(1) \times U(1)$ part is neglected. For the map $T^2 \to U(1) \times U(1)$, we can define the degree of the map as a homotopy invariant

$$\begin{aligned} &\frac{1}{(2\pi)^2} \int_{BZ} d^2k \left(\partial_{k_x} \theta_1 \partial_{k_y} \theta_2 - \partial_{k_x} \theta_2 \partial_{k_y} \theta_1 \right) \\ &= w_1^x(\mathcal{B}_1) w_1^y(\mathcal{B}_2) - w_1^x(\mathcal{B}_2) w_1^y(\mathcal{B}_1) \bmod 2, \end{aligned} \tag{B.17}$$

where we used that $\theta_{i=1,2}(\mathbf{k})$ is homotopically equivalent to $w_1^x(\mathcal{B}_i)k_x + w_1^y(\mathcal{B}_i)k_y$ because they have the same 1D winding number: $w_1^j(\mathcal{B}_i)$ along $k_{j=x,y}$. If we require that this homotopy invariant contributes to the two-dimensional topological invariant, that is, the second Stiefel-Whitney invariant, we obtain the Whitney sum formula $w_2(\mathcal{B}_1 \oplus \mathcal{B}_2) = w_2(\mathcal{B}_1) + w_2(\mathcal{B}_2) + w_1^x(\mathcal{B}_1) w_1^y(\mathcal{B}_2) - w_1^x(\mathcal{B}_2) w_1^y(\mathcal{B}_1)$. The generalization to the cases with many blocks is straightforward.

B.4 Some properties of homotopy groups

In this section, we prove some properties of homotopy groups we use in the main text. The main tool to be used is the long exact sequence of homotopy groups [11, 113, 159]:

$$\begin{aligned} \ldots &\xrightarrow{\partial_{p+1}} \pi_p(X) \xrightarrow{i_p^*} \pi_p(M) \xrightarrow{j_p^*} \pi_p(M, X) \\ &\xrightarrow{\partial_p} \pi_{p-1}(X) \xrightarrow{i_p^*} \ldots, \end{aligned} \tag{B.18}$$

where $i_p : X \to M$ and $j_p : M \to (M, X)$ are inclusions, i_p^* and $j_p^*$are maps for homotopy groups induced by i_p and j_p, and ∂ is the restriction to the boundary.

This sequence is *exact* because the image of a map is the kernel of the next map, e.g., $\mathrm{im}\, i_p^* = \ker j_p^*$. It is also valid when $\pi_p(M, X)$ is substituted by $\pi_p(M/X)$ because the two homotopy groups are isomorphic [11, 159].

$$\begin{aligned} \ldots \xrightarrow{\partial_{p+1}} \pi_p(X) \xrightarrow{i_p^*} \pi_p(M) \xrightarrow{j_p^*} \pi_p(M/X) \\ \xrightarrow{\partial_p} \pi_{p-1}(X) \xrightarrow{i_p^*} \ldots . \end{aligned} \tag{B.19}$$

B.4.1 Equivalence between real and smooth gauges

Let us prove Eq. (B.8), that is, $\pi_d[U(N)/O(N)]/\mathrm{im}\, j_d^* \simeq \pi_{d-1}[O(N)]$ when $d \neq 4n$ for a positive integer n. It can be proved for arbitrary N when $d = 1, 2$, which are dimensions studied in the main text, whereas we need the large N limit in general dimensions, This follows from the exact sequence in Eq. (B.19). In our case, $M = U(N)$, and $X = O(N)$. We have

$$\begin{aligned} \ldots \to \pi_d[U(N)] \xrightarrow{j_d^*} \pi_d[U(N)/O(N)] \\ \xrightarrow{\partial_d} \pi_{d-1}[O(N)] \xrightarrow{i_{d-1}^*} \pi_{d-1}[U(N)] \to \ldots . \end{aligned} \tag{B.20}$$

Then, we have

$$\frac{\pi_d[U(N)/O(N)]}{\mathrm{im}\, j_d^*} \simeq \ker i_{d-1}^*, \tag{B.21}$$

where we used the exactness of maps $\ker \partial_d = \mathrm{im}\, j_d^*$ and $\mathrm{im}\, \partial_d = \ker i_{d-1}^*$ and the group isomorphism theorem $\pi_d[U(N)/O(N)]/\ker \partial_d \simeq \mathrm{im}\, \partial_d$. Notice that i_{d-1}^* is a trivial map for $d \neq 4n$ for a positive integer n when N is large enough. When d is odd, it is because $\pi_{d-1}[U(N)] = 0$ for $d \leq 2N$. In particular, $\pi_0[U(N)] = \pi_2[U(N)] = 0$ for all N. When $d = 2$, i_{d-1}^* is trivial because orthogonal group elements have quantized determinants, $+1$ or -1, so that they cannot have a winding of the determinant (recall that $\pi_1[U(N)]$ is characterized by the winding number of the determinant of the unitary matrix). When $d = 6$,

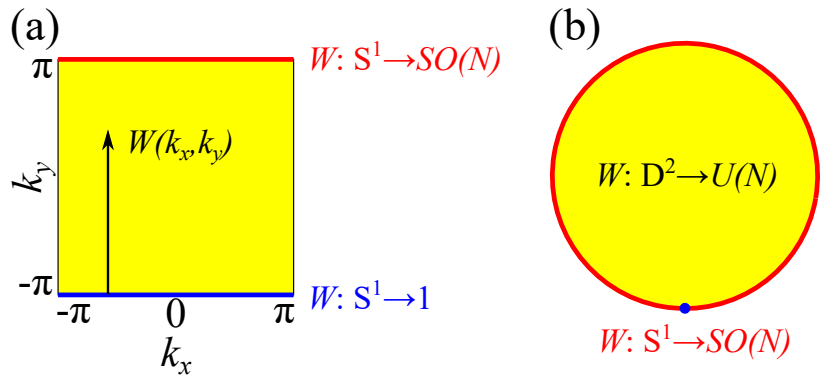

Figure B.4 Wilson line operator in a $I_{\rm ST}$-invariant Brillouin zone. (a) $W(k_x, k_y)$ is the Wilson line operator $W_{(k_x,-\pi)\to(k_x,k_y)}$. (b) Deformation of (a) after $k_x = -\pi$, $k_x = \pi$, and $k_y = -\pi$ lines are contracted to a point. From Ref. [23].

the map i_5^* is trivial because $\pi_5[O(N)] = 0$. Bott periodicity then shows that the same is true for $2 + 8m$ and $6 + 8m$ dimensions for a positive integer m when N is large enough, i.e., $d \le 2N$ and $d \le N - 1$. On the other hand, when $d = 4n$ for a positive integer n, i_{d-1}^* is not trivial. This is related to the fact that the reality condition on wave functions (equivalently, PT symmetry) does not require that the $2n$-th Chern class vanishes, and the Chern class in a real gauge is called the Pontrjagin class [9]. Let us recall that the $2n$-th Chern number is given by the $(4n-1)$-th nontrivial homotopy of the transition function. The $2n$-th Chern class of real wave functions does not vanish because the nontrvial homotopy class of the transition function in $\pi_{d-1}[O(N)]$ survives as an element in $\pi_{d-1}[U(N)]$. Accordingly,

$$\ker i_{d-1}^* \simeq \pi_{d-1}[O(N)] \text{ for } d \notin 4\mathbb{Z}_+, \tag{B.22}$$

where $\mathbb{Z}_+$ is the set of positive integers. This finishes the proof.

B.5 Wilson loop method

In this section, we show the connection between the second homotopy class of the sewing matrix for $I_{\rm ST}$ and the winding number of the Wilson loop spectrum in an invariant plane. This provides a new insight into the Wilson loop method [7, 13, 17, 19, 20, 40, 41, 45].

We first define a Wilson line operator for the occupied states on the line connecting $\mathbf{k}$ and $\mathbf{k}'$ by

$$W_{\mathbf{k}\to\mathbf{k}'} = \lim_{\boldsymbol{\delta}\to 0} F_{\mathbf{k}'-\boldsymbol{\delta}} F_{\mathbf{k}'-2\boldsymbol{\delta}} ... F_{\mathbf{k}+\boldsymbol{\delta}} F_{\mathbf{k}}, \tag{B.23}$$

where

$$(F_{\mathbf{k}})_{mn} = \langle u_{m\mathbf{k}+\boldsymbol{\delta}} | u_{n\mathbf{k}} \rangle \,, \tag{B.24}$$

and m, n are indices for occupied states. The transition matrix F satisfies the following equation in $I_{\rm ST}$-symmetric systems.

$$\begin{aligned}
(F^*_{\mathbf{k}})_{mn} &= \langle u_{m\mathbf{k}+\boldsymbol{\delta}} | u_{n\mathbf{k}} \rangle^* \\
&= \langle I_{\rm ST} u_{m\mathbf{k}+\boldsymbol{\delta}} | I_{\rm ST} u_{n\mathbf{k}} \rangle \\
&= G^*_{pm}(\mathbf{k}+\boldsymbol{\delta}) \, \langle u_{p\mathbf{k}+\boldsymbol{\delta}} | u_{q\mathbf{k}} \rangle \, G_{qn}(\mathbf{k}) \\
&= [G^\dagger(\mathbf{k}+\boldsymbol{\delta}) F_{\mathbf{k}} G(\mathbf{k})]_{mn}.
\end{aligned} \tag{B.25}$$

It follows that

$$\begin{aligned}
W^*_{\mathbf{k}\to\mathbf{k}'} &= \lim_{\boldsymbol{\delta}\to 0} F^*_{\mathbf{k}'-\boldsymbol{\delta}} F^*_{\mathbf{k}'-2\boldsymbol{\delta}} ... F^*_{\mathbf{k}+\boldsymbol{\delta}} F^*_{\mathbf{k}} \\
&= G^\dagger(\mathbf{k}') W_{\mathbf{k}\to\mathbf{k}'} G(\mathbf{k}).
\end{aligned} \tag{B.26}$$

Therefore, we find that

$$G(\mathbf{k}') = W_{\mathbf{k}\to\mathbf{k}'} G(\mathbf{k}) W^T_{\mathbf{k}\to\mathbf{k}'} \tag{B.27}$$

For simplicity, we assume that all 1D topological invariants are trivial. Then, we can take a gauge $G(k_x, -\pi) = 1$ such that

$$G(k_x, k_y) = W_{(k_x,-\pi)\to(k_x,k_y)} W^T_{(k_x,-\pi)\to(k_x,k_y)} \tag{B.28}$$

Because we are in a smooth gauge, we have

$$\begin{aligned} 1 &= G(k_x, -\pi) \\ &= G(k_x, \pi) \\ &= W_{(k_x,-\pi)\to(k_x,\pi)} W^T_{(k_x,-\pi)\to(k_x,\pi)}, \end{aligned} \tag{B.29}$$

so the Wilson loop operator belong to the orthogonal group at $k_y = \pi$:

$$W_{(k_x,-\pi)\to(k_x,\pi)} \in SO(N). \tag{B.30}$$

It belongs to $SO(N) \subset O(N)$ because it is continously connected to the identity element $W_{(k_x,-\pi)\to(k_x,-\pi)} = 1$.

Let us contract the $k_x = -\pi$, $k_x = \pi$, and $k_y = -\pi$ lines to a point, which is possible due to the assumption that the 1D topology is trivial, as shown in Fig. B.4(a,b). As we show in Sec. B.4, the relative homotopy class of $\pi_2[U(N), SO(N)]$ of $W(k_x, k_y) \equiv W_{(k_x,-\pi)\to(k_x,k_y)}$ is determined by its homotopy class on the boundary $\pi_1[SO(N)]$. Notice that the relative homotopy class of W is one-to-one correspondence with the second homotopy class of G as derived in Sec. B.4. Also, the homotopy class in $\pi_1[SO(N)]$ is given by the winding number of the Wilson loop operator $W[k_x] \equiv W_{(k_x,-\pi)\to(k_x,\pi)}$. Therefore, we conclude that the second homotopy class of $G(k_x, k_y)$ is in one-to-one correspondence with the 1D winding number of the Wilson loop operator $W[k_x]$. In practice, one obtains the winding number of the Wilson loop operator from the winding pattern of its spectrum, which can be calculated in a gauge-invariant way.

Appendix C

Parity indices of odd-parity superconductors.

In Chapter 8, we define parity indices ν_{2^n} that counts the number of 2^n band inversion occuring at each time-reversal-invariant momentum (TRIM):

$$\nu_{2^n} = \sum_{\mathbf{K}\in\mathrm{TRIM}} \left[\frac{n_-^{\mathrm{o}}(\mathbf{K})}{2^n}\right]_{\mathrm{floor}}, \tag{C.1}$$

where we define $n_{\pm}^{\mathrm{o(u)}}(\mathbf{K})$ as the number of occupied (unoccupied) states at $\mathbf{K}$ with inversion parity ± 1. One of our main result is the decomposition of the parity indices for the odd-parity BdG Hamiltonian into

$$\begin{aligned}\nu_{2^n}^{\mathrm{BdG}} = &\sum_{\mathbf{K}\in\mathrm{TRIM}} \left[\frac{n^{\mathrm{u}}(\mathbf{K})}{2^n}\right]_{\mathrm{floor}} + \sum_{\mathbf{K}\in\mathrm{TRIM}} \left[\frac{n_-^{\mathrm{o}}(\mathbf{K})}{2^{n-1}}\right]_{\mathrm{floor}} \\ &+ \sum_{\mathbf{K}\in\mathrm{TRIM}} \left[\frac{n_-(\mathbf{K})}{2^n}\right]_{\mathrm{floor}} + \sum_{\mathbf{K}\in\mathrm{TRIM}} \delta_{2^n}(\mathbf{K})\end{aligned} \tag{C.2}$$

modulo two, where $n^{\mathrm{u}}(\mathbf{K}) = n^{\mathrm{u}}_{+}(\mathbf{K}) + n^{\mathrm{u}}_{-}(\mathbf{K})$, $n_{-}(\mathbf{K}) = n^{\mathrm{o}}_{-}(\mathbf{K}) + n^{\mathrm{u}}_{-}(\mathbf{K})$, and $\delta_{2^n}(\mathbf{K})$ is defined below. Here, we derive the decomposition Eq. (C.2) as follows:

$$
\begin{aligned}
\nu^{\mathrm{BdG}}_{2^n} &= \sum_{\mathbf{K}\in\mathrm{TRIM}} \left[\frac{n^{\mathrm{o,BdG}}_{-}(\mathbf{K})}{2^n} \right]_{\mathrm{floor}} \\
&= \sum_{\mathbf{K}\in\mathrm{TRIM}} \left[\frac{n^{\mathrm{u}}_{+}(\mathbf{K}) + n^{\mathrm{o}}_{-}(\mathbf{K})}{2^n} \right]_{\mathrm{floor}} \\
&= \sum_{\mathbf{K}\in\mathrm{TRIM}} \left[\frac{n^{\mathrm{u}}_{+}(\mathbf{K}) + n^{\mathrm{u}}_{-}(\mathbf{K}) + 2n^{\mathrm{o}}_{-}(\mathbf{K}) - n^{\mathrm{o}}_{-}(\mathbf{K}) - n^{\mathrm{u}}_{-}(\mathbf{K})}{2^n} \right]_{\mathrm{floor}} \\
&= \sum_{\mathbf{K}\in\mathrm{TRIM}} \left[\frac{n^{\mathrm{u}}(\mathbf{K})}{2^n} + \frac{n^{\mathrm{o}}_{-}(\mathbf{K})}{2^{n-1}} - \frac{n_{-}(\mathbf{K})}{2^n} \right]_{\mathrm{floor}} \\
&= \sum_{\mathbf{K}\in\mathrm{TRIM}} \left(\left[\frac{n^{\mathrm{u}}(\mathbf{K})}{2^n} \right]_{\mathrm{floor}} + \left[\frac{n^{\mathrm{o}}_{-}(\mathbf{K})}{2^{n-1}} \right]_{\mathrm{floor}} - \left[\frac{n_{-}(\mathbf{K})}{2^n} \right]_{\mathrm{floor}} + \delta_{2^n}(\mathbf{K}) \right) \\
&= \sum_{\mathbf{K}\in\mathrm{TRIM}} \left[\frac{n^{\mathrm{u}}(\mathbf{K})}{2^n} \right]_{\mathrm{floor}} + \sum_{\mathbf{K}\in\mathrm{TRIM}} \left[\frac{n^{\mathrm{o}}_{-}(\mathbf{K})}{2^{n-1}} \right]_{\mathrm{floor}} + \sum_{\mathbf{K}\in\mathrm{TRIM}} \left[\frac{n_{-}(\mathbf{K})}{2^n} \right]_{\mathrm{floor}} \\
&\quad + \sum_{\mathbf{K}\in\mathrm{TRIM}} \delta_{2^n}(\mathbf{K})
\end{aligned}
\tag{C.3}
$$

modulo two, where $\delta_{2^n}(\mathbf{K})$ is defined by the fourth and fifth lines, and we flip the sign of the third term in the last line, which is possible because we count only mod 2.

Bibliography

[1] M. Z. Hasan and C. L. Kane, *Colloquium: topological insulators*, *Rev. Mod. Phys.* **82** (2010) 3045.

[2] N. Armitage, E. Mele and A. Vishwanath, *Weyl and dirac semimetals in three-dimensional solids*, *Reviews of Modern Physics* **90** (2018) 015001.

[3] S. Murakami, *Phase transition between the quantum spin hall and insulator phases in 3d: emergence of a topological gapless phase*, *New Journal of Physics* **9** (2007) 356.

[4] X. Wan, A. M. Turner, A. Vishwanath and S. Y. Savrasov, *Topological semimetal and fermi-arc surface states in the electronic structure of pyrochlore iridates*, *Phys. Rev. B* **83** (2011) 205101.

[5] C. Fang and L. Fu, *New classes of three-dimensional topological crystalline insulators: Nonsymmorphic and magnetic*, *Phys. Rev. B* **91** (2015) 161105(R).

[6] J. Ahn and B.-J. Yang, *Unconventional topological phase transition in two-dimensional systems with space-time inversion symmetry*, *Phys. Rev. Lett.* **118** (2017) 156401.

[7] J. Ahn, D. Kim, Y. Kim and B.-J. Yang, *Band topology and linking structure of nodal line semimetals with Z2 monopole charges*, *Phys. Rev. Lett.* **121** (2018) 106403.

[8] A. Bouhon, R.-J. Slager and T. Bzdušek, *Non-abelian reciprocal braiding of weyl nodes*, *arXiv preprint arXiv:1907.10611* (2019) .

[9] M. Nakahara, *Geometry, Topology and Physics*. CRC Press, 2003.

[10] A. Hatcher, *Vector bundles and k-theory*, *http://pi.math.cornell.edu/ hatcher/VBKT/VB.pdf* (unpublished) .

[11] A. Hatcher, *Algebraic Topology*. Cambridge University Press, 2002.

[12] K. Shiozaki, M. Sato and K. Gomi, *Topological crystalline materials: General formulation, module structure, and wallpaper groups*, *Phys. Rev. B* **95** (2017) 235425.

[13] T. Bzdušek and M. Sigrist, *Robust doubly charged nodal lines and nodal surfaces in centrosymmetric systems*, *Phys. Rev. B* **96** (2017) 155105.

[14] J. Ahn, S. Park and B.-J. Yang, *Failure of Nielsen-Ninomiya theorem and fragile topology in two-dimensional systems with space-time inversion symmetry: Application to twisted bilayer graphene at magic angle*, *Phys. Rev. X* **9** (2019) 021013.

[15] H. C. Po, H. Watanabe and A. Vishwanath, *Fragile topology and wannier obstructions*, *Phys. Rev. Lett.* **121** (2018) 126402.

[16] J. Cano, B. Bradlyn, Z. Wang, L. Elcoro, M. Vergniory, C. Felser et al., *Topology of disconnected elementary band representations*, *Phys. Rev. Lett.* **120** (2018) 266401.

[17] A. Bouhon, A. M. Black-Schaffer and R.-J. Slager, *Wilson loop approach to fragile topology of split elementary band representations and topological crystalline insulators with time-reversal symmetry*, *Phys. Rev. B* **100** (2019) 195135.

[18] Z. Wang, B. J. Wieder, J. Li, B. Yan and B. A. Bernevig, *Higher-order topology, monopole nodal lines, and the origin of large fermi arcs in transition metal dichalcogenides x te 2 (x= mo, w)*, *Phys. Rev. Lett.* **123** (2019) 186401.

[19] B. Bradlyn, Z. Wang, J. Cano and B. A. Bernevig, *Disconnected elementary band representations, fragile topology, and wilson loops as topological indices: An example on the triangular lattice*, *Physical Review B* **99** (2019) 045140.

[20] Z. Song, Z. Wang, W. Shi, G. Li, C. Fang and B. A. Bernevig, *All magic angles in twisted bilayer graphene are topological*, *Phys. Rev. Lett.* **123** (2019) 036401.

[21] H. C. Po, L. Zou, T. Senthil and A. Vishwanath, *Faithful tight-binding models and fragile topology of magic-angle bilayer graphene*, *Phys. Rev. B* **99** (2019) 195455.

[22] S. Liu, A. Vishwanath and E. Khalaf, *Shift insulators: rotation-protected two-dimensional topological crystalline insulators*, *Phys. Rev. X* **9** (2019) 031003.

[23] J. Ahn and B.-J. Yang, *Symmetry representation approach to topological invariants in c 2 z t-symmetric systems*, *Phys. Rev. B* **99** (2019) 235125.

[24] J. Ahn, S. Park, D. Kim, Y. Kim and B.-J. Yang, *Stiefel–whitney classes and topological phases in band theory*, *Chinese Physics B* **28** (2019) 117101.

[25] J. Ahn and B.-J. Yang, *Higher-order topological superconductivity of spin-polarized fermions*, *arXiv preprint arXiv:1906.02709* (2019) .

[26] R. Kirby and L. Taylor, *Pin structures on low-dimensional manifolds*, vol. 2 of *London Mathematical Society Lecture Note Series*. Cambridge University Press, 1991, 10.1017/CBO9780511629341.015.

[27] W. Su, J. Schrieffer and A. J. Heeger, *Solitons in polyacetylene*, *Phys. Rev. Lett.* **42** (1979) 1698.

[28] S. M. Young and C. L. Kane, *Dirac semimetals in two dimensions*, *Physical review letters* **115** (2015) 126803.

[29] B. J. Wieder and C. Kane, *Spin-orbit semimetals in the layer groups*, *Physical Review B* **94** (2016) 155108.

[30] B. A. Bernevig, T. L. Hughes and S.-C. Zhang, *Quantum spin hall effect and topological phase transition in hgte quantum wells*, *Science* **314** (2006) 1757.

[31] M. König, S. Wiedmann, C. Brüne, A. Roth, H. Buhmann, L. W. Molenkamp et al., *Quantum spin hall insulator state in hgte quantum wells*, *Science* **318** (2007) 766.

[32] J. Kim, S. S. Baik, S. W. Jung, Y. Sohn, S. H. Ryu, H. J. Choi et al., *Two-dimensional dirac fermions protected by space-time inversion symmetry in black phosphorus*, *Physical review letters* **119** (2017) 226801.

[33] S. Park and B.-J. Yang, *Classification of accidental band crossings and emergent semimetals in two-dimensional noncentrosymmetric systems*, *Physical Review B* **96** (2017) 125127.

[34] Y. Chen, Y. Xie, S. A. Yang, H. Pan, F. Zhang, M. L. Cohen et al., *Nanostructured carbon allotropes with weyl-like loops and points*, *Nano letters* **15** (2015) 6974.

[35] H. Weng, Y. Liang, Q. Xu, R. Yu, Z. Fang, X. Dai et al., *Topological node-line semimetal in three-dimensional graphene networks*, *Physical Review B* **92** (2015) 045108.

[36] L. S. Xie, L. M. Schoop, E. M. Seibel, Q. D. Gibson, W. Xie and R. J. Cava, *A new form of ca3p2 with a ring of dirac nodes*, *Apl Materials* **3** (2015) 083602.

[37] Y.-H. Chan, C.-K. Chiu, M. Chou and A. P. Schnyder, *Ca 3 p 2 and other topological semimetals with line nodes and drumhead surface states*, *Physical Review B* **93** (2016) 205132.

[38] Y. Kim, B. J. Wieder, C. L. Kane and A. M. Rappe, *Dirac line nodes in inversion-symmetric crystals*, *Phys. Rev. Lett.* **115** (2015) 036806.

[39] R. Yu, H. Weng, Z. Fang, X. Dai and X. Hu, *Topological node-line semimetal and dirac semimetal state in antiperovskite cu 3 pdn*, *Physical review letters* **115** (2015) 036807.

[40] C. Fang, Y. Chen, H.-Y. Kee and L. Fu, *Topological nodal line semimetals with and without spin-orbital coupling*, *Phys. Rev. B* **92** (2015) 081201.

[41] Y. X. Zhao and Y. Lu, *PT-symmetric real Dirac fermions and semimetals*, *Phys. Rev. Lett.* **118** (2017) 056401.

[42] Z. Song, T. Zhang and C. Fang, *Diagnosis for nonmagnetic topological semimetals in the absence of spin-orbital coupling*, *Phys. Rev. X* **8** (2018) 031069.

[43] V. V. Prasolov, *Elements of combinatorial and differential topology*, vol. 74. American Mathematical Soc., 2006.

[44] Y. Chooquet-Bruhat, *Analysis, Manifolds, and Physics – Part II*. Elsevier, Amsterdam, 2000.

[45] R. Yu, X. L. Qi, A. Bernevig, Z. Fang and X. Dai, *Equivalent expression of z 2 topological invariant for band insulators using the non-abelian berry connection*, *Physical Review B* **84** (2011) 075119.

[46] A. Alexandradinata, Z. Wang and B. A. Bernevig, *Topological insulators from group cohomology*, *Phys. Rev. X* **6** (2016) 021008.

[47] A. A. Soluyanov and D. Vanderbilt, *Smooth gauge for topological insulators*, *Phys. Rev. B* **85** (2012) 115415.

[48] T. Nomura, T. Habe, R. Sakamoto and M. Koshino, *Three-dimensional graphdiyne as a topological nodal-line semimetal*, *Phys. Rev. Materials* **2** (2018) 054204.

[49] Y. Hwang, J. Ahn and B.-J. Yang, *Fragile topology protected by inversion symmetry: Diagnosis, bulk-boundary correspondence, and wilson loop*, *Phys. Rev. B* **100** (2019) 205126.

[50] S. T. Ramamurthy and T. L. Hughes, *Patterns of electromagnetic response in topological semimetals*, *Phys. Rev. B* **92** (2015) 085105.

[51] Y. X. Zhao, A. P. Schnyder and Z. D. Wang, *Unified theory of pt and cp invariant topological metals and nodal superconductors*, *Phys. Rev. Lett.* **116** (2016) 156402.

[52] B. J. Wieder and B. A. Bernevig, *The axion insulator as a pump of fragile topology*, *arXiv:1810.02373* (2018) .

[53] F. Zhang, C. L. Kane and E. J. Mele, *Surface state magnetization and chiral edge states on topological insulators*, *Phys. Rev. Lett.* **110** (2013) 046404.

[54] C. Fang and L. Fu, *Rotation anomaly and topological crystalline insulators*, *arXiv:1709.01929* (2017) .

[55] E. Khalaf, *Higher-order topological insulators and superconductors protected by inversion symmetry*, *Phys. Rev. B* **97** (2018) 205136.

[56] S. H. Kooi, G. Van Miert and C. Ortix, *Inversion-symmetry protected chiral hinge states in stacks of doped quantum hall layers*, *Physical Review B* **98** (2018) 245102.

[57] N. Varnava and D. Vanderbilt, *Surfaces of axion insulators*, *arXiv:1809.02853* (2018) .

[58] G. van Miert and C. Ortix, *Higher-order topological insulators protected by inversion and rotoinversion symmetries*, *Phys. Rev. B* **98** (2018) 081110.

[59] C. Yue, Y. Xu, Z. Song, H. Weng, Y.-M. Lu, C. Fang et al., *Symmetry-enforced chiral hinge states and surface quantum anomalous hall effect in the magnetic axion insulator bi 2–x sm x se 3*, *Nat. Phys.* (2019) 1.

[60] F. Schindler, A. M. Cook, M. G. Vergniory, Z. Wang, S. S. Parkin, B. A. Bernevig et al., *Higher-order topological insulators*, *Science advances* **4** (2018) eaat0346.

[61] M. Ezawa, *Strong and weak second-order topological insulators with hexagonal symmetry and z3 index*, *Phys. Rev. B* **97** (2018) 241402.

[62] M. Ezawa, *Magnetic second-order topological insulators and semimetals*, *Phys. Rev. B* **97** (2018) 155305.

[63] X.-L. Qi, T. L. Hughes and S.-C. Zhang, *Topological field theory of time-reversal invariant insulators*, *Phys. Rev. B* **78** (2008) 195424.

[64] Z. Wang, X.-L. Qi and S.-C. Zhang, *Equivalent topological invariants of topological insulators*, *New J. Phys.* **12** (2010) 065007.

[65] Y. Cao, V. Fatemi, S. Fang, K. Watanabe, T. Taniguchi, E. Kaxiras et al., *Unconventional superconductivity in magic-angle graphene superlattices*, *Nature* **556** (2018) 43.

[66] Y. Cao, V. Fatemi, A. Demir, S. Fang, S. L. Tomarken, J. D. Luo, J. Y .and Sanchez-Yamagishi et al., *Correlated insulator behaviour at half-filling in magic-angle graphene superlattices*, *Nature* **556** (2018) 80.

[67] G. E. Volovik, *Graphite, graphene, and the flat band superconductivity*, *JETP Letters* **107** (2018) 516.

[68] C. Xu and L. Balents, *Topological superconductivity in twisted multilayer graphene*, *Physical review letters* **121** (2018) 087001.

[69] B. Roy and V. Juričić, *Unconventional superconductivity in nearly flat bands in twisted bilayer graphene*, *Physical Review B* **99** (2019) 121407.

[70] H. Guo, X. Zhu, S. Feng and R. T. Scalettar, *Pairing symmetry of interacting fermions on a twisted bilayer graphene superlattice*, *Physical Review B* **97** (2018) 235453.

[71] G. Baskaran, *Theory of emergent josephson lattice in neutral twisted bilayer graphene (moiré is different)*, *arXiv preprint arXiv:1804.00627* (2018) .

[72] B. Padhi, C. Setty and P. W. Phillips, *Wigner crystallization in lieu of mottness in twisted bilayer graphene*, *arXiv preprint arXiv:1804.01101* (2018) .

[73] V. Y. Irkhin and Y. N. Skryabin, *Dirac points, spinons and spin liquid in twisted bilayer graphene*, *JETP Letters* (2018) 1.

[74] J. F. Dodaro, S. A. Kivelson, Y. Schattner, X.-Q. Sun and C. Wang, *Phases of a phenomenological model of twisted bilayer graphene*, *Physical Review B* **98** (2018) 075154.

[75] T. Huang, L. Zhang and T. Ma, *Antiferromagnetically ordered mott insulator and d+ id superconductivity in twisted bilayer graphene: A quantum monte carlo study*, *Science Bulletin* **64** (2019) 310.

[76] L. Zhang, *Lowest-energy moiré band formed by dirac zero modes in twisted bilayer graphene*, *Science Bulletin* **64** (2019) 495.

[77] S. Ray, J. Jung and T. Das, *Wannier pairs in superconducting twisted bilayer graphene and related systems*, *Physical Review B* **99** (2019) 134515.

[78] C.-C. Liu, L.-D. Zhang, W.-Q. Chen and F. Yang, *Chiral sdw and d+ id superconductivity in the magic-angle twisted bilayer-graphene*, *arXiv preprint arXiv:1804.10009* (2018) .

[79] X. Y. Xu, K. Law and P. A. Lee, *Kekulé valence bond order in an extended hubbard model on the honeycomb lattice with possible applications to twisted bilayer graphene*, *Physical Review B* **98** (2018) 121406.

[80] L. Rademaker and P. Mellado, *Charge-transfer insulation in twisted bilayer graphene*, *Physical Review B* **98** (2018) 235158.

[81] H. Isobe, N. F. Yuan and L. Fu, *Unconventional superconductivity and density waves in twisted bilayer graphene*, *Physical Review X* **8** (2018) 041041.

[82] F. Wu, A. MacDonald and I. Martin, *Theory of phonon-mediated superconductivity in twisted bilayer graphene*, *Physical review letters* **121** (2018) 257001.

[83] J. Pizarro, M. Calderón and E. Bascones, *The nature of correlations in the insulating states of twisted bilayer graphene*, *Journal of Physics Communications* **3** (2019) 035024.

[84] T. J. Peltonen, R. Ojajärvi and T. T. Heikkilä, *Mean-field theory for superconductivity in twisted bilayer graphene*, *Physical Review B* **98** (2018) 220504.

[85] Y.-Z. You and A. Vishwanath, *Superconductivity from valley fluctuations and approximate so (4) symmetry in a weak coupling theory of twisted bilayer graphene*, *npj Quantum Materials* **4** (2019) 16.

[86] Y. W. Choi and H. J. Choi, *Strong electron-phonon coupling, electron-hole asymmetry, and nonadiabaticity in magic-angle twisted bilayer graphene*, *Physical Review B* **98** (2018) 241412.

[87] X.-C. Wu, K. A. Pawlak, C.-M. Jian and C. Xu, *Emergent superconductivity in the weak mott insulator phase of bilayer graphene moiré superlattice*, *arXiv preprint arXiv:1805.06906* (2018) .

[88] H. K. Pal, *On magic angles and band flattening in twisted bilayer graphene*, *arXiv preprint arXiv:1805.08803* (2018) .

[89] M. Ochi, M. Koshino and K. Kuroki, *Possible correlated insulating states in magic-angle twisted bilayer graphene under strongly competing interactions*, *Physical Review B* **98** (2018) 081102.

[90] M. Fidrysiak, M. Zegrodnik and J. Spałek, *Unconventional topological superconductivity and phase diagram for an effective two-orbital model as applied to twisted bilayer graphene*, *Physical Review B* **98** (2018) 085436.

[91] A. Thomson, S. Chatterjee, S. Sachdev and M. S. Scheurer, *Triangular antiferromagnetism on the honeycomb lattice of twisted bilayer graphene*, *Phys. Rev. B* **98** (2018) 075109.

[92] F. Guinea and N. R. Walet, *Electrostatic effects, band distortions, and superconductivity in twisted graphene bilayers*, *Proceedings of the National Academy of Sciences* **115** (2018) 13174.

[93] L. Zou, H. C. Po, A. Vishwanath and T. Senthil, *Band structure of twisted bilayer graphene: Emergent symmetries, commensurate approximants, and wannier obstructions*, *Physical Review B* **98** (2018) 085435.

[94] H. C. Po, L. Zou, A. Vishwanath and T. Senthil, *Origin of mott insulating behavior and superconductivity in twisted bilayer graphene*, *Physical Review X* **8** (2018) 031089.

[95] M. Koshino, N. F. Yuan, T. Koretsune, M. Ochi, K. Kuroki and L. Fu, *Maximally localized wannier orbitals and the extended hubbard model for twisted bilayer graphene*, *Physical Review X* **8** (2018) 031087.

[96] N. F. Yuan and L. Fu, *Model for the metal-insulator transition in graphene superlattices and beyond*, *Physical Review B* **98** (2018) 045103.

[97] J. Kang and O. Vafek, *Symmetry, maximally localized wannier states, and a low-energy model for twisted bilayer graphene narrow bands*, *Physical Review X* **8** (2018) 031088.

[98] J. M. B. Lopes dos Santos, N. M. R. Peres and A. H. Castro Neto, *Graphene bilayer with a twist: Electronic structure*, *Phys. Rev. Lett.* **99** (2007) 256802.

[99] R. Bistritzer and A. H. MacDonald, *Moiré bands in twisted double-layer graphene*, *PNAS* **108** (2011) 12233.

[100] S. Shallcross, S. Sharma, E. Kandelaki and O. Pankratov, *Electronic structure of turbostratic graphene*, *Phys. Rev. B* **81** (2010) 165105.

[101] E. S. Morell, J. Correa, P. Vargas, M. Pacheco and Z. Barticevic, *Flat bands in slightly twisted bilayer graphene: Tight-binding calculations*, *Phys. Rev. B* **82** (2010) 121407.

[102] G. Trambly de Laissardiere, D. Mayou and L. Magaud, *Localization of dirac electrons in rotated graphene bilayers*, *Nano Lett.* **10** (2010) 804.

[103] J. Jung, A. Raoux, Z. Qiao and A. H. MacDonald, *Ab-initio theory of moiré superlattice bands in layered two-dimensional materials*, *Phys. Rev. B* **89** (2014) 205414.

[104] Y. Cao, J. Y. Luo, V. Fatemi, S. Fang, J. Sanchez-Yamagishi, K. Watanabe et al., *Superlattice-induced insulating states and valley-protected orbits in twisted bilayer graphene*, *Phys. Rev. Lett.* **117** (2016) 116804.

[105] H. B. Nielsen and M. Ninomiya, *No-go theorem for regularizing chiral fermions*, tech. rep., Science Research Council, 1981.

[106] E. Witten, *Three lectures on topological phases of matter*, *La Rivista del Nuovo Cimento* **39** (2016) 313.

[107] C.-K. Chiu, J. C. Y. Teo, A. P. Schnyder and S. Ryu, *Classification of topological quantum matter with symmetries*, *Rev. Mod. Phys.* **88** (2016) 035005.

[108] V. Mathai and G. C. Thiang, *Differential topology of semimetals*, *Communications in Mathematical Physics* **355** (2017) 561.

[109] R. Bott and L. W. Tu, *Differential forms in algebraic topology*, vol. 82. Springer Science & Business Media, 2013.

[110] Y. Choquet-Bruhat and C. DeWitt-Morette, *Analysis, Manifolds and Physics: Graph. Darst.* Gulf Professional Publishing, 2013.

[111] L. Fu, C. L. Kane and E. J. Mele, *Topological insulators in three dimensions*, *Phys. Rev. Lett.* **98** (2007) 106803.

[112] T. L. Hughes, E. Prodan and B. A. Bernevig, *Inversion-symmetric topological insulators*, *Phys. Rev. B* **83** (2011) 245132.

[113] A. M. Turner, Y. Zhang, R. S. K. Mong and A. Vishwanath, *Quantized response and topology of magnetic insulators with inversion symmetry*, *Phys. Rev. B* **85** (2012) 165120.

[114] H. C. Po, A. Vishwanath and H. Watanabe, *Symmetry-based indicators of band topology in the 230 space groups*, *Nat. Commun.* **8** (2017) 50.

[115] M. Sato and Y. Ando, *Topological superconductors: a review*, *Rep. Prog. Phys.* **80** (2017) 076501.

[116] J. Alicea, *New directions in the pursuit of Majorana fermions in solid state systems*, *Rep. Prog. Phys.* **75** (2012) 076501.

[117] S. Das Sarma, M. Freedman and C. Nayak, *Majorana zero modes and topological quantum computation*, *npj Quant. Inf.* **1** (2015) 15001.

[118] A. Kitaev, *Fault-tolerant quantum computation by anyons*, *Ann. Phys.* **303** (2003) 2.

[119] C. Nayak, S. H. Simon, A. Stern, M. Freedman and S. Das Sarma, *Non-abelian anyons and topological quantum computation*, *Rev. Mod. Phys.* **80** (2008) 1083.

[120] L. Fu and E. Berg, *Odd-parity topological superconductors: theory and application to* $Cu_xBi_2Se_3$, *Phys. Rev. Lett.* **105** (2010) 097001.

[121] M. Sato, *Topological properties of spin-triplet superconductors and fermi surface topology in the normal state*, *Physical Review B* **79** (2009) 214526.

[122] M. Sato, *Topological odd-parity superconductors*, *Phys. Rev. B* **81** (2010) 220504(R).

[123] Y. You, D. Litinski and F. Von Oppen, *Higher-order topological superconductors as generators of quantum codes*, *Phys. Rev. B* **100** (2019) 054513.

[124] M. Geier, L. Trifunovic, M. Hoskam and P. W. Brouwer, *Second-order topological insulators and superconductors with an order-two crystalline symmetry*, *Phys. Rev. B* **97** (2018) 205135.

[125] L. Trifunovic and P. W. Brouwer, *Higher-order bulk-boundary correspondence for topological crystalline phases*, *Phys. Rev. X* **9** (2019) 011012.

[126] Y. Wang, M. Lin and T. L. Hughes, *Weak-pairing higher order topological superconductors*, *Phys. Rev. B* **98** (2018) 165144.

[127] T. E. Pahomi, M. Sigrist and A. A. Soluyanov, *Braiding Majorana corner modes in a two-layer second-order topological insulator*, *arXiv:1904.07822* (2019) .

[128] T. Liu, J. J. He, F. Nori et al., *Majorana corner states in a two-dimensional magnetic topological insulator on a high-temperature superconductor*, *Phys. Rev. B* **98** (2018) 245413.

[129] Q. Wang, C.-C. Liu, Y.-M. Lu and F. Zhang, *High-temperature Majorana corner states*, *Phys. Rev. Lett.* **121** (2018) 186801.

[130] Z. Yan, F. Song and Z. Wang, *Majorana corner modes in a high-temperature platform*, *Phys. Rev. Lett.* **121** (2018) 096803.

[131] C.-H. Hsu, P. Stano, J. Klinovaja and D. Loss, *Majorana Kramers pairs in higher-order topological insulators*, *Phys. Rev. Lett.* **121** (2018) 196801.

[132] X. Zhu, *Second-order topological superconductors with mixed pairing*, *Phys. Rev. Lett.* **122** (2019) 236401.

[133] K. Laubscher, D. Loss and J. Klinovaja, *Fractional topological superconductivity and parafermion corner states*, *Phys. Rev. Research* **1** (2019) 032017(R).

[134] X. Zhu, *Tunable Majorana corner states in a two-dimensional second-order topological superconductor induced by magnetic fields*, *Phys. Rev. B* **97** (2018) 205134.

[135] Y. Volpez, D. Loss and J. Klinovaja, *Second-order topological superconductivity in π-junction rashba layers*, *Phys. Rev. Lett.* **122** (2019) 126402.

[136] Y.-T. Hsu, W. S. Cole, R.-X. Zhang and J. D. Sau, *Inversion-protected topological crystalline superconductivity in monolayer WTe_2*, *arXiv:1904.06361* (2019) .

[137] Y.-J. Wu, J. Hou, X. Luo, Y. Li and C. Zhang, *In-plane Zeeman field induced Majorana corner and hinge modes in an s-wave superconductor heterostructure*, *arXiv:1905.08896* (2019) .

[138] R.-X. Zhang, W. S. Cole, X. Wu and S. Das Sarma, *Higher order topology and nodal topological superconductivity in Fe(Se,Te) heterostructures*, *Phys. Rev. Lett.* **123** (2019) 167001.

[139] Z. Wu, Z. Yan and W. Huang, *Higher-order topological superconductivity: Possible realization in fermi gases and Sr_2RuO_4*, *Phys. Rev. B* **99** (2019) 020508(R).

[140] S. Franca, D. Efremov and I. Fulga, *Phase-tunable second-order topological superconductor*, *Phys. Rev. B* **100** (2019) 075415.

[141] M. Kheirkhah, Y. Nagai, C. Chen and F. Marsiglio, *Majorana corner flat bands in two-dimensional second-order topological superconductors*, *arXiv:1904.00990* (2019) .

[142] S. Ono, Y. Yanase and H. Watanabe, *Symmetry indicators for topological superconductors*, *Physical Review Research* **1** (2019) 013012.

[143]

[144] A. Skurativska, T. Neupert and M. H. Fischer, *Atomic limit and inversion-symmetry indicators for topological superconductors*, *arXiv:1906.11267* (2019) .

[145] A. Y. Kitaev, *Unpaired majorana fermions in quantum wires*, *Physics-Uspekhi* **44** (2001) 131.

[146] E. Khalaf, H. C. Po, A. Vishwanath and H. Watanabe, *Symmetry indicators and anomalous surface states of topological crystalline insulators*, *Phys. Rev. X* **8** (2018) 031070.

[147] M. Eschrig, J. Kopu, J. C. Cuevas and G. Schön, *Theory of half-metal/superconductor heterostructures*, *Phys. Rev. Lett.* **90** (2003) 137003.

[148] D. Aoki, K. Ishida and J. Flouquet, *Review of U-based ferromagnetic superconductors: Comparison between UGe_2, URhGe, and UCoGe*, *J. Phys. Soc. Jpn.* **88** (2019) 022001.

[149] S. S. Saxena, P. Agarwal, K. Ahilan, F. M. Grosche, R. K. W. Haselwimmer, M. J. Steiner et al., *Superconductivity on the border of itinerant-electron ferromagnetism in UGe_2*, *Nature* **406** (2000) 587.

[150] A. Huxley, I. Sheikin, E. Ressouche, N. Kernavanois, D. Braithwaite, R. Calemczuk et al., *UGe_2: A ferromagnetic spin-triplet superconductor*, *Phys. Rev. B* **63** (2001) 144519.

[151] D. Aoki, A. Huxley, E. Ressouche, D. Braithwaite, J. Flouquet, J.-P. Brison et al., *Coexistence of superconductivity and ferromagnetism in URhGe*, *Nature* **413** (2001) 613.

[152] N. T. Huy, A. Gasparini, D. E. De Nijs, Y. Huang, J. C. P. Klaasse, T. Gortenmulder et al., *Superconductivity on the border of weak itinerant ferromagnetism in UCoGe*, *Phys. Rev. Lett.* **99** (2007) 067006.

[153] A. D. Huxley, *Ferromagnetic superconductors*, *Physica C* **514** (2015) 368.

[154] S. Ran, C. Eckberg, Q.-P. Ding, Y. Furukawa, T. Metz, S. R. Saha et al., *Nearly ferromagnetic spin-triplet superconductivity*, *Science* **365** (2019) 684.

[155] X. Liu, Z. Hao, E. Khalaf, J. Y. Lee, K. Watanabe, T. Taniguchi et al., *Spin-polarized correlated insulator and superconductor in twisted double bilayer graphene*, *arXiv:1903.08130* (2019) .

[156] J. Y. Lee, E. Khalaf, S. Liu, X. Liu, Z. Hao, P. Kim et al., *Theory of correlated insulating behaviour and spin-triplet superconductivity in twisted double bilayer graphene*, *Nat. Commun.* **10** (2019) 5333.

[157] C. Shen, N. Li, S. Wang, Y. Zhao, J. Tang, J. Liu et al., *Observation of superconductivity with tc onset at 12K in electrically tunable twisted double bilayer graphene*, *arXiv:1903.06952* (2019) .

[158] Q. Wu, A. A. Soluyanov and T. Bzdušek, *Non-abelian band topology in noninteracting metals*, *Science* **365** (2019) 1273.

[159] X.-Q. Sun, S.-C. Zhang and T. Bzdušek, *Conversion rules for Weyl points and nodal lines in topological media*, *Phys. Rev. Lett.* **121** (2018) 106402.

초록

이 논문에서는 시공간 반전대칭이 있는 계에서의 위상적인 상에 대해 연구한다. 여기서 시공간 반전 I_{ST} 은 운동량을 바꾸지 않는 반(anti)유니터리 대칭 연산자이면서 $I_{\mathrm{ST}}^2 = 1$을 만족시키는 것을 말한다. 이러한 조건을 만족시키는 I_{ST}는 스핀궤도결합이 3차원 물질에서 공간 반전 P와 시간 반전 T의 조합인 PT 혹은 스핀궤도결합의 유무와 상관없이 2차원 물질에서 수직 축으로 180도 회전 C_2 와 시간 반전 T 의 결합인 C_2T가 있다. 시공간 반전 대칭은 운동량 공간 내에서 해밀토니안과 블로흐 파동함수에 실수 조건을 주고, 따라서 베리 곡률과 천 숫자가 항상 0이 된다. 따라 실수 파동함수의 위상적인 성질은 천 숫자 대신에 다른 위상 불변량으로 기술되어야 한다. 우리는 실수 파동함수의 위상적인 성질이 슈티펠-휘트니 숫자라는 위상불변량으로 기술된다는 것을 보여주고, 이 불변량의 일반적인 성질과 물리적인 의미에 대해 설명한다. 제 1 슈티펠-휘트니 숫자와 제 2 슈티펠-휘트니 숫자는 1차원과 2차원 위상 불변량으로 양자화된 베리 위상과 Z_2 홀극 전하에 대응된다. 우리는 먼저 제 1 슈티펠-휘트니 숫자로 설명되는 위상적인 상에 대해서 다룬다. 1차원에서 양자화된 전기 편극을 가지는 부도체, 2차원 디락 준금속과 3차원 마디 선 준금속이 이에 해당된다. 다음으로 제 2 슈티펠-휘트니 숫자가 3차원 마디 선이 Z_2 홀극 전하를 가지는 것을 어떻게 설명할 수 있는 지 얘기한다. 특히 제 2 슈티펠-휘트니 숫자, Z_2 홀극 전하, 그리고 마디 선들의 연결 수 의 관계에 대해서 설명한다. 그 다음 제 2 슈티펠-휘트니 숫자로 설명되는 2차원과 3차원 위상 부도체에 관해서 다룬다. 일반적인 이론에 대한 설명을 마친 다음, 2차원에서 닐슨과 니노미야의 정리의 재정립을 우리 이론의 재미있는 응용으로서 설명한다. 이 모든 이론적인 분석들은 시공간 반전 대칭만을 필요로 한다. 하지만 스핀궤도결합이 없는 경우에 시간 반전 대칭과 공간 반전 대칭이 각각 존재하면 공간 반전 연산자의 고유값을 이용해서 제 2 슈티펠-휘트니 숫자를 간단하게 계산할 수 있다. 이러한 관계와 이미 알려져 있는 결과들을 조합해서 스핀이 정렬되어 있는 계에서

나타나는 홀반전성을 가지는 위상 초전도의 연구에 적용해본다.

주요어: 띠 위상, 시공간 반전 대칭,위상 준금속, 위상 부도체, 위상 초전도체, 위상 불변량

학번: 2013-20372